UNC-4 CONTROLS SYNAPTIC SPECIFICITY BY MODULATING

ANTAGONISTIC WNT PATHWAYS IN THE C. ELEGANS

MOTOR CIRCUIT

By

JUDSEN DANIEL SCHNEIDER

Dissertation

Submitted to the Faculty of the

Graduate School of Vanderbilt University

in partial fulfillment of the requirements

for the degree of

DOCTOR OF PHILOSOPHY

in

Cell and Developmental Biology

May, 2010

Nashville, Tennessee

Approved:

David M. Miller, III, Ph.D.

Guoqiang Gu, Ph.D.

Kendal Broadie, Ph.D.

Kathy Gould, Ph.D.

To my lovely wife Natasha,
my beautiful daughter Diem,
and the baby on the way

AKNOWLEDGEMENTS

The journey towards this thesis actually began one morning back in 2003 when I swam with the masters group the Nashville Aquatic Club. At that time, I was fresh out of college swimming and still in great swimming shape. Afterwards, the swimmer in the next lane commented on how he was trying to keep up with me. I told him my story, and asked who he was. "Hi, I'm David Miller." he said.

Sometimes fate intervenes and brings people into your life. I am very thankful to have met David Miller that morning. Graduate school has been a long, punctuated journey filled with periods of sheer elation, distraught, and pleasant monotony. Having a mentor who takes a strong interest in your progress, pushes you to succeed, and appreciates your effort in both success and failure, has shaped not only my scientific life, but also my personal journey. It's a rare person that can allow one of his students to torture him as a swimming coach for an hour each morning, and then provide a meaningful critique of an experimental result later on. A less confident and sincere individual would struggle with that change in hierarchy. In order to be a great teacher, you must first be a student. David, you exemplify that statement. Thank you.

I'd also like to thank my committee members for their assistance with this project. Special thanks for Kathy Gould and her willingness to chair my committee. Having a chair that is direct and fair is a fantastic asset. I'd also like to thank Kendal Broadie for bringing a wealth of neuroscience expertise and

of good beer. Kathie, you inspire me with your kindness. To anyone I have not mentioned, thank you for making this experience enjoyable.

My greatest supporter through graduate school has been my wife, Natasha. This experience would have been a lot more challenging without you by my side to cheer me on when things were going well, and to push me when things were slowing down. I love you more than words can say. Thank you.

A big thank you goes out to the rest of my family. To my daughter Diem: you radiate joy and love. I have never met anyone like you. To my parents: thanks for being my tireless supporters, and providing me with a strong faith. To my brother: thanks for being my best friend. To my in-laws: for raising my wonderful wife and listening to my esoteric scientific presentations.

I'd also like to thank Sam at J & J's coffee shop for a daily dose of fine coffee and a bolt of sunshine.

I'd also like to thank the financial support I've received. After joining David's lab, I was awarded the Program in Developmental Biology training grant, which supported me for two years. I have also been awarded several Vanderbilt travel grants, to attend scientific conferences, as well as a dissertation enhancement grant, which allowed me to perform a risky experiment. A thank you to Vanderbilt for making these opportunities available.

TABLE OF CONTENTS

LIST OF TABLES

Page

LIST OF FIGURES

CHAPTER I

WNT SIGNALING PATHWAYS PATTERN NEURAL CONNECTIONS

INTRODUCTION

I have divided this introduction into three main sections. First, I will

describe canonical and non-canonical Wnt signaling pathways and their

relevance to development. This section will highlight examples of the Wnt

pathways that antagonize each other. Second, I will review the literature

describing the role of Wnt signaling in neuronal development. Third, I will

describe the role of gap junction connections in a neural system. A common

theme will emerge; Wnt signaling plays an indispensible role in multiple different

aspects of synaptic development.

Section 1: Wnt Signaling

What is Wnt signaling? First discovered in Drosophila based on a mutant

fly with no wings, the extracellular ligand Wingless, is the starting point for this

pathway. Here, I will provide an overview of the canonical Wnt pathway, but I

direct your attention to several recent reviews for a more comprehensive

discussion of the Wnt signaling pathway (Clevers 2006; Angers and Moon 2009;

Macdonald et al. 2009).

Drosophila Wingless is homologous to the oncogene int-1; the term "Wnt"

was adopted for this conserved signal in homage to both findings (Clevers 2006).

Wnt is a secreted glycoprotein that functions by interaction with a variety of receptors, the most well known are homologs of the Drosophila Frizzled protein. Frizzled receptors are seven transmembrane domain proteins that bind Wnt through a cysteine rich domain (CRD) (Clevers 2006). Distinct Wnt receptors, such as ROR kinase and MuSK, also bind Wnt through a CRD sequence (Clevers 2006; Jing et al. 2009). The interaction of Wnt with a receptor can trigger a variety of downstream signaling pathways.

The canonical Wnt signaling pathway.

The canonical Wnt signaling pathway (Figure 1.1) controls cytosolic levels of the effector protein, β-catenin (Macdonald et al. 2009). Normally, β-catenin is kept low by a 'destruction complex', consisting of the scaffold proteins Axin and *adenomatous polyposis coli* (APC), and the kinases Glycogen Synthase Kinase 3 (GSK3) and Casein Kinase 1α (CK1α) (Macdonald et al. 2009). Axin, the central scaffold protein binds APC, GSK3, CK1α to form the destruction complex and recruits cytosolic β-catenin into the complex. Upon binding, β-catenin is initially phosphorylated by CK1α, which in turn leads to additional phosphorylation of β-catenin by GSK3. Phosphorylated β-catenin is then covalently linked to ubiquitin via the E3 ligase β-TRCP. This linkage targets β-catenin for degradation by the ubiquitin proteosome system (Macdonald et al. 2009). Thus, in the absence of Wnt signaling, Axin and the destruction complex function to keep cytosolic β-catenin levels low and thereby maintain the Wnt pathway in an 'off' state (Macdonald et al. 2009).

When Wnt binds to a Frizzled receptor, the intracellular concentration of β-catenin is allowed to rise through inhibition of the destruction complex (Macdonald et al. 2009). The most well characterized mechanism for Wnt induced stabilization of cytosolic β-catenin occurs via direct interaction between the intracellular domain (ICD) of the co-receptor protein LRP5/6 with GSK3. The LRP5/6 ICD directly inhibits GSK3-dependant phosphorylation of β-catenin (Cselenyi et al. 2008) (Figure 1.1). In addition, Frizzled receptors signaling through the membrane-associated protein, disheveled, cause the disassembly of the destruction complex, ultimately leading to the degradation of Axin by an unknown mechanism (Macdonald et al. 2009). The net outcome of these events, the elevation of cytosolic β-catenin and concomitant reduction of Axin, is a characteristic feature of β-catenin dependent Wnt signaling.

The stabilization of cytosolic β-catenin results in its translocation to the nucleus where it interacts with the transcription factor TCF/LEF to activate gene expression (Macdonald et al. 2009). In the absence of β-catenin, TCF associates with the co-repressor protein Groucho, to mediate transcriptional repression. β-catenin recruits the nuclear adaptor proteins Legless/BCL-9 and Pygopus after binding to TCF and displacing Groucho. Legless/BCL-9 and Pygopus then interact with the mediator complex to activate transcription. Therefore, activated canonical Wnt signaling ultimately functions to convert TCF from a transcriptional repressor protein to an activator protein (Macdonald et al. 2009) (Table 1.1).

Migration of the Q neuroblast in *C. elegans* provides a well-characterized example of canonical Wnt signaling in neural development. The QL and QR
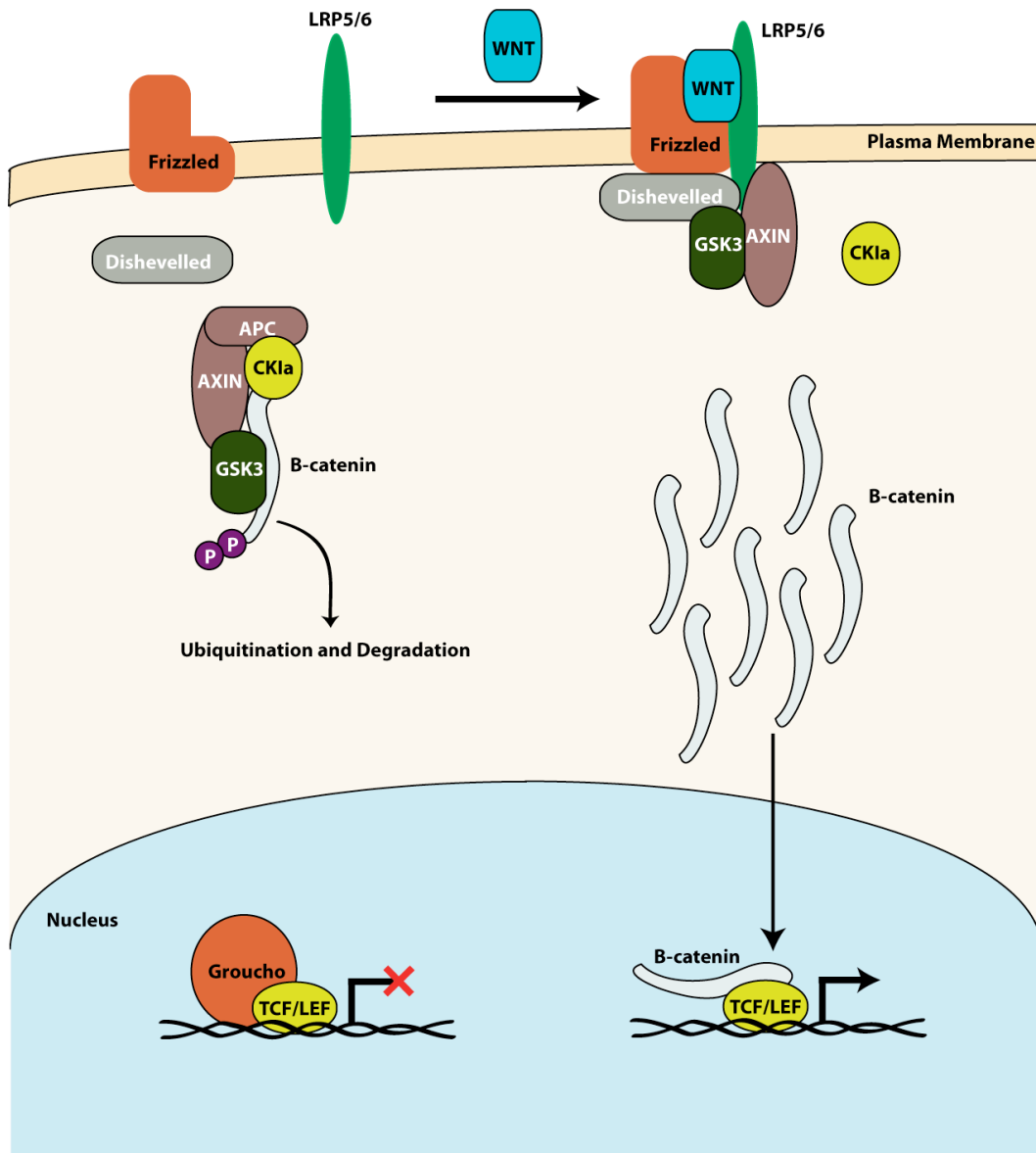
Figure 1.1. The Canonical Wnt signaling pathway.

Left. In an inactive pathway, cytosolic levels of β-catenin are kept low by a destruction complex consisting of Axin, GK3, APC, and CKIα. In the nucleus, Groucho interacts with TCF/LEF to prepress transcription. Right. Wnt activates the pathway through its interaction with Frizzled and co-receptor lrp5/6. This inhibits the destruction complex by Disheveled's recruitment of Axin, blocking the destruction complex. The intracellular domain of LRP5/6 further inactivates the destruction complex by inhibiting GSK3. This allows cytosolic β-catenin to accumulate and leads to its subsequent translocation into the nucleus. β-catenin then interacts with TCF to displace Groucho. Legless/BCL-9 and Pygopus then interact with β-catenin and the mediator complex, effectively turning TCF from a repressor into an activator.

	Drosophila	*C. elegans*
Secretion Complex		
Wntless	Wntless/Evenness interrupted	*mig-14/mom-3*
porcupine	porcupine	*mom-1*
retromer complex		*vps-35*
Ligand		
Wnt	Wingless(wg)	*lin-44, egl-20, cwn-1, cwn-2, mom-2*
Receptor		
Frizzled	Frizzled, dFz2	*lin-17, mig-1, mom-5, cfz-2*
Ror		*cam-1*
Ryk	Derailled	*lin-18*
LRP5/6	Arrow	*N.C.*
Intracellular		
Disheveled	Disheveled	*dsh-1, dsh-2, mig-5*
Gαo		*goa-1?*
Destruction Complex		
GSK-3	Shaggy	*gsk-3*
Axin	Axin	*pry-1*
Caesin Kinase I		*kin-19*
Adenomatous Polyposis Coli	apc	*apr-1*
Beta-Catenin	Armadillo	*bar-1*
Transcription Factor		
TCF	dTCF	*pop-1*
Pygopus	Pygopus	N.C.
Legless	Legless	N.C.
Groucho	Groucho	*unc-37*

Table 1.1. Comparison of *Drosophila*, and *C. elegans* compoents of the canonical Wnt signaling pathway.

Each of these components has been implicated in canonical Wnt signal transduction. Many of these components are conserved, but remain uncharacterized. (NC = not characterized).

neuroblasts are born on opposite sides of the embryo (Sulston and Horvitz 1977). After hatching, each neuroblast undergoes additional rounds of division to produces 3 distinct types of neurons and a cell that undergoes apoptosis. The hox gene, *mab-5*, is selectively activated in QL and its descendants as they migrate posteriorly whereas QR does not express *mab-5* and moves toward the anterior. The different locations of the mechanosensory neurons AVM (daughter of QR) in the anterior and PVM (daughter of QL) in the posterior are a direct result of the opposite directions of migration adopted by these distinct neuroblast lineages (Maloof et al. 1999). The posterior migration of QL and its descendents depend on *mab-5* (Harris et al. 1996; Maloof et al. 1999). Genetic results indicate that a canonical Wnt signaling pathway controls expression of *mab-5* (Maloof et al. 1999). For example, mutations in *egl-20*/Wnt or in the frizzled genes, *mig-1* or *lin-17,* which act redundantly in this pathway, cause a loss of *mab-5* expression that induces QL descendants to reverse direction and migrate toward the anterior (Harris et al. 1996). The anterior direction of QR is also perturbed by these mutations such that AVM ends up in a more posterior position than in wildtype animals. Thus, QL and QR display opposite responses to EGL-20/Wnt with the QR lineage migrating anteriorly and QL and its descendents moving to the posterior. Wnt pathway components that drive the anterior migration of QR are unknown. However, the migration toward the posterior depends on canonical Wnt signaling. Mutations in the negative regulator of canonical Wnt signaling, *pry-1*/Axin, result in ectopic *mab-5* expression in the QR daughter cells and induce their posterior migration (Maloof et al. 1999).

Mutations in β-catenin, *bar-1* block the *pry-1* phenotype indicating that *bar-1* is required downstream of *pry-1*/Axin (Maloof et al. 1999) as predicted for canonical Wnt signaling. The transcription factor *pop-1*/TCF also functions in this pathway and is required for expression of *mab-5* (Herman 2001). Thus, a canonical Wnt signaling pathway comprised of *egl-20*/Wnt, *mig-1/ Frz and lin-17/Frz, bar-1*/β-catenin, and *pop-1*/TCF drives *mab-5* expression and posterior migration of QL and its lineal descendents.

Non-canonical Wnt signaling.

Wnt signals may also activate alternative downstream transduction pathways in different cell types (Clevers 2006). Several of these so-called "non-canonical" Wnt signaling pathways do not involve the phosphorylation and degradation of β-catenin. The planar cell polarity pathway (PCP) and the Wnt Ca^{2++} pathway are two examples of non-canonical pathways with important roles in development (Angers and Moon 2009). PCP signaling is required for the uniform orientation of specific cellular structures, such as hair on the Drosophila wing (Fanto and McNeill 2004). One critical aspect of Wnt/PCP signaling is asymmetric distribution of Wnt pathway components within the cell. For example, in the Drosophila imaginal wing disk, Frizzled, the ankryin repeat protein Diego, Dishevled, and the atypical cadherin Flamingo, localize to the distal portions of the cell. Opposing this, Flamingo, Diego, the transmembrane protein VanGoh/Strabizimus, and the LIM domain containing protein Prickle localize to the proximal cell membrane. This asymmetric distribution of pathway

components helps to create a polarized cell (Fanto and McNeill 2004). The Wnt

Ca^{2++} pathway functions by mediating the release of intracellular calcium by

activating PIP_3 (phosphoinositol) signaling. Here, Frizzled activates

phospholipase C (PLC), via G-protein signaling. PLC then converts IP_2 into IP_3,

causing IP_3 to interact with its receptor, IP_3R, in the endoplasmic reticulum and

trigger the release of intracellular calcium from the endoplasmic reticulum (Kühl

2004). One common feature of non-canonical Wnt signaling pathways, is that

they do not function by modulating cytosolic levels of β-catenin.

Non-canonical Wnt signaling plays an important role in the developing *C.

elegans* embryo (Figure 1.2). However, these pathways are distinguished from

non-canonical signaling pathways in other animals in that some involve β-

catenin. The non-canonical, β-catenin-dependant, asymmetric cell division

pathway is critical for differentiating between anterior versus posterior cellular

fates (Figure 1.3) (Huang et al. 2007). The critical determinant for this pathway's

output is the nuclear ratio of SYS-1/β-catenin to *pop-1*/TCF. A high SYS-1:POP-

1 ratio results in a posterior cell fate whereas a low ratio produces in an anterior

cell fate (Huang et al. 2007). For example, in the 4-cell stage embryo, the ventral

blastomere EMS divides to produce two cells, the posterior daughter, E, which

gives rise to gut cells (endoderm), and the anterior daughter MS, which

generates muscle cells and other tissue (mesoderm) (Sulston et al. 1983). This

asymmetric division is dependant upon a MOM-2/Wnt (MOM = MOre

Mesoderm). Mutations in *mom-5*/Frizzled, *apr-1*/APC, and *wrm-1*/β-catenin also

result in the loss of endodermal tissue. These effects are mimicked by laser
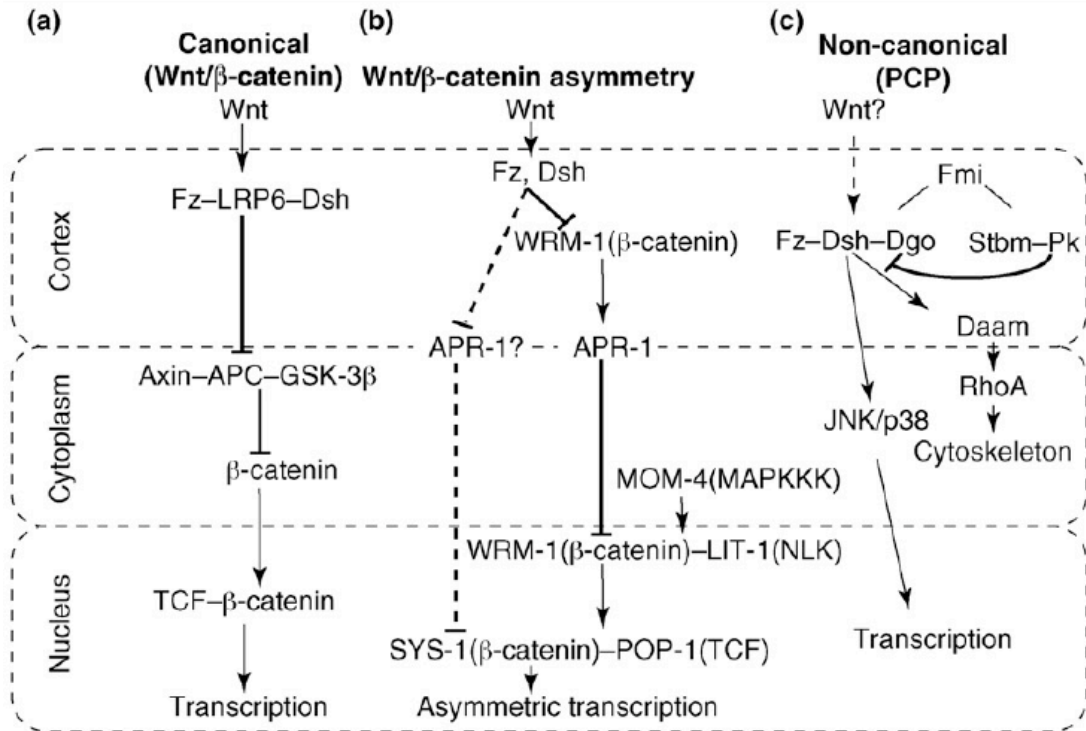
Figure 1.2. Non-canonical Wnt signaling in *C. elegans* early embryo.

Divergence of the cytosolic processes in three *C. elegans* Wnt pathways. A. Canonical Wnt signaling functions through a well characterized mechanism and appears preserved in some developmental processes such as vulval development and Q cell migration. B. Wnt/β-catenin asymmetry pathway. This pathway likely functions through disheveled to regulate two β-catenins, WRM-1 and SYS-1. Ultimately, this pathway regulates the SYS-1 to POP-1/TCF ratio in the nucleus to regulate gene transcription. WRM-1 nuclear levels are also thought to be regulated by *apr-1*(APC) through a branch in the pathway. C. non-canonical planar cell polarity pathway (PCP) in vertebrates and *Drosophila*. Fz-Dsh-dgo (Diego) and Stbm-(Strabismus)-Pk(Prickle) show opposite, polarized locations at the cell cortex. This pathway regulates the actin cytoskeleton through RhoA, and transcription through JNK/p38 MAP kinase cascade. Wnt may not actually be required in *Drosophila* to activate PCP signaling.

Figure taken from Figure 1 of (Mizumoto and Sawa 2007)

ablation of the P2 blastomere, the source of the MOM-2/Wnt signal (Rocheleau et al. 1997). These experiments are consistent with a model in which MOM-2/Wnt from P2 signals to EMS blastomere through the frizzled receptor MOM-5 which in turn activates the disheveled homologs, *dsh-2* and *mig-5*. DSH-2 is recruited to the cell surface and signals through an unknown mechanism to activate *kin-19*/CKIα*, gsk-3*/GSK3*, apr-1*/APC (Walston et al. 2004; King et al. 2009). In this case, these components actually *promote* Wnt signal transduction, a role opposite to their antagonistic roles in the canonical pathway function. Once the pathway is activated, WRM-1/β-catenin interacts with LIT-1/Nemo-like-kinase (NLK) (Rocheleau et al. 1999). Activation of this pathway also causes a MOM-4(Map Kinase Kinase Kinase)/LIT-1(NLK) complex to form, which then activates the WRM-1/LIT-1 complex (Shin et al. 1999). The WRM-1/LIT-1 complex phosphorylates POP-1 causing its association with a 14-3-3 protein, PAR-5, and POP-1 export from the nucleus. The net effect of these interactions is to reduce the level of nuclear POP-1 in the anterior daughter cell (Lo et al. 2004). MOM-2/Wnt signaling also elevates nuclear SYS-1/β-catenin, thus effectively increasing the SYS-1:POP-1 ratio. This promotes an anterior cell fate by converting POP-1 from an activator protein into a repressor, turning off transcription factors required for endoderm fate (Huang et al. 2007) (Figure 1.3).

As in PCP pathways in *Drosophila*, the asymmetric localization of frizzled receptors is required for non-canonical signaling (Park et al. 2004; Angers and Moon 2009). For example, MOM-5/Frizzled asymmetric localization is required
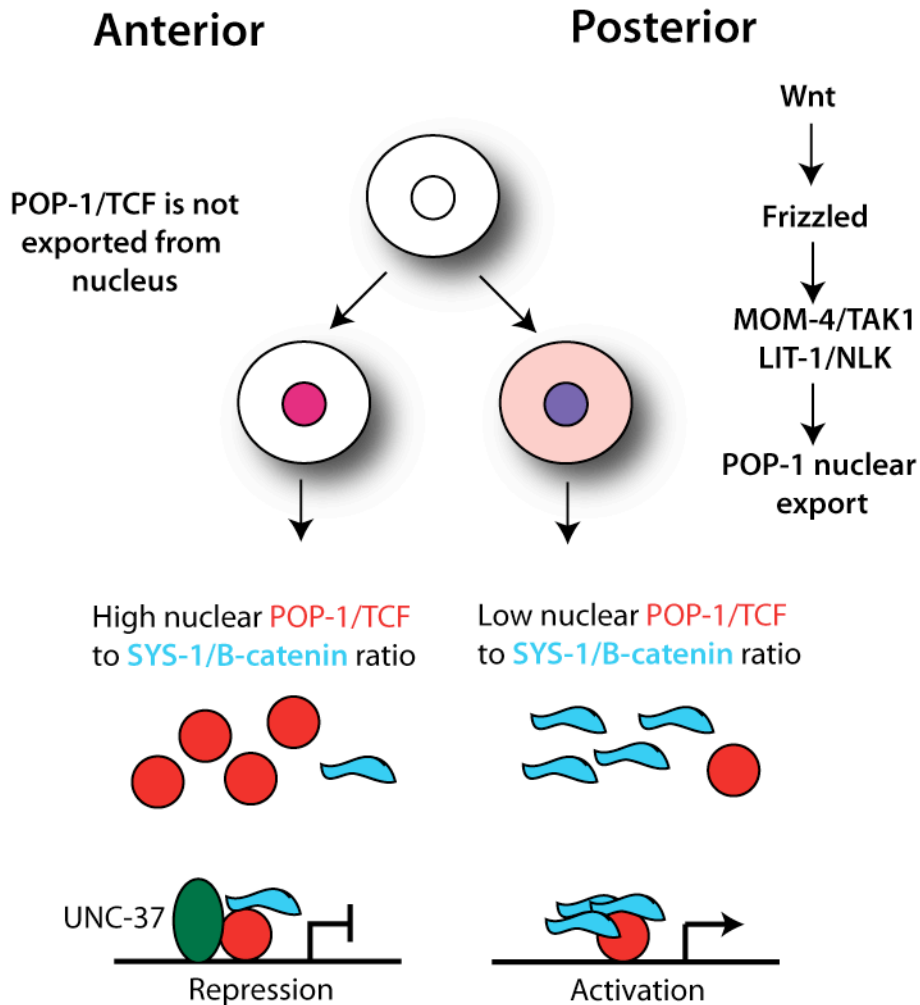
Figure 1.3. The *C. elegans* non-canonical asymmetry pathway.

Global regulation of anterior-posterior fate is regulated by a non-canonical, β-catenin dependant Wnt signaling pathway coined the non-canonical asymmetry pathway. Here, the level of nuclear POP-1/TCF is controlled, in contrast to the canonical pathway's tight regulation of cytosolic β-catenin. Anterior fate is established by a high SYS-1(β-catenin) to POP-1(TCF) ratio, which turns the SYS-1:POP-1 complex into a transcriptional repressor. In contrast, posterior fate is induced by a posterior Wnt signal. This causes the MOM-4/LIT-1 complex to export POP-1 from the nucleus, reducing the SYS-1 to POP-1 ratio and activating gene transcription.

for normal development. MOM-5::GFP is enriched at the posterior pole of dividing cells. MOM-5::GFP expression is up-regulated when the embryo has reached the 32 cell stage. MOM-5::GFP asymmetric distribution has also been observed in several different larval cell divisions (Park et al. 2004). Asymmetric localization of *dsh-2*/Disheveled at the P2/EMS boundary has also been reported (Walston et al. 2004). These events have not been observed at the four-cell stage, however, the asymmetric localization of Frizzled and Disheveled do appear to occur in asymmetric postembryonic cell divisions later during development, and thus may represent a common mechanism characteristic of the asymmetric Wnt pathway (Wu and Herman 2007).

A different, non-canonical Wnt signaling pathway controls localization of the mitotic spindle (Schlesinger et al. 1999). In this case, MOM-5::GFP puncta are associated with the centromere of dividing cells (Park et al. 2004). *mom-5* is required for normal spindle orientation in the mitotic cell ABar, but *mom-2*/Wnt is not, suggesting additional signals that may function to orient this pathway (Rocheleau et al. 1997; Schlesinger et al. 1999). Genetic results have also implicated several additional Wnt pathway components in this process including *dsh-1*/Dsh, *dsh-2*/Dsh, *mig-5*/Dsh, *gsk-3*/GSK3β and kin-19/CKIα. KIN-19/CKIα localization at the mitotic spindle was also observed, suggesting that these pathway components are acting on microtubules (Walston et al. 2004). This non-canonical pathway, however, does not require downstream genes including, *wrm-1*/β-catenin, *apr-1*/APC and *pop-1*/TCF, which do not show a spindle orientation defect. Thus, it is likely that this signaling pathway is not dependant

12

upon transcription (Rocheleau et al. 1997). This model suggests that GSK3 and other destruction complex proteins are acting directly on the mitotic spindle to regulate its orientation. It is also possible, however, that these Wnt pathway components may function in a separate pathway that determines the timing of mitotic spindle orientation during mitosis instead of acting to turn the spindle directly (Walston et al. 2004).

Non-canonical Wnt signaling has been implicated in additional developmental events. For example, a non-canonical asymmetry pathway is thought to be involved fate determination of terminal asymmetric cell division in *C. elegans*, although it is unclear if the pathway is also required for all postembryonic cell divisions (Bertrand and Hobert 2009; Hingwing et al. 2009). One report also implicated non-canonical Wnt signaling during gastrulation in *C. elegans* through regulation of myosin contractility (Lee et al. 2006).

Wnts function redundantly to specify tissues in *C. elegans*.

Many of the Wnt-dependant signaling pathways in *C. elegans* function through the interaction of multiple Wnts and Frizzled receptors to promote a common developmental event. One example of this functional redundancy between receptors and lignads occurs during the development of the *C. elegans* vulva (Sternberg 2005). Adult vulval epithelial cells are derived from six vulval precursor cells (VPC) in the ventral epidermis. Several competing signals control VPC differentiation including the LIN-3/EGF, which functions through LET-60/Ras, LIN-12/Notch, and Wnt (Sternberg 2005).

13

Vulval induction is initiated by a LIN-3/EGF signal from the anchor cell, which is positioned in the gonad directly above the developing vulval epithelium. LIN-44/Wnt and MOM-2/Wnt are also expressed within the anchor cell. The combined LIN-3/EGF and Wnt signals induce expression of the hox gene *lin-39*, which in turn prevents VPC fusion with the hypodermal syncytium and stimulates VPC division (Sternberg 2005). Further genetic studies have provided a picture of a highly redundant system: all five Wnt ligands, four of the five Frizzled receptors, and a canonical signaling pathway all interact to coordinate development of the vulval epithelium (Gleason et al. 2006).

An intriguing regulatory mechanism has been proposed for the developmental event in which the CAM-1/Ror Wnt receptor modulates the strength of Wnt signaling through a non-cell autonomous mechanism. In this model, the essential role of CAM-1/Ror is to act as a sink to prevent Wnt ligands from triggering Wnt signaling pathways that affect VPC fate. It will be interesting to determine if Wnt receptors adopt similar non-cell autonomous roles in other Wnt depdendent developmental pathways (Green et al. 2007).

Antagonistic Wnt pathways regulate development.

Xenopus laevis, the African clawed frog, is a model system used to study early embryonic development. One of the first Wnt experiments was conducted in Xenopus. Injection of the oncogene int-1 into the developing embryo was found to induce a secondary axis (McMahon and Moon 1989b; McMahon and Moon 1989a). Subsequent experiments revealed that induction of the Spemann

organizer, which is critical to axis specification, is dependant upon the nuclear accumulation of β-catenin (and dorsal TGFβ signaling) (Moon and Kimelman 1998).

One of the first experiments to suggest a functional antagonism between Wnt ligands was also performed in the Xenopus system. Xwnt8 normally induces a secondary axis, however, a pre-injection of the embryo with Xwnt5a can block this Xwnt8 induced effect (Torres et al. 1996). Experiments in zebrafish have also detected Wnt-5 and Wnt-8 antagonism (Slusarski et al. 1997; Westfall et al. 2003). Additional experiments in the Zebrafish blastomere have shown that reduced levels of the 'non-canonical' Wnt-5 phenocopies over-activation of canonical Wnt signaling; Wnt-5 loss-of-function animals display a dorsalized phenotype and some animals show induction of a secondary axis that is characteristic of hyperactivated canonical Wnt signaling (Westfall et al. 2003). Consistent with these results are data showing that non-canonical Wnt signaling, via Wnt-11 and Wnt-5, promotes a ventralized fate (Westfall et al. 2003). Thus, these findings support a model of antagonism between a canonical Wnt signaling pathway that favors a dorsal fate versus a non-canonical pathway that promotes ventral fate (Westfall et al. 2003).

Recent results have shown a more direct interaction between the co-receptor protein, lrp5/6, and the non-canonical Wnt signaling pathway that drives convergent extension movements (Tahinci et al. 2007). Animal caps, cultured *in vitro,* normally differentiate into balls of epidermis. However, treatment with activin, a TGF-β homolog, causes cells to become mesoderm and intercalate into

the cap, creating an enlongated structure. Activin-induced animal cap elongation

is blocked by injection of the non-canonical Wnt, Xwnt11, known to induce

convergent and extension and antagonize activin-mediated mesoderm induction.

Furthermore, co-injection of suboptimal amounts of lrp5/6 morpholino reinforces

Xwnt11 injection, suggesting that lrp5/6 may antagonize non-canonical Wnt

signaling. Inhibition of non-canonical Wnt signaling, is caused by a specific part

of the intracellular domain of lrp5/6 (Tahinci et al. 2007). These experiments

have revealed a mechanism whereby antagonistic interactions between Wnt

pathways may result from direct interactions between canonical and non-

canonical pathway components.

Antagonism between competing Wnt pathways is also observed in *C.*

elegans vulval development (Figure 1.4). For example, the effects of EGL-

20/Wnt on P7.p are antagonized by two Wnt ligands, LIN-44 and MOM-2

(Eisenmann and Kim 2000). Recent work has suggested that the Wnt ligand

EGL-20 serves as a mechanism to define a 'ground' polarity for defining the

asymmetric divisions of P7.p (Green et al. 2008). This EGL-20/Wnt signal

functions through interactions with the PCP component *vang-*

1/VanGogh/Strabizimus and serves to orient the asymmetric cell divisions of both

2 cells (P5.p and P7.p) in a wildtype P5.p manner (Green et al. 2008). However,

EGL-20/Wnt is a long-range signal (secreted in the tail), and although it has clear

effects in the mid-body, the Wnt ligands expressed from the anchor cell, *lin-44*

16
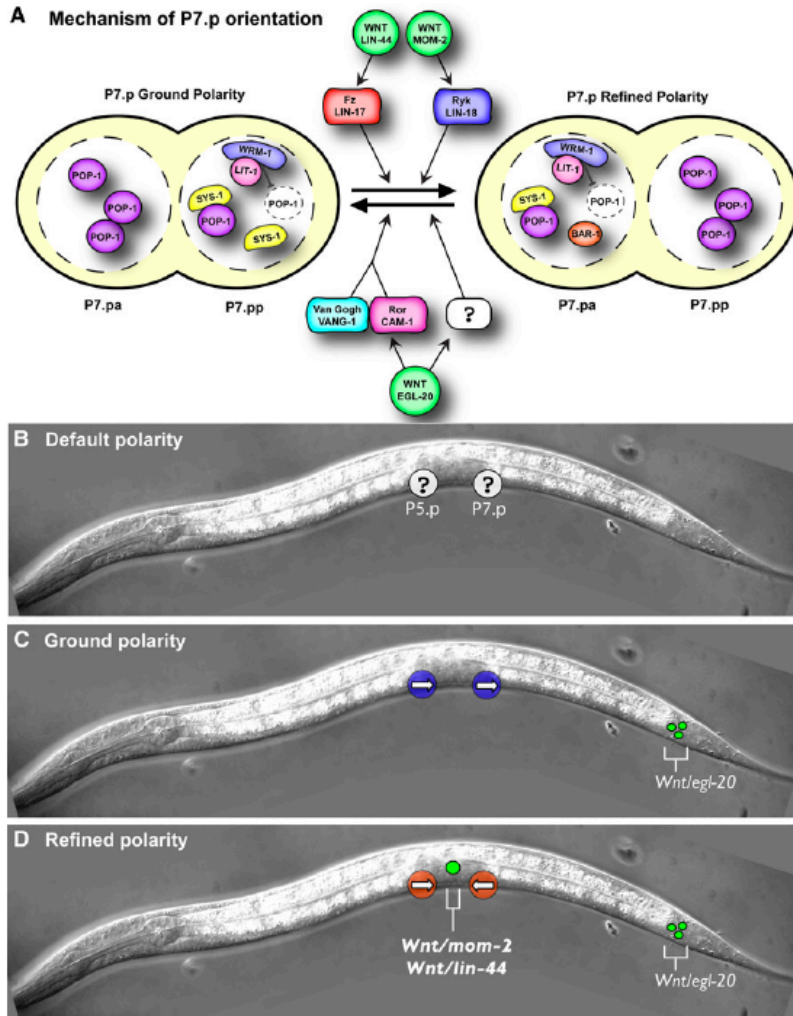
Figure 1.4. Antagonistic Wnt signaling pathways in *C. elegans* vulval development

A. Two competing Wnt signals function to orient asymmetric divisions of the vulval epithelium via the non-canonical asymmetry pathway. B. During development P5.p. and P7.p. do not establish an intrinsic polarity. C. The posterior Wnt ligand, EGL-20, establishes a 'ground' polarity, orienting P5.p. and P7.p. in a posterior direction. D. The Wnt ligands, MOM-2 and LIN-44, expressed between P5.p. and P7.p. above the vulval epithelium, induce a 'refined' polarity effectively reversing the orientation of P7.p. This allows the vulval epithelium to divide along a central axis and form the symmetrical vulval structure.

Figure taken from figure 5 of (Green et al. 2008)

and *mom-2*, are able to dominate *lin-17*/Frizzled and *lin-18*/Ryk mediated signaling. Thus, although the 'ground polarity' is established by EGL-20, orienting cells to divide in one direction, this polarity is later 'refined' by LIN-44 and MOM-2 such that P5.p. and P7.p. divide as mirror images of each other (Green et al. 2008). In this refinement mechanism, LIN-44/Wnt and MOM-2/Wnt are hypothesized to re-orient P7.p. cell fate via the non-canonical β-catenin asymmetry pathway. Wnt signaling induces expression of transcription factors *cog-1*/Nkx6 and *lin-11*/LIM, which promote cell fate in the posterior daughters of P7.p (Inoue et al. 2005). The exact role of canonical Wnt signaling in vulval induction remains unclear. Genetic studies have implicated all the major intracellular pathway components (BAR-1/β-catenin, GSK-3/GSK3, KIN-19/CKIα, PRY-1/Axin, POP-1/TCF), and the genetic model for their function in vulval epithelial division seems to mirror the canonical pathway mechanism although the system appears to be highly redundant (Olson et al. 1991; Gleason et al. 2006).

Although the axis of embryonic blastomere asymmetry may be established via non-canonical Wnt signaling, it is important to note that mutations in non-canonical pathway components do not induce severe defects in the vulval epithelium (Green et al. 2008). These results stand in contrast to *bar-1*/β-catenin mutations, which exhibit a highly penetrant defect (Eisenmann and Kim 2000). One possible explanation is suggested by the finding that EGL-20 regulates a SYS-1 asymmetry, as well as a BAR-1 asymmetry, in primary VPCs (Green et al.

2008). This result suggests that there maybe an asymmetry in the VPC

responsiveness to canonical Wnt signaling.

Section 2: Wnt Signaling in Neurons

Wnt signaling regulates multiple aspects of neuronal development.

Wnt signaling has multiple roles in neuronal development, including roles

in dendritic patterning (Rosso et al. 2005), axon guidance (Krylova et al. 2002;

Hilliard and Bargmann 2006; Maro et al. 2009), the localization of synapses

(Klassen and Shen 2007), and the assembly of pre-synaptic vesicle components

(Ahmad-Annuar et al. 2006). Here, we will focus strictly on the role of Wnt in

synapse formation, and discuss the various model systems used to study

synapse development. This discussion will start with vertebrates and then move

to invertebrate synapse development, highlighting parallels between these

systems along the way. We will finish with a discussion of the role of Wnt

signaling in synaptic development in *C. elegans*, the model system used in this

dissertation.

**Wnt plays a role in the classical model for synaptic specificity, Agrin/MuSK
signaling at the vertebrate neuromuscular junction.**

The classical model for the induction of neuromuscular junction (NMJ)

formation by an extracellular ligand is derived from studies with the secreted

protein Agrin (Kummer et al. 2006). Secreted by motor neurons as they enter the

neuromuscular junction target area, Agrin organizes smaller pre-clusters of

acetylcholine receptors (AChR) into larger domains, which are eventually localized immediately below the presynaptic membrane. Agrin functions through the receptor MuSK (Kummer et al. 2006). However, clever experiments to test this model suggest that Agrin is in fact dispensable for the initial clustering of AChRs but is required to maintain these pre-established AChR clusters at the site of innervation (Kummer et al. 2006). New information has revealed an early role for Wnt signaling in NMJ assembly.

Previous studies of the Agrin-MuSK signaling detected interaction with the Wnt pathway to establish AChR clustering at neuromuscular junctions. For example, one study showed that a component of the destruction complex, APC, binds to the β subunit of an acetylcholine receptor and is necessary to mediate clustering upon stimulation with Agrin (Wang et al. 2003). Mutations in Disheveled 1 (*Dvl1*) also display reduced AChR clustering in the mouse diaphragm (Henriquez et al. 2008).

Recently, lrp4, a low-density lipoprotein receptor with structural similarity to the Frizzled co-receptor, lrp5/6, has been shown to function as a co-receptor for MuSK (Kim et al. 2008). Mice with mutations in lrp4 phenocopy MuSK mutants with severe neuromuscular defects and die at birth (Kim et al. 2008). MuSK and lrp4 are expressed in post-synaptic muscle cells (Weatherbee et al. 2006). Cell-specific expression of lrp4 in muscle rescues Agrin-induced phosphorylation of MuSK, indicating that lrp4 is required for Agrin-induced phosphorylation of MuSK (Kim et al. 2008). The results of these experiments and others have lead to a model in which lrp4 functions in a complex with MuSK, is

necessary for the activation of MuSK by Agrin, and binds Agrin with MuSK (Kim et al. 2008). The critical domains for the binding and activation of MuSK are the transmembrane and extracellular domains of lrp4 (Kim et al. 2008).

Recently, work in zebrafish has provided direct evidence that the Agrin/MuSK signaling pathway and the Wnt pathway interact to coordinate neuromuscular junction development. *Unplugged*, the MuSK homolog in zebrafish, directly binds Wnt11, *in vitro*, through the interaction of the *unplugged*/MuSK CRD domain, the Wnt binding domain shared among other ROR and Frizzled receptors (Jing et al. 2009). Wnt11 is also required for pre-patterning the AChR clusters before innervation, which involves MuSK, but happens before Agrin expressing neurons innervate the muscle, suggesting Agrin is not required (Jing et al. 2009). Furthermore, Wnt11 and MuSK seem to function via a disheveled-dependant mechanism, and therefore the AChR pre-patterning may occur via a non-canonical mechanism (Jing et al. 2009). These studies provide strong support for a model in which Wnt signaling fulfills a synergistic role with Agrin/MuSK to regulate synaptogenesis.

Studies in the mouse neuromuscular junction, specifically the innervation of the diaphragm, suggest a similar mechanism. Recent work in this system has also suggested that Wnt signaling patterns AChR clusters (Henriquez et al. 2008). Analysis of the Dvl1 mutant mouse reveals significant differences in the gross structure of diaphragm neuromuscular junctions with an increase in the overall width of the area that is innervated, a similar phenotype observed in *unplugged* mutants (Henriquez et al. 2008).

In the developing chick neuromuscular junction, a beautiful set of cell implantation studies shows that over-expressing Wnt3 increases acetylcholine receptor clustering, suggesting Wnt3 can induce AChR clustering. On the other hand, treatment of the NMJ with exogenous secreted Frizzled-related proteins (sFRPs), which bind and sequester extracellular Wnt3 decreasing the amount of Wnt3 available at the NMJ, results in a significant decrease in the number of AChR clusters. Thus, by manipulating the amount of extracellular Wnt3 available to the developming NMJ, it is possible to change the density of AChR clusters. Wnt3 was also shown to cooperate with Agrin to increase the total number of AChR clusters in cultured myotubes. Through this mechanism, Wnt appears to increase the number of microclusters prior to Agrin-mediated aggregation of these clusters, presumably through Rac1 (Henriquez et al. 2008).

Antagonistic Wnt pathways function at the vertebrate NMJ.

There is also evidence that antagonistic Wnt pathways regulate parallel mechanisms to regulate AChR cluster formation. One study, involving Wnt3, suggests that a non-canonical mechanism functions to increase AChR clusters at the NMJ (Henriquez et al. 2008). The authors propose that Rac1 is involved during Wnt3 mediated promotion of AChR clustering (Henriquez et al. 2008). This is suggestive of a non-canonical mechanism promoting AChR assembly, as Rac1 has been previously associated with a non-canonical Wnt signaling mechanism (Angers and Moon 2009). The authors also propose that Wnt3 and Agrin function through a non-canonical mechanism based on the pharmacologic

inhibition of GSK3 (Henriquez et al. 2008). These experiments show that inhibiting GSK3 does not *increase* the number of AChR clusters in the presence of Wnt3, which would be the anticipated result if a canonical pathway were involved, but in fact, antagonizes Wnt3 or Agrin mediated induction of AChR clustering. These results suggest that induction of AChR clustering by Wnt3 or Agrin functions through GSK3 *activation* (Henriquez et al. 2008). This result is especially interesting because GSK3 activation functions to silence canonical Wnt signaling. This result alludes to the potential involvement of an antagonistic canonical Wnt pathway that opposes AChR clustering.

Induction of AChR clustering by Wnt3 is antagonized by the related ligand Wnt3**a** (Wang et al. 2008). This effect is mediated by down regulation of the synaptic protein Rapsyn and appears to depend on a canonical mechanism. Activation of canonical Wnt signaling, using the non-specific GSK3 inhibitor, LiCl, causes a decrease in the amount of Rapsyn expressed, consistent with this hypothesis (Wang et al. 2008). Activation of β-catenin also decreased rapsyn mRNA. Curiously, this down regulation of Rapsyn appears to function without the terminal effector protein TCF, and thus, the Wnt3a pathway must regulate Rapsyn expression via a different, TCF-independent mechanism (Zhang et al. 2007; Wang et al. 2008). Thus, the two Wnt ligands, Wnt3 and Wnt3a have opposite effects on AChR clustering: Wnt3 functions by a non-canonical mechanism involving Rac1 and GSK3 *activation*, to increase the number of AChR clusters, whereas Wnt3a, functions through a TCF-independent canonical mechanism, and GSK3 inhibition to regulate Rapsyn levels and AChR cluster

density. This antagonistic relationship may function to fine-tune AChR clustering at the vertebrate NMJ.

Other roles for Wnt pathway components are known at the synapse. For example, β-catenin has been shown to interact with rapsyn at the NMJ, although the role of this relationship in synaptic assembly is unclear (Zhang et al. 2007). Curiously, although overexpression of activated β-catenin causes a decrease in AChR clustering, the effector of the pathway, TCF/LEF does not appear to be involved in this transcriptional mechanism. This result may be indicative of a β-catenin dependant pathway that does not involve TCF/LEF.

Wnt signaling regulates synapse formation in the vertebrate nervous system.

Studies of vertebrate neural development have revealed that Wnt signaling regulates many aspects of the assembly and specificity of synapses. During cerebellum development, Granule cells secrete Wnt7a to signal mossy fiber axon termini to remodel and differentiate into pre-synaptic structures (Hall et al. 2000). Mossy fiber neurons innervate granule cells with 'en passant' synapses, a basic geometry that also applies to most other synapses in the CNS. (*en passant* synapses are also observed between side-by-side neuronal processes in *C. elegans* (White et al. 1976b).) Wnt-7a mutant mice have less mature glomerular rosettes (pre-synaptic structures produced by a single mossy fiber neuron making synapses onto several granule cells) suggesting a decrease in synaptic complexity (Hall et al. 2000). Other studies show that *in vitro* addition of Wnt-7a induces the clustering of synapsin 1, thereby indicating that Wnt-7a

may stimulate presynaptic assembly (Hall et al. 2000). Consistent with these results, Dvl1 also localizes to presynaptic sites, and is important for pre-synaptic assembly. Double mutants of Wnt7a and Dvl1 genetically enhance each other, and decrease the accumulation of synapsin 1 at glomerular rosettes. This genetic interaction is suggestive of a functional redundancy between Wnt pathway components (Ahmad-Annuar et al. 2006).

A recent study of mouse hippocampal development has revealed a role for Wnt7a in activity-dependent enhancement of synaptic assembly (Gogolla et al. 2009). Exposure to an enriched environment is correlated with increased synaptic number and the complexity of synaptic markers in hippocampal CA3 neurons. The enriched environment also induced increased levels of Wnt7a (Gogolla et al. 2009). Synaptic activity is presumptively required for increased Wnt7a activity, because treatment with tetrodotoxin reduces Wnt7a immunoreactivity in hippocampal slice cultures. However, the mechanism that links neural activity to Wnt7a secretion is unknown. An attractive model for these effects suggests that Wnt7a plays an active role at the adult hippocampal synapse, to increase the complexity of synaptic structures in response to environmental stimuli. This model has direct implications for learning and memory since this effect can be reversed by treatment with sFRP-1, an extracellular Wnt antagonist, or by removal from the enriched environment (Gogolla et al. 2009).

Wnt signaling functions in *Drosophila* synaptic development.

A large number of studies of Wnt signaling at the neuromuscular junction have been performed in *Drosophila melanogaster*. The first mutants of Wnt pathway components were identified by their distinctive phenotypes: Wingless (Wg), Disheveled (Dsh), Frizzled, Shaggy(Sgg)/GSK3, and Armadillo (Arm). Since these initial discoveries, roles for these components in Wingless signaling have been discovered in various neuronal processes including axon guidance, neuronal polarity, and synaptic development (Korkut and Budnik 2009).

The *Drosophila* larval NMJ is readily visualized and the pattern of neuronal connectivity is stereotypic. A central role for Wnt signaling in NMJ development is suggested by the finding that Wg mutations alter NMJ morphology and glutamate receptor distribution (Packard et al. 2002). These mutations also disrupt pre-synaptic bouton morphology and a key structural component of the post-synaptic zone, the subsynaptic reticulum, is missing or severely disrupted.

Wg is believed to have both pre-synaptic and post-synaptic functions at the Drosophila NMJ (Figure 1.5). This hypothesis is consistent with the finding that both Wg and Frizzled 2 (Dfz2), its receptor, are both localized to the neuromuscular junction, with Dfz2 positioned at both pre- synaptic and post-synaptic locations (Packard et al. 2002). Upon stimulation of the pre-synaptic neuron, Wg is secreted from the neuromuscular synapse, crosses the synaptic cleft and binds to Dfz2. Both Dfz2 and Wg are endocytosed by muscle
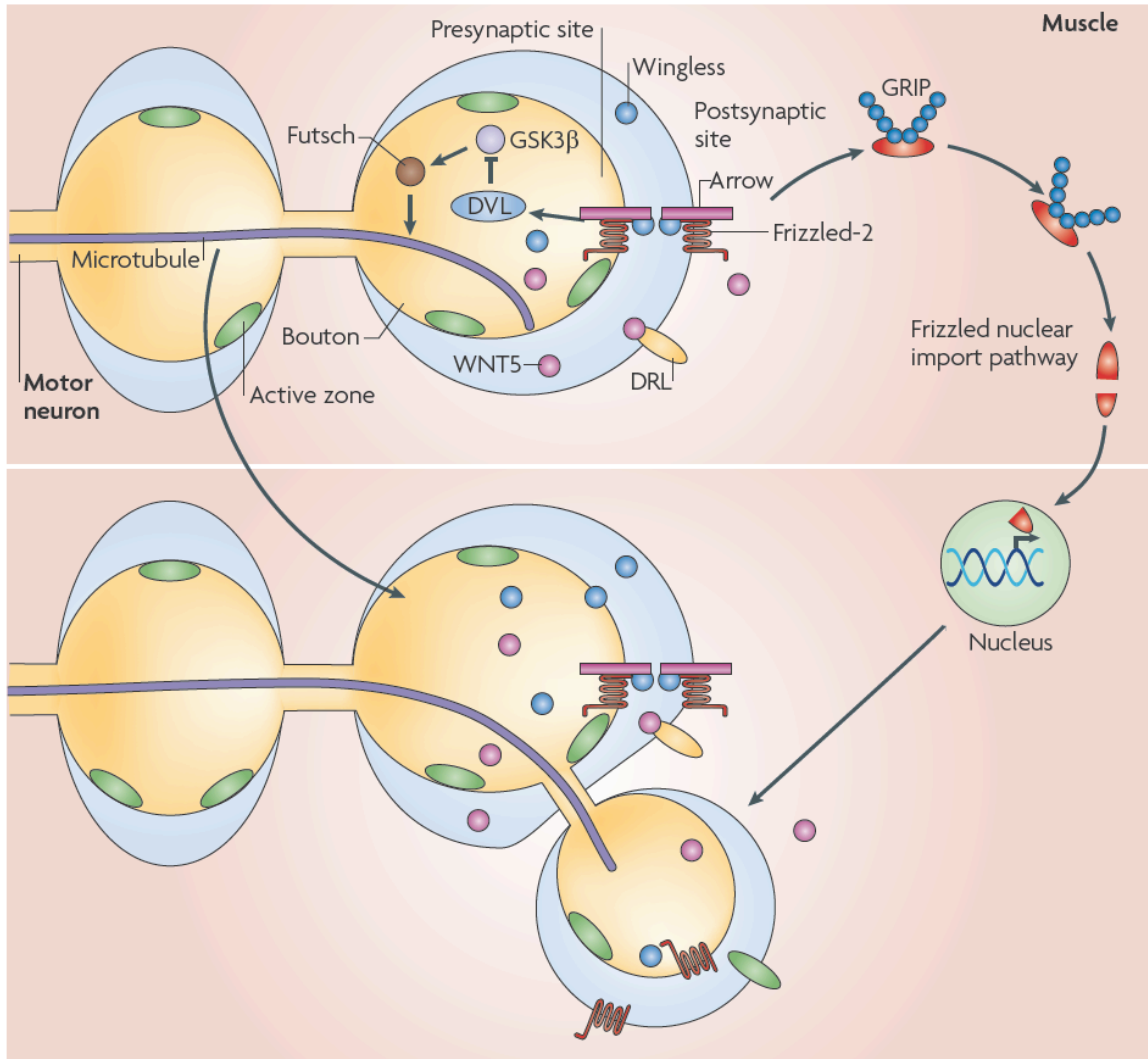
Figure 1.5. Wingless signaling at the *Drosophila* NMJ regulates synaptic development.

Pre-synaptic secretion of Wg activates responses in both the presynaptic neuron and the postsynaptic muscle. Frizzled and lrp5/6 respond to Wg on either side of the synapse. Post-synaptically, Frizzled is internalized by GRIP. Frizzled is then cleaved sending its C-terminus into the nucleus. Presynaptic response to Wg is to activate a non-canonical signaling pathway that ultimately leads to GSK3 phosphorylation of Futsch. This phosphorylation of Futsch ultimately leads to its association with microtubules.

Figure and legend taken from Figure 2 of (Korkut and Budnik 2009)

27

cells (Packard et al. 2002; Miech et al. 2008). Endocytosis of Dfz2 leads to a cleavage of the receptor C terminus, and both halves of Dfz2 are translocated to the nucleus. Antibodies to the N and C terminus of the protein have revealed different sub-cellular localizations for either half of the protein. At the synapse, the two Dfz2 antibodies co-localize at the membrane, but inside the cytoplasm the N-terminal antibody shows a peri-nuclear staining pattern, whereas the C terminal antibody localizes to distinct, punctate cytosolic and nuclear structures. Intranuclear staining of the Dfz2 C-terminus did not mark transcriptionally inactive heterochromatin, thus suggesting an active transcriptional role for the C-terminal fragment (although this remains to be confirmed). The protease that cleaves Dfz2 is unknown but a likely candidate is suggested by the presence of an ADAM protease consensus sequence at the cleavage site in the C-terminus of Dfz2. This Dfz2 internalization mechanism is Wg responsive and is blocked by mutants in the endocytosis pathway (*Shibire*). The cleavage of Dfz2 is also required for activation of the pathway. Furthermore, the fact that both N and C termini of Dfz2 are required for rescue of the Dfz2 mutant phenotype suggests that this mechanism may be critical for proper synaptic development of the Drosophila NMJ (Mathew et al. 2005).

More recent work has shown that dGRIP, a 7-PDZ domain-containing protein, is important for trafficking of Dfz2 to the peri-nuclear membrane. In Wg, Dfz2, and dGRIP mutants, the occurrence of 'ghost boutons' was dramatically increased. These boutons are rounded structures filled with synaptic vesicles and synaptic vesicle associated proteins, such as synapsin and CSP, but lack a

functional active zone and other pre-synaptic structures. Post-synaptic proteins such as glutamate receptors, Scribble, Bazooka, Dfz2 and Spectrin are also missing, suggesting that post-synaptic structures have not been completely formed (Ataman et al. 2006). In one hypothesis, ghost boutons are proposed to correspond to immature pre-synaptic structures that have not fully differentiated. Recent evidence has shown that activity-dependant modifications in synaptic structure depend on bi-directional Wg signaling and formation of 'ghost boutons' requires Wg signaling in the pre-synaptic neuron. A non-canonical mechanism, via inhibition of GSK3/shaggy, appears to be required pre-synaptically. The postsynaptic response to secreted Wg functions through the frizzled nuclear importation pathway (FNI) (Ataman et al. 2008).

Wg protein is secreted pre-synapticaly via exosome-like vesicles. The transmembrane protein, Evenness interrupted/Wntless, Evi, is required for pre-synaptic secretion, as well as post-syaptic internalization of Wg. Evi and Wg are secreted via exosome-like vesicles, which are then internalized by the postsynaptic membrane and ultimately lead to Dfz2 internalization and cleavage. The exosome secretion mechanism is yet unknown, but points to an intriguing mechanism for trans-synaptic communication (Korkut et al. 2009).

Although the presence of Sgg, Dsh, Arrow/lrp5/6 and Wg at the Drosophila synapse is consistent with a classical canonical pathway, Armadillo/β-catenin (Arm) does not localize to the synaptic bouton. This thus suggests that a non-canonical Wnt pathway (non-β-catenin dependant) may be active at the synapse. Consistent with this model, Arrow/lrp5/6 mutants display a disrupted

synaptic bouton morphology that phenocopies Wg mutants (Miech et al. 2008).

Moreover, the microtubule-associated protein Futsch/MAP1b, which normally

localizes with microtubule loops and is critical for NMJ development, does not

associate with microtubules in Arrow mutants (Roos et al. 2000). However,

proper bouton morphology is not completely dependant upon Arrow expression

within the pre-synaptic neuron, as only a subset of boutons, in arrow mutants,

display a disrupted morphology (Miech et al. 2008). Pre-synaptic expression of

Arrow can rescue this defect, suggesting that Arrow does function pre-

synaptically, but is not required for postsynaptic morphology (Miech et al. 2008).

Other rescue experiments show that Disheveled and shaggy/GSK3 are

required pre-synapticaly for the formation of Futsch microtubule loops (Miech et

al. 2008). Furthermore, Shaggy/GSK3 phosphorylates Futsch at a conserved site

(Gögel et al. 2006). Overexpression experiments of an active Armadillo/β-

catenin, or dominant negative pangolin/TCF did not show a role for these

proteins in Futsch/microtubuole association. Thus, it is likely that shaggy,

disheveled, and arrow are operating via a local, non-canonical pathway to

regulate futsch loops and pre-synaptic differentiation (Miech et al. 2008) (Figure

1.5). Although, the authors suggest that their model depends upon a divergent

Wnt signaling pathway mediated by shaggy to control microtubule dynamics,

they also show that young bouton formation is dependant upon transcription and

translation (Ataman et al. 2008).

Synaptic location in *C. elegans* is controlled by local, extracellular cues.

Studies in *C. elegans* have also revealed important roles for extracellular cues in synaptogenesis. Three examples of this local regulation are known: First, UNC-6/Netrin is responsible for positioning synapses between the interneurons AIY and RIA (Colón-Ramos et al. 2007). Second, the immunoglobulin containing protein SYG-1 and SYG-2 function together to direct the localization of synapses between the HSN and VC motor neurons in the egg-laying circuit (Shen and Bargmann 2003). Third, Wnt signaling is critical for NMJ position and localization in the ventral cord motor neuron DA9 (Klassen and Shen 2007; Poon et al. 2008). Each of these examples is discussed below.

UNC-6/Netrin coordinates the position of a central synapse.

The AIY and RIA interneurons are components of a sensory circuit in *C. elegans*. AIY receives *en passant* inputs from specific sensory neurons and provides output to selected interneurons, including RIA. AIY inputs to RIA are strictly localized to the AIY ventral process (White et al. 1976b). Mutations in the UNC-6/netrin receptor *unc-40*/DCC result in the loss of active zone markers within this AIY region (Colón-Ramos et al. 2007). Surprisingly, these synaptic defects are not a consequence of disrupted axon guidance despite the key roles of UNC-6 and UNC-40 in growth cone guidance; AIY and RIA processes that contribute to the active zone, are not misplaced in *unc-6/unc-40* mutants. Thus, the authors concluded in this instance, that both UNC-6 and UNC-40 are acting directly at the synapse. The cephalic sheath cell envelops the AIY afferent
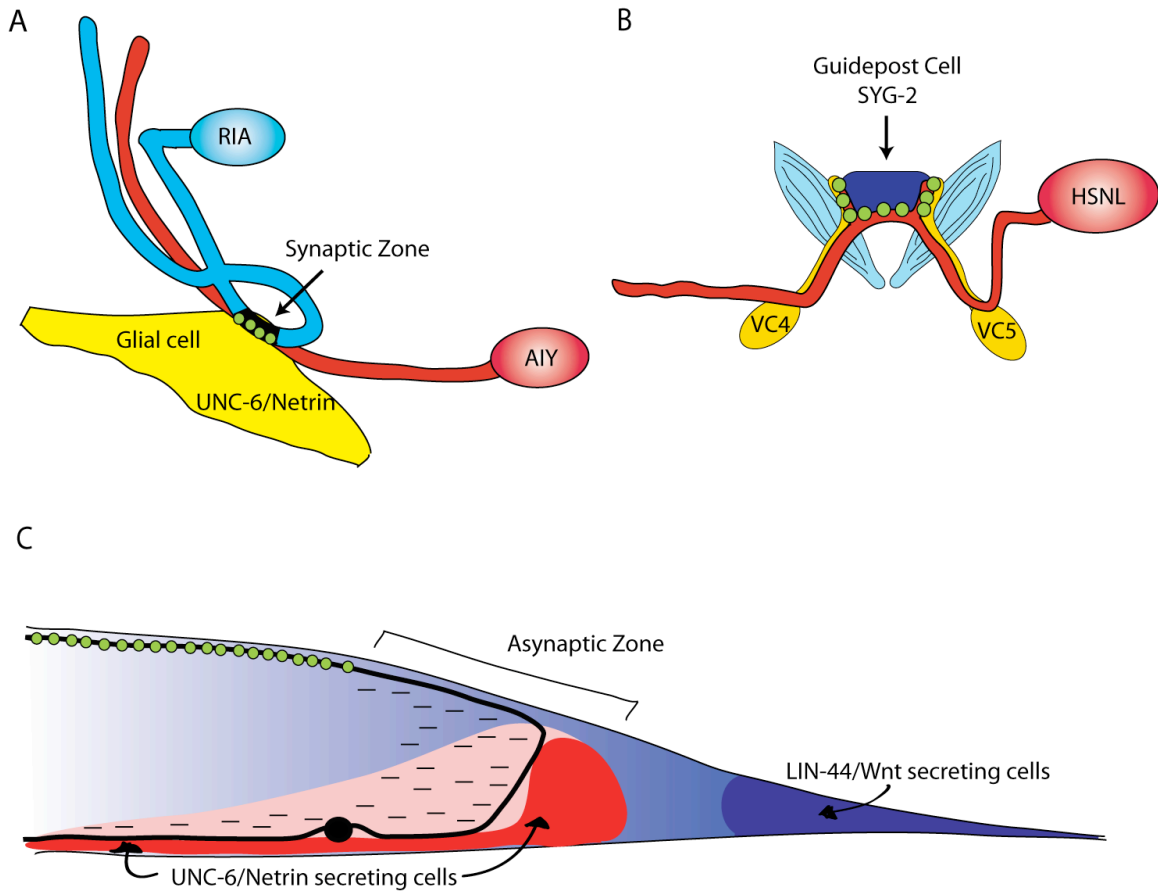
Figure 1.6. Transient interactions coordinate synaptic specificity.

Examples in *C. elegans* where local environmental signals are responsible for coordinating synaptic specificity. A. RIA to AIY synaptic location is controlled by an UNC-6/Netrin signal from a local glial cell. B. HSN to VC synapses are controlled SYG-2 expression on the guidepost cell. C. UNC-6/Netrin and LIN-44/Wnt are critical for establishing an asynaptic domain in the DA9 process.

process and appears to function as a glial cell. This sheath cell also expresses UNC-6/Netrin and its proximal location, adjacent to the AIY to RIA synapse, is critical for the correct localization of this synaptic connection. Thus, the location of the synapse is specified by an UNC-6/Netrin signal, secreted from a local glial cell process, which signals through the UNC-40 receptor in AIY to establish the physical location of the presynaptic apparatus (Colón-Ramos et al. 2007). Important questions for future studies include the signal transduction pathway that links UNC-40 to presynaptic assembly and the identification of additional signals that induce post-synaptic assembly in RIA.

Transmembrane proteins SYG-1 and SYG-2 determine synaptic location.

A more detailed mechanism for extracellular regulation of synaptic connectivity has been established for the hermaphrodite specific neuron, HSN. The HSN synapses with VC motor neurons near the vulval epithelium. The creation of the HSN presynaptic zone in this location depends on the provision of a membrane bound cue, the Ig domain protein SYG-2, on the surface of a nearby vulval epithelial cell (Shen and Bargmann 2003). Interaction of SYG-2 with a second related type of Ig domain protein, SYG-1, on the HSN neuron triggers presynaptic assembly (Shen et al. 2004) (Figure 1.7). This model is supported by a series of elegant experiments in by Kang Shen's group. The HSN to VC connections are stereotypic and are located on either side of the vulva opening where these two neurons initially contact one another. Mutations in SYG-1 result
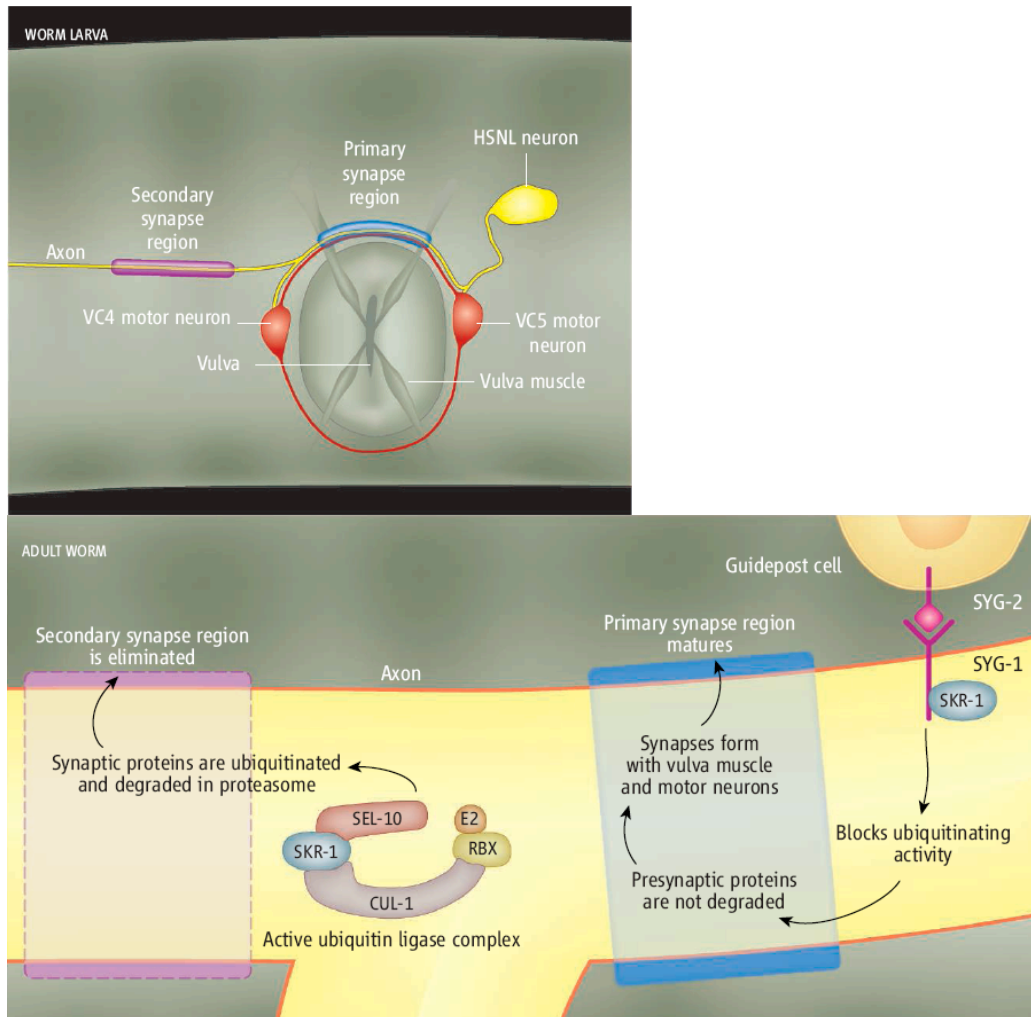
Figure 1.7. VC to HSN synaptic location is specified by non-autonomous signals

Signals from the vulval epithelium are critical for establishing the location of HSN to VC synapses. Top. Anatomy of neuromuscular architecture in the *C. elegans* vulva. The HSN neuron makes synaptic connections onto the VC motor neuron and muscle in the primary synapse region. Mutations in *syg-1* and *syg-2*, cause these synapses to relocate to the secondary synapse region. Bottom. SYG-2 is expressed in a non-neural, guidepost cell that interacts with receptors expressed within HSN. This cell-cell contact causes SKR-1 to interact with SYG-1 and blocks formation of the SEL-10, SKR-1, CUL-1 E3 ubiquitin ligase complex in that local environment. The E3 ligase complex is active in the secondary synapse region and degrades synaptic proteins in that location. In the absense of *syg-1/2*, the E3 ligase complex is assembled and degrades the primary synaptic region.

Figure taken from (Miller 2007).

34

in the displacement of the presynaptic marker, RAB-3, to a distal, anterior location in the HSN process after its entry into the ventral nerve cord. A cell autonomous role for SYG-1 in the HSN neuron is supported by transgenic rescue with an HSN-specific promoter (Shen and Bargmann 2003). Additional genetic studies revealed a that SYG-2 expression in a vulval epithelial "guidepost" cell is required for the normal location of SYG-1 and the HSN synapse (Shen et al. 2004). The interaction of the SYG-2 extracellular domain with SYG-1 on the HSN cell surface triggers local accumulation of presynaptic components. This effect depends in part on the inhibition of proteolysis by SYG-1. The SYG-1 intracellular domain prevents local activation of an E3 ubiquitin ligase (the SCF complex) by sequestering one of the SCF components, SKR-1. Constitutive SCF activity in *syg-1* and *syg-2* mutants prevents local presynaptic assembly. In that case, presynaptic domains emerge at a distal secondary location. The mechanism that accounts for the differential stability of these secondary synapses is unclear but may be indirectly stimulated by SYG-1 inhibition of the proteolytic pathway at the primary synapse (Ding et al. 2007). Although these studies have uncovered an elegant intercellular signaling mechanism for defining the location of the presynaptic apparatus, and its dependency upon extracellular cues, mechanisms that regulate postsynaptic assembly at this connection are unknown.

Wnt signaling antagonizes the posterior localization of DA9 neuromuscular junctions.

Frizzled receptors also regulate the intracellular location of the presynaptic zone of a specific cholinergic motor neuron, DA9 (Klassen and Shen 2007). The DA9 cell soma is located at the posterior end of the ventral nerve cord and extends a single axon to the dorsal side of the animal to innervate dorsal body muscles (White et al. 1976b). In the wildtype, the DA9 NMJ is created in a stereotypical location. The Shen lab used a GFP-labeled presynaptic marker, GFP::RAB-3, to detect the posterior displacement of the DA9 synapses in a *lin-44*/Wnt mutant (Klassen and Shen 2007). A similar phenotype was also observed in a *lin-17*/Frz mutant. In both *lin-44* and *lin-17* mutants, the DA9 presynaptic zone occupies a more posterior compartment than in the wild type. The origin of this phenotype is informed by the known expression of LIN-44/Wnt in specific cells in the tail region, posterior to the DA9 synapse. Thus, the authors proposed that LIN-44/Wnt functions to prevent the posterior displacement of DA9 pre-synaptic assembly. The LIN-17/Frz protein is localized to this posterior asynaptic DA9 axonal compartment and therefore appears to function in this region to exclude pre-synaptic assembly. In fact, in this case, LIN-44/Wnt may provide key positional information; the location of LIN-17/Frz is perturbed by experiments that modify the position or strength of LIN-44/Wnt expression in the tail region. Genetic tests detected a role for *dsh-1*/Disheveled in this pathway, but surprisingly did not reveal necessary functions for any other known component of either canonical or non-canonical Wnt signaling in *C. elegans* (Klassen and Shen 2007).

Additional studies revealed the *surprising* finding that UNC-6/Netrin and its receptor UNC-5 also function to exclude pre-synaptic assembly from inappropriate DA9 compartments (Poon et al. 2008). In this case, a ventral source of UNC-6 acts locally to prevent localization of pre-synaptic components to the DA9 dendrite in the ventral nerve cord (Figure 7). Additional experiments suggest that LIN-44 and UNC-6 can function interchangeably to limit proximal pre-synaptic assembly (Poon et al. 2008). For example, ectopic expression of UNC-6 from posterior cells in the tail was sufficient to rescue the posterior synaptic mislocalization defects of *lin-44* and *lin-17* mutants. These results suggest that UNC-6 and LIN-44 may regulate a common intracellular pathway to limit pre-synaptic assembly. Thus, two morphogen gradients, Wnt and Netrin, are responsible for patterning the location of pre-synaptic components in a single neuron.

Although this work clearly established a role for UNC-6 in regulating assembly of pre-synaptic components, UNC-6 does not appear to be required for proper localization of gap junctions. A YFP-tagged innexin, UNC-9, is largely restricted to the ventral DA9 dendrite and appears as discrete puncta that likely correspond to gap junctions with the interneuron AVA (White et al., 1986). The localization of the YFP::UNC-9 puncta is not altered in *unc-6* mutants. This result suggests that *unc-6* is required for the polarized localization of a specific subset of motor neuron proteins but that other components such as UNC-9/innexin may depend on other signaling pathways for proper polarized trafficking in the developing neuron (Poon et al. 2008). Unfortunately, this work did not ask if the

LIN-44/Wnt – LIN-17/Frz pathway is required for the polarized localization of UNC-9 gap junctions and therefore did not explore the interesting possibility that Wnt signaling regulates gap junction assembly.

SECTION 3: THE ROLE OF GAP JUNCTIONS

In the following section, I will explore the role of gap junctions in neuronal connectivity. At the end, I will review the surprisingly sparse literature that connects Wnt signaling and gap junction assembly.

Gap junction proteins: convergent evolution.

Gap junctions provide direct connections between the cytoplasm of neighboring cells (Figure 1.8). In the nervous system, gap junctions regulate ion flow between coupled neurons and can thus propagate changes in electrical potential from one coupled neuron to the next. Gap junction proteins form hexameric, transmembrane rings which interdigitate at the surface of adjacent cells from the mature pore-like structure. Three major classes of gap junction proteins have been identified, connexins – found only in vertebrate species, innexins – found in invertebrates, and pannexins – found in both invertebrates and vertebrates (D'hondt et al. 2009). All three classes of gap junction proteins share a similar functional mechanism, but little sequence homology; a classical example of convergent evolution.
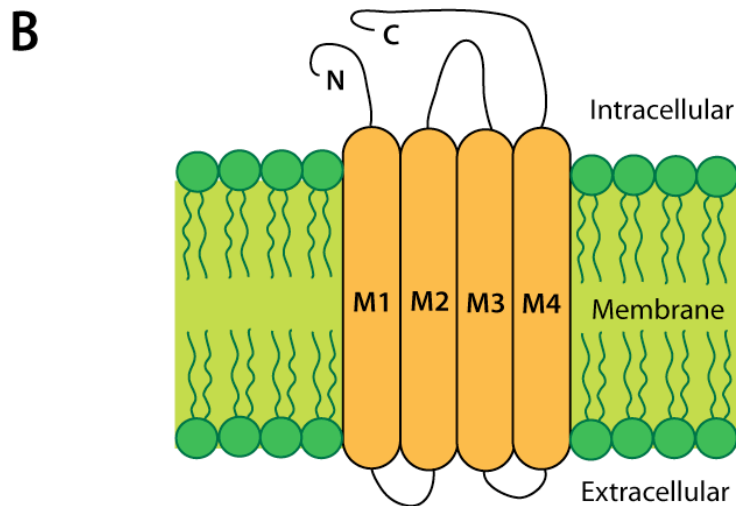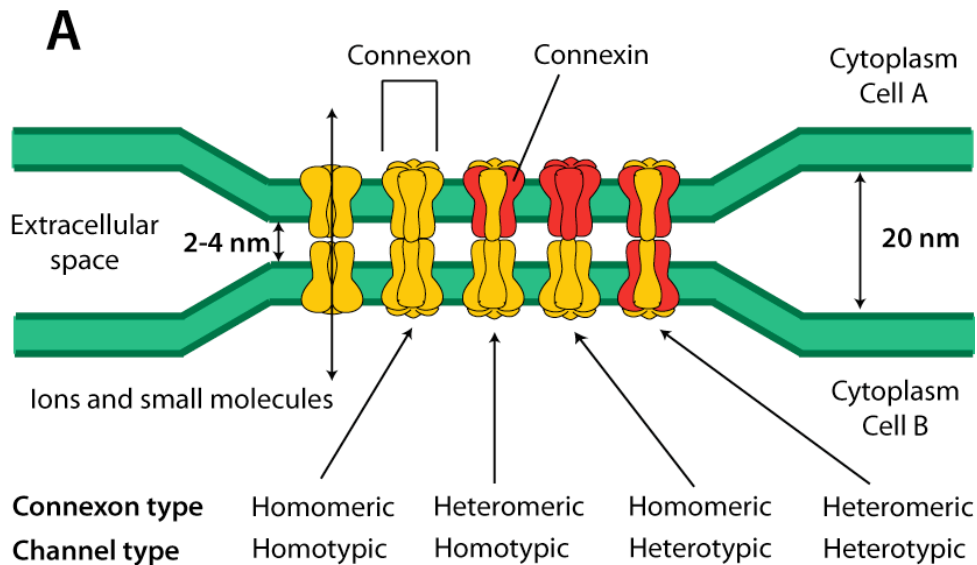
Figure 1.8. Structure of neuronal gap junctions

A. Graphic of a gap junction in a vertebrate system. Connexin proteins form hemichannels from 6 subunits. Homomeric hemichannels consist of the same protein. Hetermeric hemichannels consist of different subunits. A homotypic gap junction consists of a single protein subunit that makes up both hemichannels. Heterotypic gap junctions consist of two protein subunits that make a gap junction channel. In the *C. elegans* VNC, UNC-7 and UNC-9 make homomeric hemichannels and heterotypic gap junctions. B. Gap junction proteins have 4 transmembrane domains with 2 extracellular loops.

Most gap junctions are permeable to cations but their subunit composition may determine the specific cation transport properties of each channel (D'hondt et al. 2009). For example, gap junctions composed of Cx43 respond to a high extracellular $[Ca^{2+}]$ by closing, thus regulating the flow of Ca^{2+} into the cell, whereas gap junctions of Cx37 show a biphasic response, and close in response to both high and low concentrations of intracellular Ca^{2+}.

Furthermore, gap junctions can be composed of either a single subunit type (homomeric) or multiple subunit types (heteromeric) within a hemichannel (D'hondt et al. 2009). Also, two hemichannels of different compositions can form a complete gap junction (heterotypic) (Figure 1.8). These different combinations of subunits may contribute to different functional properties of the channel itself (D'hondt et al. 2009).

Gap junctions function as electrical synapses in the vertebrate brain.

Gap junction networks are hypothesized to regulate coordinated action within a group of interconnected neurons (Christie et al. 2005; Zufall 2005; Fukuda 2007). In the vertebrate CNS, gap junction connectivity has been extensively documented for cortical GABAergic interneurons but has been observed less frequently in other classes of brain neurons. For example, gap junctions between GABA interneurons and glutamatergic interneurons have been observed in EM studies of both the rat and cat neocortex, but are rare compared to GABAergic interconnections (Fukuda and Kosaka 2003; Fukuda et al. 2006; Fukuda 2007). Because GABAergic interneurons modulate the excitation

40

threshold and output of glutamatergic interneurons, gap junction synchrony among GABAergic interneurons is proposed to coordinate the output of glutamatergic interneurons. Physiological evidence is suggestive of subnetworks of GABAergic interneurons (Hestrin and Galarreta 2005) within the larger system, locally regulating specific populations of glutamatergic interneurons (Fukuda 2007). About half of the 20 known vertebrate connexin genes are expressed in the brain. Members of the related pannexin family of gap junction proteins are also expressed in the brain in specific subsets of neurons (Connors and Long 2004). These observations offer the attractive possibility that subsets of gap junctions are composed of selected classes of connexin or pannexin subunits. The functional importance of connexin to brain development and function is dramatically demonstrated in a knockout mouse that eliminates the connexin, CX36. Gap junction networks in the inferior olive (associated with the cerebellum) are eliminated in the CX36 mutant. Behavioral studies revealed significant impairment of learning and memory in these animals, although gross motor coordination appears to be unaffected (Van Der Giessen et al. 2008). Physiological measurements indicate that electrical synapses may be important for regulating rhythmic activity in spinal locomotory circuits after birth (Connors and Long 2004). These experiments suggest that gap junction connections are created between specific neurons for specific functions and have roles in the adult nevous system. Although much is understood about the function of these gap junctions, nothing is known about how this specificity is achieved.

Gap Junctions in the *C. elegans* nervous system.

Gap junctions are important for normal physiological processes in *C.elegans*. For example, the gap junction INX-16 is responsible for propagating a calcium wave along the *C. elegans* intestine that is critical for moving lumen contents in concert with the defecation cycle (Peters et al. 2007). Gap junctions comprised of the innexins, INX-6 or EAT-5, coordinate pharyngeal pumping by electrically coupling pharyngeal muscle cells (Starich et al. 1996; Li et al. 2003). Gap junctions also provide important developmental roles. For example, gap junctions comprised of the innexin NSY-5 are required for the establishment of a specific left-right asymmetry between a pair of chemosensory neurons (Chuang et al. 2007). Two AWC neurons, AWCL and AWCR, arise from similar cell lineages on the left and right sides, respectively, of the developing *C. elegans* embryo (Sulston et al. 1983). Despite the bilateral symmetry of this neuron pair, each AWC neuron senses different odorants. These alternative sensory modalities are randomly adopted with one fate on either the left or right side. The decision is regulated by a feedback loop involving a calcium-dependant kinase signaling cascade that prevents the opposite cell from adoping a default state (defined as the fate adopted when one of the cells is killed with a laser). Physical interaction between the two AWC cells is critical for making this distinction (Chuang et al. 2007). The decision also depends on the formation of transient networks of gap junctions comprised of the innexin, NSY-5, involving each AWC and adjacent embryonic neurons (Chuang et al. 2007).

Genetic analysis has confirmed a critical role for the innexin proteins UNC-7 and UNC-9 in motor circuit function (Starich et al. 1993; Barnes and Hekimi 1997). *unc-7* and *unc-9* mutants show similar jerky movements during forward locomotion (Starich et al. 1993; Starich et al. 1996; Barnes and Hekimi 1997; Starich et al. 2009b). In each case, the phenotype can be rescued by expression of the corresponding wildtype protein in the nervous system (Chen et al. 2007b; Starich et al. 2009b). UNC-7 and UNC-9 are components of prominent gap junctions between the interneuron AVB and B-class motor neurons, DB and VB, in the ventral nerve cord. These structures can be specifically labeled by transgenic expression of GFP-tagged UNC-7 and UNC-9 proteins. Mutation of either gene disrupts localization of the other innexin at this location. For example, the diffuse staining of UNC-7S::GFP expressed in AVB interneurons in an *unc-9* mutant is rescued by expression of UNC-9 in B-class motor neurons. These results are consistent with physiological experiments performed in *Xenopus* oocytes showing that UNC-7 and UNC-9 assemble to form homotypic hemichannels (i.e., hemichannels comprised of either UNC-7 or UNC-9 subunits) that can interact to produce functional heterotypic gap junctions (Starich et al. 2009b). This model is also supported by cell-specific microarray data from the Miller lab showing that the *unc-9* transcript is the only *C. elegans* innexin that is highly enriched in ventral cord motor neurons (Fox et al. 2005b) (D. Miller, personal communication).

EM reconstruction has revealed that UNC-7 containing gap junctions with AVB are consistently localized to the soma of B-class motor neuron partners

(White et al., 1986). This finding was confirmed by recent experiments showing that UNC-7::GFP expression in AVB results in discrete, GFP-stained puncta adjacent to the cell bodies of B-class motor neurons (counter-stained with the fluorescent DNA dye, DAPI) (Von Stetina et al. 2007b; Starich et al. 2009b). In contrast, gap junctions between the interneuron AVA and A-class motor neuron partners appear to be randomly located at different positions with respect to the motor neuron soma (White et al. 1976b). These results indicate that assembly of gap junction proteins is not only limited to specific neuron partners but may also be restricted to specific membrane domains. The mechanisms that regulate the intracellular trafficking and neuron specificity of gap junction protein assembly are unknown.

A recent report suggests that hemichannels formed by UNC-7 might be required for chemical synaptic assembly (Yeh et al. 2009). This model was initially suggested by the observation that localization of the SYD-2 (α-liprin) to GABAergic synapses with body muscle is disrupted in *unc-7* mutants (Yeh et al. 2009). A GFP fusion of UNC-10/Rim, also a marker of the active zone, was similarly disorganized but localization of the synaptic vesicle associate proteins synaptobrevin and synaptogyrin were normal. This finding suggested that the *unc-7* mutation disrupts active zone assembly but not localization of synaptic vesicles to the presynaptic region. An *unc-9* mutant produced similar results suggesting that UNC-7 and UNC-9 may function in a common pathway (Yeh et al. 2009). Mutants in *unc-7* also show resistance to aldicarb, a cholinesterase inhibitor, suggesting a defect in synaptic transmission (Yeh et al. 2009).

Immunostaining revealed that the UNC-7 protein localized to small, punctate

domains in a peri-synaptic region surrounding a central domain that

counterstains with active zone markers (i.e., UNC-49, SYD-2, UNC-10). EM

analysis did not detect classical gap junctions in these locations leading these

authors to propose that UNC-7 and UNC-9 are likely assembling into

hemichannels in the motor neurons. The mechanism whereby gap junction

hemichannel function might regulate synaptic assembly is unknown (Ai et al.

2000; Yeh et al. 2009).

Gap junction regulation by Wnt signaling?

Several experiments have suggested that gap junction connectons may

be regulated by the Wnt signaling pathway. Injection of Wnt-1 mRNA into the

developing Xenopus embryo increases gap junctional communication between

ventral cells; brighter staining for gap junction proteins was correlated with

enhanced intercellular transfer of Lucifer yellow (Olson and Moon 1992). Xwnt-8,

a canonical Wnt, also had a similar function, but injection with Xwnt-5A, a non-

canonical Wnt, did not. The authors speculate that gap junction communication

may be a target of Wnt signaling but the mechanism of this effect is unknown

(Olson et al. 1991). Additional studies in vertebrate systems have linked Wnt

signaling with the expression of connexin proteins (van der Heyden et al. 1998;

Ai et al. 2000; Robinson et al. 2006; Du et al. 2008). Most studies linking Wnt

signaling to connexin expression were conducted *in vitro* with cultured vertebrate

cells. For example, studies in PC12 cells, skeletal myoblasts and MC3T3-E1

cells, showed upregulation of connexin 43 mRNA and protein with application of exogenous Wnt ligands or treatment with lithium chloride to activate the Wnt pathway (van der Heyden et al. 1998; Du et al. 2008). Treatment of cardiomyocytes with exogenous Wnt increased a co-localization of β-catenin and connexin 43 (Ai et al. 2000). This result is especially suggestive of a relationship between Wnt signaling and gap junction formation as β-catenin was originally characterized as a component of tight junctions. It is possible that gap junction proteins and therefore gap junction assembly may be controlled by the canonical Wnt signaling pathway.

This link appears to be conserved in other model organisms. In *Drosophila*, foregut development is regulated by a combination of wingless and hedgehog signaling (Bauer et al. 2002). A mutation in the innexin2 gene, kropf, disrupted foregut development by preventing an outward buckling of the endoderm at a specific anatomical location in the midgut known as the "keyhole." Normally, cells surrounding the keyhole express Wingless. Gain-of-function experiments suggest the involvement of a canonical wingless signaling pathway as ectopic Armadillo/β-catenin expression causes an increase in the mRNA of innexin 2. Wingless expression also induces transcription of innexin 2 mRNA in cell culture (Bauer et al. 2002).

In *C. elegans*, Wnt signaling opposes the pruning of lateral processes between left and right AIM neurons that terminate in a gap junction connection (Hayashi et al. 2009). This contact between AIM neurons is normally established during early embryonic development but is eliminated during the first larval stage.

Local expression of the ligand CWN-2 is required to maintain this process.

Pruning is incomplete in the wildtype but is significantly enhanced by mutations

that disable specific Wnt signaling components. Of particular interest is the

finding that the Wnt receptor and Ror kinase homolog, CAM-1, is specifically

involved (Hayashi et al. 2009). Although it is not known if the gap junction

connection between AIML and AIMR is regulated directly by Wnt signaling, this

finding provides an intriguing example of a potential role for Wnt signaling in the

stability of electrical synaptic connections between specific neurons.

UNC-4 controls synaptic specificity in the *C. elegans* motor circuit.

In *C. elegans*, coordinated movement depends on specific connections in

the motor circuit involving both chemical synapses and gap junctions (Miller et al.

1992; White et al. 1992a; Starich et al. 2009a). To create this circuit, interneurons

from the head extend processes into the ventral nerve cord where they make

connections with specific motor neuron targets. In turn, motor neurons synapse

with body muscles (White et al. 1976b). Subnetworks within this circuit are

correlated with movement in either forward or backward directions. Forward

movement is controlled by inputs from interneurons AVB (gap junctions) and

PVC (chemical synapses) to VB and DB motor neurons (Figure 1.9). The

backward motor circuit consists of a separate set of interneurons AVA (gap

junction and chemical synapse), AVD (chemical synapse), and AVE (chemical

synapse) that synapse with VA and DA motor neurons (White et al. 1976b). The
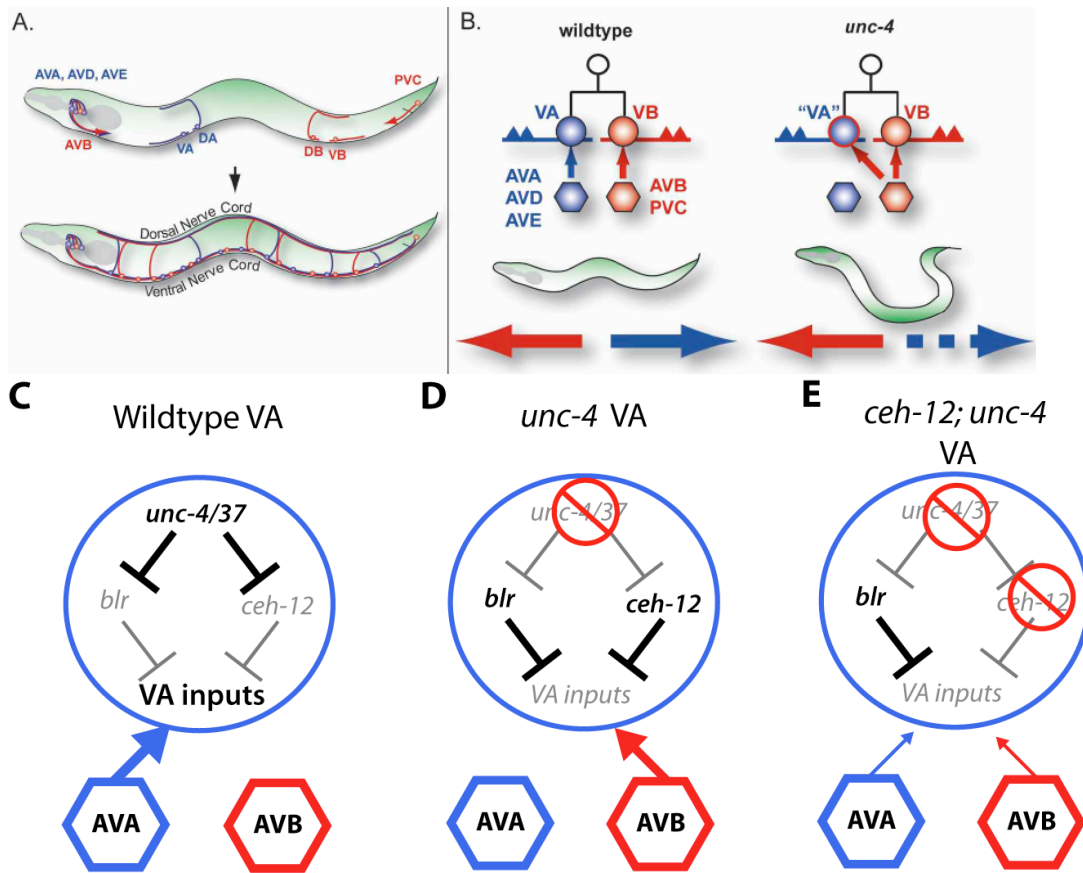
Figure 1.9. *unc-4* **controls multiple pathways to coordinate synaptic specificity**

A. Structure of the ventral nerve cord of C. elegans. The VNC contains two basic motor circuits: the interneurons (AVB, PVC) and motor neurons in red (DB, VB) mediate forward locomotion, whereas the neurons in blue mediate backward locomotion. B. The VA and VB motor neurons are lineal sister cells that divide and send processes into the opposite directions. They then receive inputs from different circuits and intercalate themselves into the existing nerve fascicle. C. UNC-4 functions to repress VB genes in VA motor neurons in wildtype animals. In *unc-4* mutants, parallel pathways, downstream of *unc-4* block normal AVA to VA inputs in favor of inputs from AVB. Mutations in the transcription factor, *ceh-12*, partially restores normal wiring. *blr* indicates genes that function in parallel to unc-4 that are discussed in Chapter 3.

A and B are taken from (Von Stetina et al. 2007b).

distinct locomotory functions of these circuits are consistent with laser ablation experiments and genetic results (Chalfie et al. 1985; White et al. 1992b).

Motor neurons within each circuit are comprised of two classes, A-class motor neurons (DA and VA) that mediate backward movement and B-class motor neurons that are required for forward locomotion. The members of each class share common features with A-class motor neurons having anteriorly directed axonal processes and inputs from AVA, AVD, and AVE and B-class motor neurons with posteriorly directed axons and connections from AVB and PVC. These motor neuron classes can be re-grouped according to developmental origin and other shared morphological features. DA and DB motor neurons are generated in the embryo and extend commissural processes to the dorsal nerve cord to synapse with dorsal body muscles whereas VA and VB motor neurons arise during the first larval stage and extend axons that are retained in the ventral cord. VA and VB motor neurons are also distinguished by their origins from a common progenitor cell; VAs arise from the anterior daughter of each neuroblast Pn.a cell and VBs are generated from the posterior daughter. Because these neurons arise after the embryonic ventral nerve cord is in place, VA and VB processes must intercalate themselves into the existing nerve fascicle (Sulston 1976; White et al. 1976a).

Mutations in the transcription factor *unc-4* disrupt backward locomotion (Brenner 1974). In *unc-4* mutants, the usual inputs to VAs from AVA, AVD and AVE are replaced with connections normally reserved for their VB sisters (i.e., gap junction with AVB and chemical synapse from PVC) (Miller et al. 1992; White

et al. 1992a). Although VAs adopt the VB pattern of synaptic inputs in *unc-4*

mutants, VA morphology and process placement in the ventral nerve cord are

normal and VAs retain their anteriorly directed axons (Miller and Niemeyer 1995)

(Figure 1.9). This finding suggests that *unc-4* is a "synaptic specificity" gene that

controls synaptic choice but not other morphological features such as axon

guidance that could indirectly alter connectivity. UNC-4 is expressed in VA and

DA motor neurons. Genetic and biochemical results showing that UNC-4 function

depends on interaction with the conserved transcriptional co-repressor protein

UNC-37/Groucho, are consistent with the hypothesis that UNC-4 preserves VA

inputs by repressing VB genes (Miller et al. 1993b; Pflugrad et al. 1997a; Winnier

et al. 1999). In this model, ectopic expression of VB-specific genes in *unc-4* or

unc-37 mutant VA motor neurons results in the imposition of VB type synaptic

inputs.

The Unc-4 miswiring defect was originally deduced from reconstruction of

EM serial sections of the ventral nerve cord (White et al. 1976a; White et al.

1992b). Recently developed tools now allow us to examine specific gap junctions

and synapses between neurons in this circuit in the light microscope (Von Stetina

et al. 2007a; Feinberg et al. 2008; Starich et al. 2009a). AVB to VB gap junctions

can be visualized by using a GFP fusion with the gap junction protein UNC-7,

expressed specifically in the AVB interneuron. AVB makes stereotypic gap

junctions on the motor neuron soma (DB and VB motor neurons in the wild type)

(White et al. 1992a) thereby allowing ready identification of motor neuron

partners from the proximity of UNC-7::GFP puncta adjacent to DAPI-stained

motor neuron nuclei (Von Stetina et al. 2007a; Starich et al. 2009a). Chemical

synapses between AVA and A-class motor neurons can also be observed in the

light microscope with a different type of GFP marker. This approach exploits

split-GFP technology in which one half of GFP is expressed at the synapse by

AVA, and the other half is provided to the synaptic region by VA motor neurons.

In each case, either the N or C-terminal split GFP domains are fused to the

extracellular domain of a synaptically localized membrane protein. With this

arrangement, discrete GFP puncta are observed at AVA to VA (and AVA to DA)

synapses in the ventral cord. The specificity of this assay for AVA to A-class

synapses has been verified in *unc-4* mutant animals, which display a loss of

GRASP ventral cord puncta (Feinberg et al. 2008).

The hypothesis that UNC-4 functions as a negative regulatory of VB

genes was confirmed by the discovery in the Miller lab that UNC-4 represses

expression of the VB-specific gene, CEH-12/HB9 (Von Stetina et al. 2007a). The

founding member of the family of homeodomain transcription factors, HB9, was

originally discovered to regulate motor neuron identity in birds but has since been

shown to exercise similar roles during both *Drosophila* and vertebrate motor

circuit development (Arber et al. 1999; Broihier and Skeath 2002). *ceh-12* was

discovered as an *unc-4* target gene by cell-specific microarray profiling

experiments which compared transcripts from wildtype and *unc-37* mutant VA

motor neurons. The resulting dataset provided a glimpse of a highly complex

regulated system, with 255 genes upregulated in *unc-37* mutant animals (Von

Stetina et al. 2007a).

In *unc-4* mutant animals, CEH-12/HB9 is selectively de-repressed in a subset of VA motor neurons in the posterior region of the ventral nerve cord. Genetic epistasis experiments showed that *ceh-12* expression in these posterior VAs is required for the miswiring phenotype in *unc-4* mutants (i.e., gap junctions with AVB) but is not necessary for miswiring anterior VAs as predicted by the pattern of ectopic *ceh-12* expression (Von Stetina et al. 2007a). These results strongly suggest that *unc-4* must also regulate additional target genes that function in parallel to *ceh-12* in anterior VAs.

The quest to identify determinants of synaptic choice.

Several questions remained when I began working on the *unc-4* project. Why is *ceh-12* derepressed only in posterior VA motor neurons? What genes function in parallel to *ceh-12*? How does UNC-4 coordinate gap junction and chemical synaptic specificity in the motor circuit?

The studies described in this dissertation were designed to address these questions. In chapter 2, I present a body of work linking two antagonistic Wnt signaling pathways to the specification of electrical connections in the motor circuit of *C. elegans*. Chapter 3 describes the results of a genetic screens that identified new loci that regulate the specificity of gap junction inputs to VAs in pathways the function in parallel to *ceh-12*. Chapter 4 features experiments that highlight the conserved nature of the canonical Wnt signaling pathway in *C. elegans* by showing that a small molecule inhibitor of casein kinase Iα (CKIα) in

mammalian cells is also targets CK1α-dependent Wnt signaling pathways that

operate during *C. elegans* development.

CHAPTER II

UNC-4 REGULATES SYNAPTIC CHOICE BY MODULATING ANTAGONISTIC WNT PATHWAYS IN THE *C. ELEGANS* MOTOR CIRCUIT

INTRODUCTION

Gap junctions contribute to neuronal signaling by providing a direct electrical link between neurons. Comprised of two interlocking hemichannels in adjacent cell membranes, gap junctions allow the ready movement of ionic currents between the linked cells. This role can be important for the proper function of neuronal circuits. For example, gap junctions formed by connexin 36 in the vertebrate olfactory bulb effectively coordinate spike synchrony within signaling glomeruli (Christie et al. 2005). In this capacity, electrical synapses are thought to function as low pass filters allowing electrical current to pass between two different neurons to alter their polarized electrical potential and firing frequency (Christie et al. 2005). Gap junctions play a role in human health. During an ischemic stroke, the deregulation of gap junction gating has been implicated as a precipitating factor in neuronal death (Thompson et al. 2006).

The gap junction proteins in vertebrates (connexins) and invertebrates (innexins) appear to be evolutionarily distinct, although a conserved class of gap proteins (pannexins) has been recently discovered (Chen et al. 2007b). Despite this apparent disparity, connexin and innexin proteins share many similar characteristics (i.e., formation of hemichannels, a conserved proline residue in

the second transmembrane domain, and a hypothesized ball-and-chain gating mechanism) and therefore represent a clear example of convergent evolution (Bauer et al. 2005; Chen et al. 2007b).

Here, we describe evidence that Wnt signaling pathways control the specificity of both gap junction and chemical synaptic inputs in the *C. elegans* motor circuit. We show that the normal function of *unc-4* is to antagonize a Wnt pathway that otherwise imposes VB-type inputs onto VA motor neurons. In the absence of *unc-4* function, the frizzled receptors MOM-5 and MIG-1 respond to an available EGL-20/Wnt cue. The resultant activation of a canonical Wnt signaling pathway induces expression of the homeodomain transcription factor CEH-12/HB9 in the affected VAs. Ectopic CEH-12/HB9 expression then results in VB-like inputs. A surprising additional finding of this work is that a separate non-canonical Wnt signaling pathway, involving LIN-44/Wnt and the frizzled receptor, LIN-17, opposes the formation of VB-type inputs. Thus, our work has identified a complex regulatory mechanism in which exogenous Wnt cues function in concert with cell autonomous transcription factors to regulate the specificity of electrical and chemical synaptic connectivity in motor circuit development.

The experiments described in this chapter were conducted in collaboration with Rachel Skelton, who performed all of the *ceh-12::GFP* experiments and the experiment with the *pry-1*/Axin mutant. We also collaborated on the construction of many double mutant strains and she assisted with the verification of specific genotypes. This work would not have been possible without her contributions.

MATERIALS AND METHODS

Strains and nematode culture.

C. elegans strains were cultured at 20°C, unless otherwise stated, on NGM media agarose plates inoculated with the *E. coli* strain OP50[-1] (Brenner 1974). Mutants were obtained from the Caenorhabditis Genetics Center (CGC) [*egl-20(n585), lin-44(n1792), mig-1(e1787), lin-17(n671), mom-5(or57) dpy-5(e61)/HT2, pry-1(mu38), cfz-2(ok1201), dsh-1(ok1445)*], and by the generous donation from other labs, *mom-5(ne12) mig-1(e1781)/HT2 – Gian Garriga Lab, lin-18(e620) – Bob Horvitz*]. Specific mutants used in this study were: *unc-4(e2322ts, e2323, e120), unc-37(e262), ceh-12(gk391),* **Wnt:** *egl-20(n585), lin-44(n1792)* **Frizzled:** *mig-1(e1787), lin-17(n671), mom-5(or57) dpy-5(e61)/HT2, mom-5(ne12) mig-1(e1781)/HT2, cfz-2(ok1201),* **Ryk:** *lin-18(e620),* **Axin:** *pry-1(mu38),* **Disheveled:** *dsh-1(ok1445)*.

Molecular Biology.

wdEx611 [pmom-5::GFP, dpy-20(+)]

3kb of the *mom-5* 5' promoter was obtained by PCR from genomic DNA and cloned into the TOPO-XL vector. *mom-5* promoter was then subcloned into the pPD95.75 (a gift from Andy Fire) vector using the restriction enzymes SalI and XmaI and verified by sequencing. The resultant plasmid pSV55 was microinjected (Fire et al. 1991) with pMH86 (dpy-20+) to produce the transgenic array. *wdEx611 [pmom-5::GFP, dpy-20(+)]*

wdEx636 [punc-4::ΔNT-BAR-1; dpy-20(+)]

The *unc-4* promoter was obtained by PCR from the plasmid pSV2 with the
primers *punc-4*_F2 (CCC GGA ACT GGG ATA TAA TTT C) and *punc-4*_REV
(ACC GTAT CAT TTT CAC TTT TTG). ΔNT-BAR-1 encodes a constitutively
active β-catenin that lacks C-terminal phosphorylation sites needed for
degradation by the destruction complex (Gleason et al. 2002b). The *ΔNT-BAR-1*
sequence was generated by PCR from pHCK19 (Gift of Rik Korswagen) with
primers 3'BAR-1_NT (GCA TGT AGG GAT GTT GAA GA) and the overlap
primer ΔNT-BAR-1_OVER (CAA AAA GTG AAA ATG ATC GGT ATG GCC
GAC TAT GAG CCG AT). *punc-4::ΔNT-BAR-1* was generated by overlap PCR
(Hobert 2002) and microinjected (Fire et al. 1991) with the plasmid pMH86 (dpy-
20+) to produce the transgenic array NC1847 *wdEx636[punc-4::ΔNT-BAR-1,
dpy-20+]*.

Genetics.

Integrated GFP reporters were used in genetic crosses to mark the
chromosome *in trans* to selected mutants: *euIs82a[unc-129::GFP; dpy-20+]* (I),
juIs76[unc-25::GFP; lin-15+] (II), *rhIs2[glr-1::GFP]* (III), *ayIs2[egl-15::GFP]* (IV),
mIs11[myo-2::GFP, pes-10::GFP, gut::GFP] (IV), *ccIs9753[myo-2::GFP]* (V),
oyIs44[odr-1::RFP] (V), *oxIs12[unc-47::GFP]* (X). The deletion allele of *ceh-
12(gk391)* was verified by PCR as previously described (Von Stetina et al.
2007b) (Primers: ceh-12_il (TAT TGC CAA GGA ACAAAG GC) ceh-12_ir (GCT
TGC CAT GCA TTT ACT GA). *egl-20(n585)* was verified by the Egl trait and by

sequencing with primers: *egl-20*_SNP_F (GGC AAT ATT CTC CTC CAT CT),

*egl-20*_SNP_R (AA TGA ACT ATG CTG GCT GCC). *mig-1(e1787)* was verified

by sequencing with primers (mig-1Ex7_SEQ_F CCT AGG CCA CCA ACT TCA

AA) and (mig-1Ex7_SEQ_R CG CA GAC TTC TCA ACT CTC A). *dsh-1(ok1445)*

is a 1132 bp deletion and was linked by recombination to *unc-4(e120)* and *unc-*

4(e2322ts) and confirmed by PCR using primers (GGA TCT CAT TGC ACC AGC

TG and GG CTC TTC TCT GCT ATT CCT). Other genotypes were verified with

visible phenotypic traits (e.g. abnormal vulva: *lin-17, lin-44*. Sterility: *mom-5, pry-*

1.)

Gene expression*.*

wdEx310 [ceh-12::GFP; unc-119(+)]

     ceh-12::GFP expression was visualized using the transgenic line NC802

wdEx310[ceh-12::GFP; unc-119+] (Von Stetina et al. 2007a). VA and VB motor

neurons were identified under DIC optics by location in the ventral nerve cord.

Each VA and VB neuron was scored for *ceh-12::GFP* expression (n > 20 for each

neuron, e.g. VA2 or VB3, etc.). The experimenter was blinded to genotype to

prevent bias. L2 stage worms were scored in Figure 2.1. L3 stage worms were

scored in Figures 2.2, 2.4, and 2.7. Animals were anesthetized with either 0.25%

tricaine/0.025% tetramasol or with 10mM levamisole on a thin 2% agarose pad

and viewed through a coverslip. Statistical significance (p values) were

calculated using Fisher's Exact Test.

Frizzled receptors

  lin-17::GFP expression was scored using the line KS411 *[lin-17(n671);*
unc-119(e2498) III; him-5(e1490) V; mhIs9[lin-17::LIN-17::GFP]] obtained from
the CGC (Wu and Herman 2007). *mom-5::GFP* was scored using the line
wdEx611 and *mig-1::GFP* was scored using the line *wdEx353* as previously
published (Fox et al. 2005a). Frizzled receptor expression was scored using a
similar methodology to *ceh-12::GFP* (Von Stetina et al. 2007a).

**Anti-GFP immunostaining to detect AVB gap junctions with ventral cord
motor neurons**.

  The chromosomal integrant NC1694 *wdIs54[punc-7*::UNC-7S:GFP, *col-*
19::GFP] unc-7(*e5*) X was generated by gamma irradiation (4000 Rads) EH578
(Starich et al. 2009b) and 10X backcrossed into the wildtype N2 strain. Standard
methods were used to cross *wdIs54* into other genetic backgrounds (Brenner
1974). Embryos were obtained by hypochlorite treatment and allowed to hatch
overnight in M9 buffer. The resultant growth-arrested L1 animals were applied to
bacterial feeding plates and gap junctions staining scored in the late L4 larval
stage. AVB gap junctions with ventral cord motor neurons were detected by anti-
GFP immunostaining as previously described (Von Stetina et al. 2007a). Motor
neuron soma with adjacent UNC-7S::GFP marked puncta (AVB gap junctions)
were scored in the region of the ventral nerve cord between VA2 and VA11 [e.g.
VA2-VA11, VB3-VB11, DA2-DA7, DB3-DB7, DD2-DD5, VD3-VD11, AS2-AS10,
and VC1-VC6]. At least 10 neurons at each position for each motor neuron class
were observed for a given genotype and assigned a score of gap junction

'present' or 'absent'. The experimenter was blinded to genotype to rule out bias. A Fisher's exact test was used to calculate p values (significance is suggested if $p < 0.05$) for the presence versus absence of UNC-7S::GFP puncta for each individual neuron compared between genotypes (e.g. VA2 of wildtype was compared to VA2 of *unc-4*).

Microscopy.

ceh-12::GFP-positive neurons were scored in a Zeiss Axioplan microscope equipped with a Hammamatsu Orca camera. UNC-7S::GFP puncta (AVB gap junctions) were visualized with a 100x objective lens. Confocal images were obtained in an Olympus FV-1000 Inverted confocal microscope with a 60x/1.45 Plan-Apochromat objective lens. DAPI excitation was performed using a Near-UV/Blue 405nm UV laser, and Cy3 excitation was performed with a 543nm HeNe laser. Pseudocolors and image overlays were generated using Olympus software and Adobe Photoshop.

Movement Assay.

A movement assay was used to detect potential effects of specific mutants on *unc-4*-dependent backward locomotion (Von Stetina et al. 2007b). The experimenter was blinded to genotype to avoid bias. For each genotype, ≥ 50 L4-young adult animals, grown at 23°C, were tapped a single time on the head with a platinum wire. Backward movement was scored as either **Unc** (coiled instantly with no net backward movement) or as **Non-Unc** (detectable backward

movement of posterior region or entire body in locomotory sinusoidal waves)

Statistical tests of differential effects on backward locomotion between

geneotypes were performed using the Fisher's Exact Test.

Lithium chloride treatment.

Lithium chloride was incorporated into NGM plates, resulting in the final

media concentration of 10mM LiCl. Media was prepared as normal, and mixed

with LiCl solution after autoclaving, immediately prior to pouring. Control plates

were prepared using an equivalent amount of water in place of LiCl solution.

Worms were synchronized by hypochloride treatment and incubated in M9 buffer

for 15 hours to the L1/L2 larval stage and then placed on LiCl plates and allowed

to grow over 3 days at 20°C. The tapping assay was performed as described.

Results are compilation of 3 experimental replicates.

Statistical Analysis.

Gap junction connectivity, suppression of *unc-4* tapping assay, and *ceh-*

12::GFP expression data was quantified using a binomial rubric (e.g. GFP was

scored as 'present' or 'absent 'in a given cell). In order to accurately calculate

statistical significance between samples, we employed the Fisher's Exact Test

for significance. The Fisher's Exact Test compares binomial categorical data and

is a powerful statistical test at low sample sizes (Motulsky 2010). It is similar to

the chi-squared test, which is more appropriate to evaluate significance between

two groups with large sample sizes. Due to the low n of our data (e.g. in our gap

junction assay approximately 10-15 individual VA2 neurons were scored within a particular genotype), this test was most appropriate to evaluate statistical significance.

Pie graphs of tapping assay data, histograms of *ceh-12::GFP* data, or line graphs of *UNC-7s::GFP* data reflect a percentage of total animals scored. To generate these histograms/pie graphs, data from individual experiments were compared to those previously performed. For example, tapping assays always included several positive and negative control strains such as N2, *unc-4(e120)* and *ceh-12(gk391); unc-4(e120)*. Once the tapping assays were complete, we compared the percentage of animals in each category for a given geneotype, (e.g. Unc versus Non-Unc) to previous results. If the tapping assay results were found to be similar to previous results for our control strains, the experimental data was included in our analysis. If these controls were found to be statistically different than previous results for these controls, the data was discarded and the blind tapping assay repeated. If these controls were conclusive, the data was combined with that from previous experiments.

RESULTS

EGL-20/Wnt signaling promotes *ceh-12* expression in posterior VA motor neurons.

ceh-12::GFP is exclusively detected in VB motor neurons in the wildtype

ventral nerve cord. In unc-4 mutant animals, *ceh-12::GFP* is also expressed in a

subset of posterior VA motor neurons. This ectopic *ceh-12::GFP* expression

obeys an apparent posterior to anterior gradient and is detected more frequently

in VA10 (posterior), than VA6 (mid-body) (Figure 2.1) (Von Stetina et al. 2007b).

We noted that the graded expression of *ceh-12::GFP* in posterior VAs mimics the

decreasing posterior to anterior gradient of the Wnt ligand, EGL-20 (Whangbo

and Kenyon 1999; Forrester et al. 2004; Coudreuse et al. 2006). We constructed

egl-20; unc-4 double mutants to test the idea that EGL-20/Wnt is required for

ceh-12::GFP expression in VAs. As shown in Figure 2.1, *ceh-12::GFP* in

posterior VAs is significantly reduced by the loss-of-function *egl-20(n585)*

mutation. This result indicates that VA expression of *ceh-12::GFP* in an *unc-4*

mutant likely depends on an EGL-20/Wnt signal. The role for EGL-20/Wnt

appears to be restricted to VA motor neurons, as *ceh-12::GFP* expression in VB

motor neurons is unaffected by the *egl-20*/Wnt mutation in both a *egl-20* and *unc-4; egl-20* background.

The Frizzled receptors MOM-5, MIG-1 and the Ryk homolog, LIN-18 are required for EGL-20/Wnt dependent expression of *ceh-12*.

The *C. elegans* genome encodes four Frizzled family Wnt receptors (*lin-17, mig-1, mom-5, cfz-2*) and one Ryk receptor (*lin-18*). To identify specific Wnt receptors that mediate the EGL-20/Wnt signal, we tested mutants in *mig-1*/Frizzled, *mom-5*/Frizzled and *lin-18*/Ryk for effects on *ceh-12::GFP* expression. We determined that mutation of *mom-5*/Frizzled reduces ectopic *ceh-12::GFP* expression in posterior VA motor neurons in *unc-4(e120)* (Figure 2.1). *mom-5* suppression is weaker than that seen in the *unc-4*; *egl-20* mutant, however, which suggested that additional Wnt receptors could be involved. This idea is supported by the finding that mutations in *mig-1*/Frz and in *lin-18*/Ryk also afford partial suppression of ectopic *ceh-12::GFP* in posterior VAs in *unc-4(e120)* (Figure 2.1) (Pan et al. 2006). Our findings are consistent with earlier studies that also detected overlapping roles for MOM-5/Frz and MIG-1/Frz in other Egl-20/Wnt-dependent signaling pathways (Pan et al. 2006).

We note that single mutations in *mig-1*/Frz, *mom-5*/Frz or *lin-18*/Frz do not disrupt normal VB expression of *ceh-12::GFP*. These results are in line with the finding above that EGL-20/Wnt signaling is not required for *ceh-12* expression in VB motor neurons in the wild type ventral nerve cord.

EGL-20/Wnt expression in the head induces *ceh-12::GFP* expression in anterior VA motor neurons.

Our results indicate that the endogenous posterior source of the Wnt ligand, EGL-20, functions as an instructive cue to drive miss-expression of *ceh-*
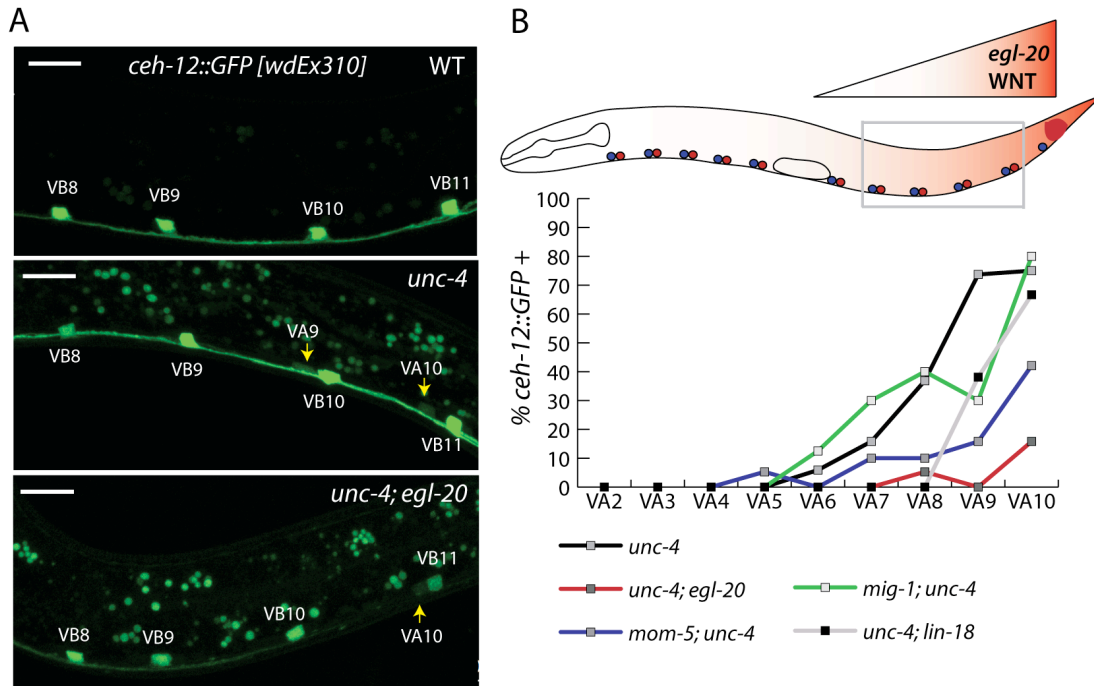
Figure 2.1. Wnt signaling is required for ectopic *ceh-12::GFP* in VA motor neurons.

A. *ceh-12::GFP* is restricted to VB motor neurons in the wildtype (WT) ventral nerve cord. In *unc-4* mutants, *ceh-12::GFP* is also detected in posterior VA motor neurons (see, VA8-VA10). B. Quantification confirms that *ceh-12::GFP* is expressed more frequently in posterior (VA6 - VA10) than anterior VA motor neurons (VA2-VA5). EGL-20/Wnt is secreted from specific cells in the tail region to produce a decreasing posterior to anterior gradient. Mutants of *egl-20*/Wnt, the frizzled receptors *mom-5, mig-1*, and the Ryk homolog *lin-18* suppress ectopic *ceh-12::GFP* in posterior VA motor neurons. Mutant alleles for these experiments were: *unc-4(e120), egl-20(n585), mom-5(or57), mig-1(e1787), lin-18(e620).*
* Indicates statistical significance (p < 0.05 Fisher's Exact Test)

12 in posterior VA motor neurons in an *unc-4* mutant (Figure 2.1). To determine if EGL-20/Wnt is also sufficient to promote *ceh-12::GFP* expression, we used a transgenic line in which EGL-20/Wnt is ectopically expressed in anterior cells (Pan et al. 2006). As shown in Figure 2.2, an anterior source of *egl-20*/Wnt enlarged the region of ectopic *ceh-12::GFP* expression to include anterior VA motor neurons in addition to the posterior VAs that normally express *ceh-12::GFP* in an *unc-4* mutant background (Figure 2.1). Ectopic *ceh-12::GFP* in anterior VAs was not observed in a WT background (data not shown) nor in an unc-4 mutant in the absence of the anterior source of egl-20/Wnt (Figure 2.1). These data confirm that loss of *unc-4* is necessary for activation of *ceh-12* expression by *egl-20*/Wnt and that *egl-20*/Wnt functions upstream of *ceh-12* (Figure 2.1). This result establishes that the *unc-4* mutation effectively sensitizes VA motor neurons throughout the length of the VNC to an available *egl-20*/Wnt cue.

To determine if the Frizzled receptor MIG-1, is required for induction of *ceh-12* by this novel anterior source of EGL-20/Wnt, we assayed a *mig-1; unc-4(0)* double mutant for *ceh-12::GFP* expression. As predicted by our model (Figure 2.3D), mutation of *mig-1*/Frz attenuated ectopic *ceh-12::GFP* expression in anterior as well as posterior VAs. We attribute residual *ceh-12::GFP* expression to the partially redundant function of *mom-5* and *lin-18* in this pathway (Figure 2.1).

EGL-20/Wnt signaling contributes to the Unc-4 movement defect.

The Miller Lab has previously shown that ectopic *ceh-12*/HB9 is partially responsible for the backward movement phenotype of *unc-4* mutants and has attributed this incomplete effect to selective de-repression of *ceh-12* in posterior but not anterior VA motor neurons (Von Stetina et al. 2007b). If *egl-20*/Wnt is required for ectopic *ceh-12* expression in posterior VAs, then this model predicts that loss-of-function mutations in *egl-20* should also partially suppress the Unc-4 backward movement defect. This phenotype can be detected in a "tapping assay" in which individual animals are touched on the head to stimulate backward locomotion. *unc-4* mutants are unable to crawl backward and instead curl dorsally ("Unc-4 phenotype"); Unc-4 suppression is readily detected as animals that can either sustain or at least initiate backward movement ("non-Unc") (see Methods). The missense mutant, *unc-4(e2323)*, was used to sensitize this assay because *ceh-12* mutations afford strong suppression of "weak" or hypomorphic *unc-4* alleles (Von Stetina et al. 2007b). As shown in Figure 2.3A, the *egl-20* mutation restores backward movement to *unc-4(e2323)* mutant animals. As expected, *egl-20* also partially suppresses the backward Unc defect of a hypomorphic mutant of the UNC-4 transcriptional cofactor, *unc-37*/Groucho (Figure 2.2A).

We employed an additional genetic test to confirm that *egl-20* and *ceh-12* function in a common pathway. For this experiment, we utilized the null allele, *unc-4(e120)* which is weakly suppressed by *ceh-12*. If *egl-20* is required for activation of a pathway functioning in parallel to *ceh-12*, then the *ceh-12; egl-20*
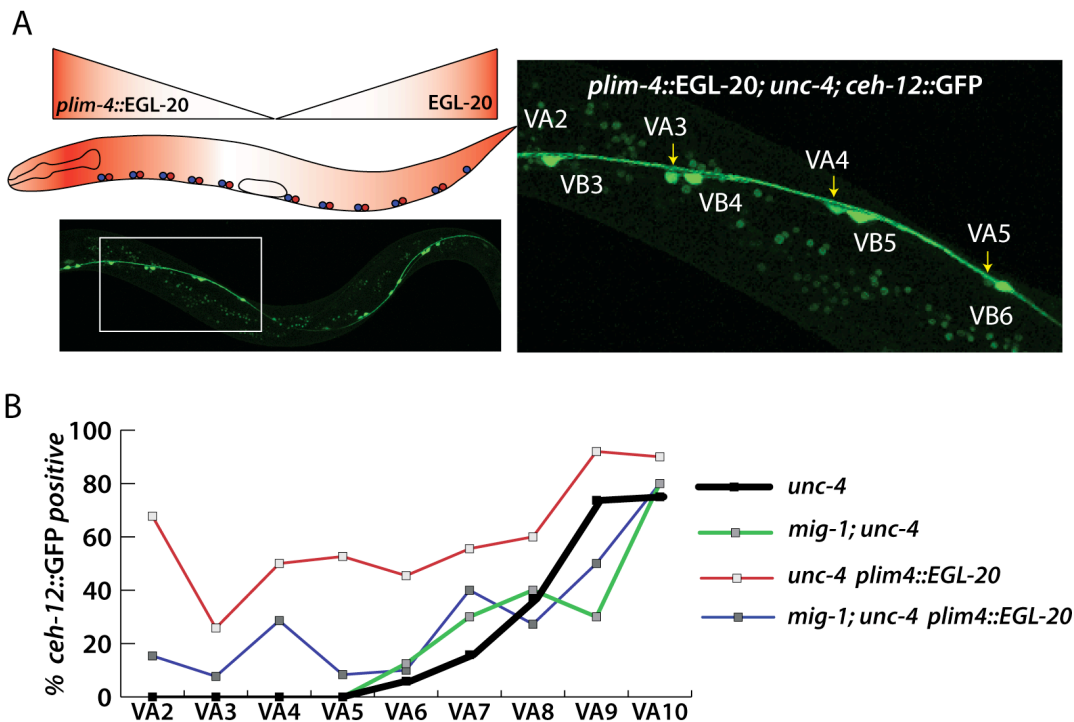
Figure 2.2. EGL-20 is sufficient to drive *ceh-12::GFP* expression in *unc-4* mutant VA motor neurons.

A. The *plim-4::*EGL-20 transgene is expressed in head neurons to produce a novel source of EGL-20/Wnt. The combined anterior and posterior EGL-20/Wnt signals induce expression of *ceh-12::GFP* in nearby *unc-4* mutant VA motor neurons. B. Inactivation of the MIG-1 frizzled receptor in a *mig-1* mutant reduces EGL-20-dependent expression of ceh-12::GFP in unc-4 mutant VA motor neurons. Mutant alleles for these experiments were: *unc-4(e120)* and *mig-1(e1787).*

double mutant should show stronger suppression of Unc-4 than either *egl-20* or *ceh-12* single mutants alone. However, this experiment shows that *egl-20* does not enhance *ceh-12* suppression of *unc-4(e120)* and therefore favors a linear model in which *egl-20*/Wnt and *ceh-12*/HB9 function in a common pathway (Figure 2.3B).

       To confirm the roles of other components of the *egl-20*/Wnt pathway in VA input specificity, we also tested alleles of *mig-1* and *mom-5* Frizzled receptors for suppression of the Unc-4 backward movement defect. For these experiments, we utilized a temperature sensitive mutant, *unc-4(e2322ts)*. In this case, this assay was sensitized by the use of an intermediate of 23°C at which *unc-4(ts)* animals can be strongly suppressed by mutations in either *egl-20* (Figure 2.3C) or *ceh-12* (Von Stetina et al. 2007b). Our results show that mutations in either *mig-1* or *mom-5* result in significant restoration of backward locomotion for *unc-4(ts)* (Figure 2.3C). *mom-5* RNAi also strongly suppresses Unc-4 movement (Figure 2.4B). These effects are consistent with the proposed overlapping roles of *mom-5*/Frz and *mig-1*/Frz in *unc-4* mutant VA motor neuron miswiring and consequent backward locomotory defects. Based on these results, we hypothesized that *mig-1* and *mom-5* frizzled receptors may function redundantly to promote VB-type inputs to VAs (Figure 2.2). Consistent with this hypothesis, *mig-1 mom-5* double mutants suppress the Unc-4 backward movement defect in null allele of *unc-4* (Figure 2.4A). A *cfz-2*/Frz mutant had no effect on the Unc-4 phenotype and is therefore unlikely to affect VA inputs (Figure 2.3C).

69
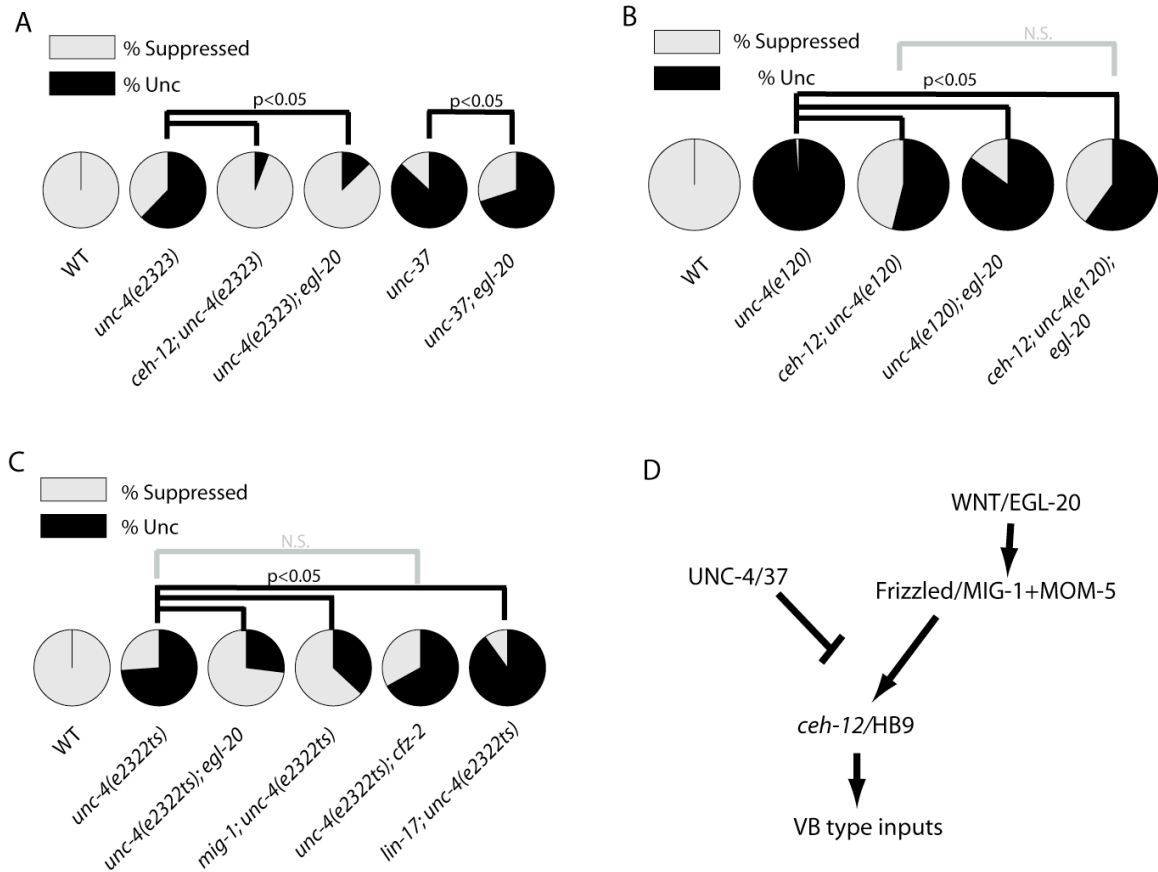
Figure 2.3. Mutants in Wnt pathway genes suppress the Unc-4 movement defect.

A. The hypomorphic mutation, *unc-4(e2323),* displays a partial Unc-4 phenotype (compare to *unc-4(e120)* in B). Mutations in *ceh-12* (transcription factor) and in *egl-20(n585)*/Wnt restore backward locomotion to *e2323* animals. The *egl-20* mutant also enhances backward locomotion for a mutation that disables the UNC-4 transcriptional co-factor protein, UNC-37 (Groucho) B. The backward locomotion defect for the null allele *unc-4(e120)* is weakly rescued by *ceh-12*/HB9 and *egl-20*/Wnt mutations; the *egl-20* mutant does not enhance *ceh-12* suppression of *unc-4(e120)*, a result consistent with model in which *egl-20*/Wnt functions upstream of *ceh-12*. C. Mutation of *mig-1(e1787)/Frz* suppresses the temperature sensitive allele, *unc-4(e2322ts)*, whereas the *cfz-2* mutation has no effect. *lin-17/Frz* enhances the Unc phenotype of *e2322ts*. D. Proposed Model: UNC-4/UNC-37 antagonize an Egl-20/Wnt signaling pathway that functions through the Frizzled receptors, MIG-1 and MOM-5 to activate *ceh-12* expression and impose VB type inputs onto VA motor neurons. p values were calculated using Fisher's exact test, n > 50 for all genotypes.
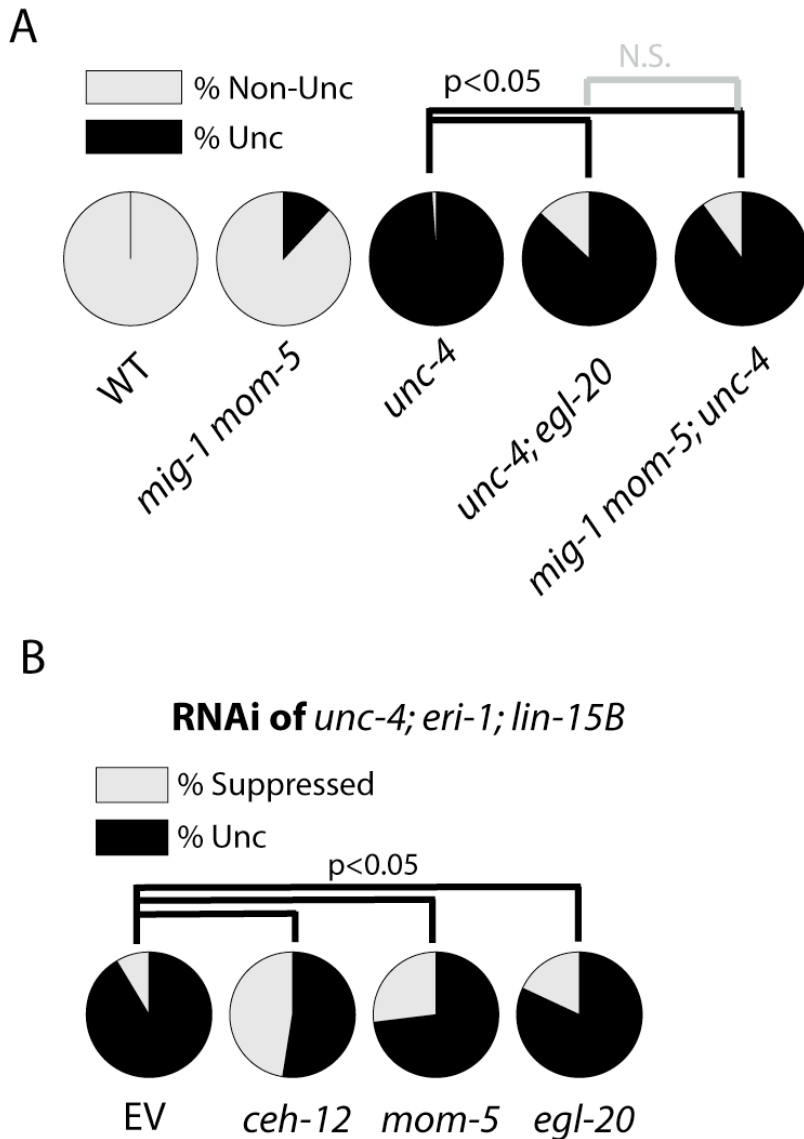
Figure 2.4. *mig-1* and *mom-5*/Frizzled suppress *unc-4*.

A. An *egl-20* mutant weakly suppresses the backward move
ment defect of an null allele unc-4(0). Comparable suppression of *unc-4(e120)*
was observed for a *mig-1, mom-5* double mutant. This result is consistent with a
model in which the Frizzled receptors MOM-5 and MIG-1 function downstream of
EGL-20/Wnt to promote miswiring of VA motor neurons in *unc-4* mutants. Mutant
alleles were *unc-4(e120), egl-20(n585), and mig-1(e1787) mom-5(ne12)*. B.
RNAi of *ceh-12, mom-5* and *mig-1* suppress the Unc-4 backward movement
defect in a non-temperature sensitive hypomorphic allele of *unc-4(e2323)*. p
values were calculated with Fisher's exact test.

LIN-44/Wnt and LIN-17/Frz oppose ectopic *ceh-12* expression in VA motor neurons.

In contrast to mutations in *mig-1*/Frz and *mom-5*/Frz, which suppress the Unc-4 backward movement defect, we discovered that a *lin-17*/Frz mutant appeared to enhance the Unc-4 phenotype (Figure 2.3C). This effect is particularly evident at the permissive temperature of 16°C at which *unc-4(ts)* animals display wildtype backward movement. Backward locomotion at 16°C is significantly impaired in the *lin-17; unc-4(ts)* double mutant in comparison to either *unc-4(ts)* or *lin-17*/Frz single mutants. In addition, *lin-17* alone shows a weak backward Unc defect (Figure 2.5A). One explanation for these results is that LIN-17/Frz normally functions to prevent ectopic expression of *ceh-12* in VA motor neurons. This model is consistent with experiments showing that over-expression of CEH-12 protein in VAs is sufficient to induce an Unc-4-like movement defect (Von Stetina et al. 2007b). To test this idea, we examined *ceh-12::GFP* expression in a *lin-17*; *unc-4(0)* double mutant. As shown in Figure 2.5B, the *lin-17* mutation expands the region of ectopic *ceh-12::GFP* to include anterior as well as posterior VAs. A mutation in *lin-44*/Wnt produces a similar effect of enhancing the Unc-4 phenotype to include ectopic *ceh-12::GFP* in anterior VAs. These results support the hypothesis that LIN-44/Wnt and LIN-17/Frizzled function to preserve wildtype VA inputs by blocking expression of *ceh-12*. We propose that the LIN-44/Wnt dependent signaling opposes the *egl-20*/Wnt pathway that promotes *ceh-12* expression and the consequent imposition of an alternative set of VB-type motor neuron input.

A *lin-17* enhances *unc-4(ts)* at permissive temperature

% Suppressed
% Unc

Fisher's Exact Test p<0.05

unc-4(e2322ts)   *lin-17*   *unc-4(e2322ts); lin-17*

B *lin-17* and *lin-44* antagonize ectopic *ceh-12::GFP*

% GFP positive VA motor neurons

unc-4
lin-17; unc-4
lin-44; unc-4

VA2 VA3 VA4 VA5 VA6 VA7 VA8 VA9 VA10

C

VA-type inputs   *Promotes VB-type inputs*

WNT/LIN-44   WNT/EGL-20

Frizzled/LIN-17   Frizzled/MIG-1+MOM-5

UNC-4/UNC-37

CEH-12/HB9

VA type inputs   VB type inputs

Figure 2.5. LIN-44/Wnt and LIN-17/Frz block *ceh-12* expression that imposes the Unc-4 movement defect.

A. A *lin-17(n671)* mutation enhances the backward movement defect of the temperature sensitive *unc-4(e2322ts)* allele at the permissive temperature of 16°C. B. *lin-44(n1792)* and *lin-17(n671)* mutations result in ectopic *ceh-12::GFP* expression in anterior VA motor neurons in an *unc-4(0)* mutant. This ectopic expression is in addition to the posterior VAs in which *ceh-12::GFP* is expressed in a *lin-17*(+) and *lin-44*(+) background. C. Proposed model: LIN-44/Wnt and LIN-17/Frz oppose *ceh-12* expression to preserve wildtype VA inputs.

Opposing Wnt signaling pathways regulate the specificity of interneuron gap junction with VA motor neurons.

Reconstruction of the *C. elegans* ventral nerve cord from serial electron micrographs (EM) established that the interneuron AVB makes gap junctions with DB and VB motor neurons (White et al. 1976a). These connections can be visualized in the light microscope with a GFP-tagged gap junction protein (innexin), UNC-7S::GFP, expressed in AVB. Localization of UNC-7S::GFP puncta adjacent to the motor neuron cell soma allows ready identification of AVB partner motor neurons in animals counter-stained with a DNA dye (DAPI) (Starich et al. 2009a). We have previously used UNC-7S::GFP to show that *ceh-12*/HB9 is required for the creation of AVB gap junctions with posterior but not anterior VAs (Von Stetina et al. 2007b). Therefore, if EGL-20/Wnt signaling is necessary for ectopic expression of *ceh-12*/HB9 in posterior VA motor neurons as our model suggests (Figure 2.5), then these aberrant AVB gap junctions with posterior VAs should be eliminated in *egl-20* mutants. As shown in Figure 2.6, the frequency of UNC-7S::GFP puncta associated with posterior VA motor neurons is substantially reduced in an *unc-4; egl-20* double mutant. A similar effect is noted for *mig-1; unc-4* in which ectopic AVB gap junctions with posterior VAs are reduced in comparison to the *unc-4* mutant alone (Figure 2.6C). These results are consistent with the proposal that EGL-20/Wnt and MIG-1/Frz function together to promote *ceh-12*/HB9 expression leading to the creation of gap junctions between AVB and VA motor neurons.
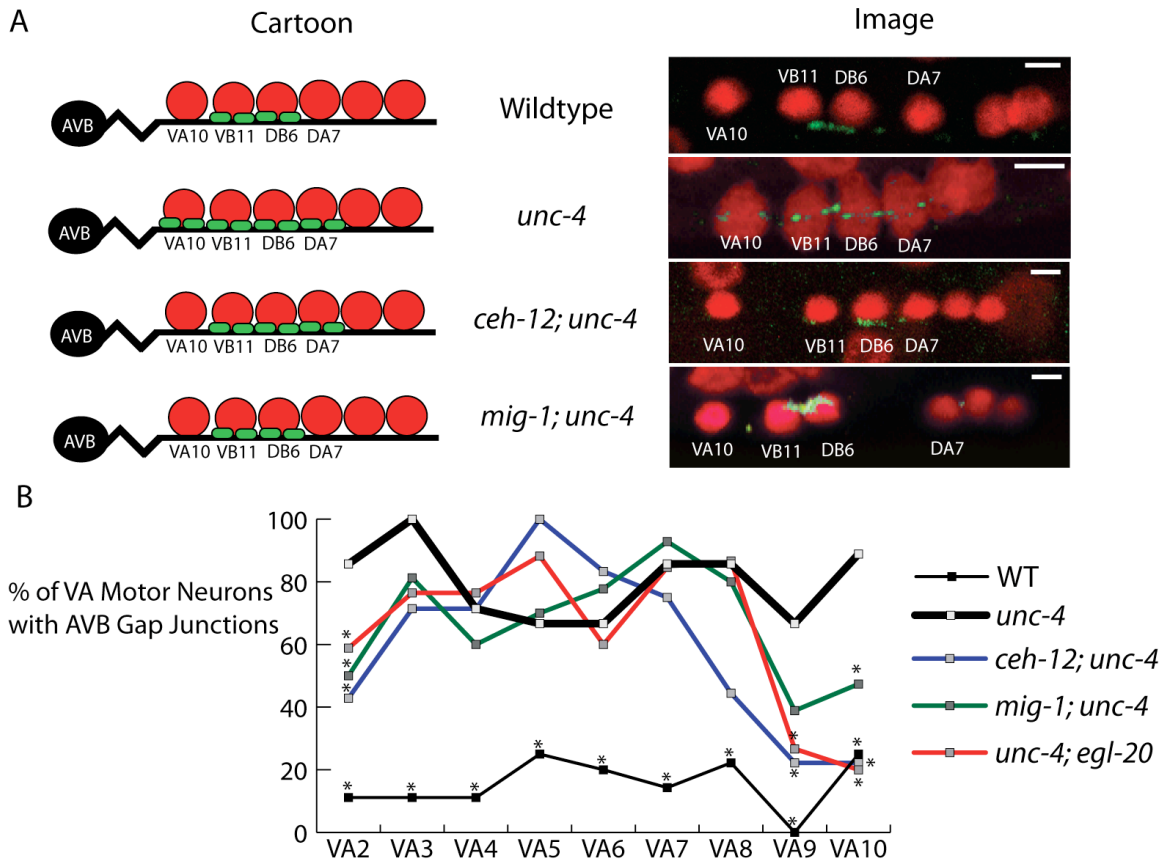
Figure 2.6. EGL-20/Wnt signaling promotes the creation of ectopic AVB gap junctions with posterior VA motor neurons.

A. Posterior ventral nerve cord depicting AVB gap junctions (green puncta) adjacent to cell soma (red filled circles) of motor neuron partners in wildtype and in *unc-4* mutants. B. Confocal images of posterior ventral nerve cord with UNC-7S::GFP puncta (green) and motor neuron nuclei stained with DAPI (red). Lateral view of adult with anterior to left, ventral down. A mutation in *mig-1* suppresses the creation of AVB gap junctions with VAs. Scale bar is 5 um. C. Mutations in *egl-20, mig-1* and *ceh-12* rescue the AVB miswiring defect for posterior *unc-4* mutant VA motor neurons and for VA2. (Mutations in *mig-1* rescue gap junctions in VA9 and VA10) (n ≥ 10 for each VA) p values were calculated with Fisher's exact test. * $p < 0.05$. Mutant alleles were *unc-4(e120), ceh-12(gk391), mig-1(e1787), egl-20(n585)*.

Our finding that mutations in *lin-17*/Frz enhance the Unc-4 movement defect and also result in ectopic *ceh-12::GFP* expression predicts that LIN-17/Frz functions to antagonize the formation of AVB to VA gap junctions. We used the UNC-7S::GFP gap junction marker to test this idea. As shown in Figure 2.7A, ectopic UNC-7S::GFP puncta are detected adjacent to VA motor neurons VA6 and VA10 in the *lin-17* mutant. Although aberrant AVB gap junctions are limited to a subset of VAs in this experiment, these effects are statistically significant and are also consistent with the mild backward movement defect of the *lin-17* mutant (Figure 2.5A). The strong *lin-17*-dependent enhancement of the Unc-4 movement phenotype (Figure 2.5A) suggests that LIN-17/Frz is likely to function in all VAs to oppose the creation of AVB to VA gap junctions. Taken together, the results of our assays with the UNC-7S::GFP marker support the hypothesis that LIN-17/Frz prevents the imposition of AVB inputs with VA motor neurons by opposing the activity of an EGL-20/Wnt signaling pathway that functions through *mom-5*/Frz, *mig-1*/Frz and *lin-18*/Ryk.

Frizzled receptors are expressed in VA motor neurons.

Our model predicts that the MOM-5, MIG-1, and LIN-17 frizzled receptors and LIN-18/Ryk function cell autonomously in VA motor neurons. *mig-1* expression in VAs is supported by cell-specific microarray results and experiments with a *mig-1::GFP* reporter gene (Von Stetina et al. 2007a). *lin-17* is expressed in the closely-related embryonic DA motor neurons
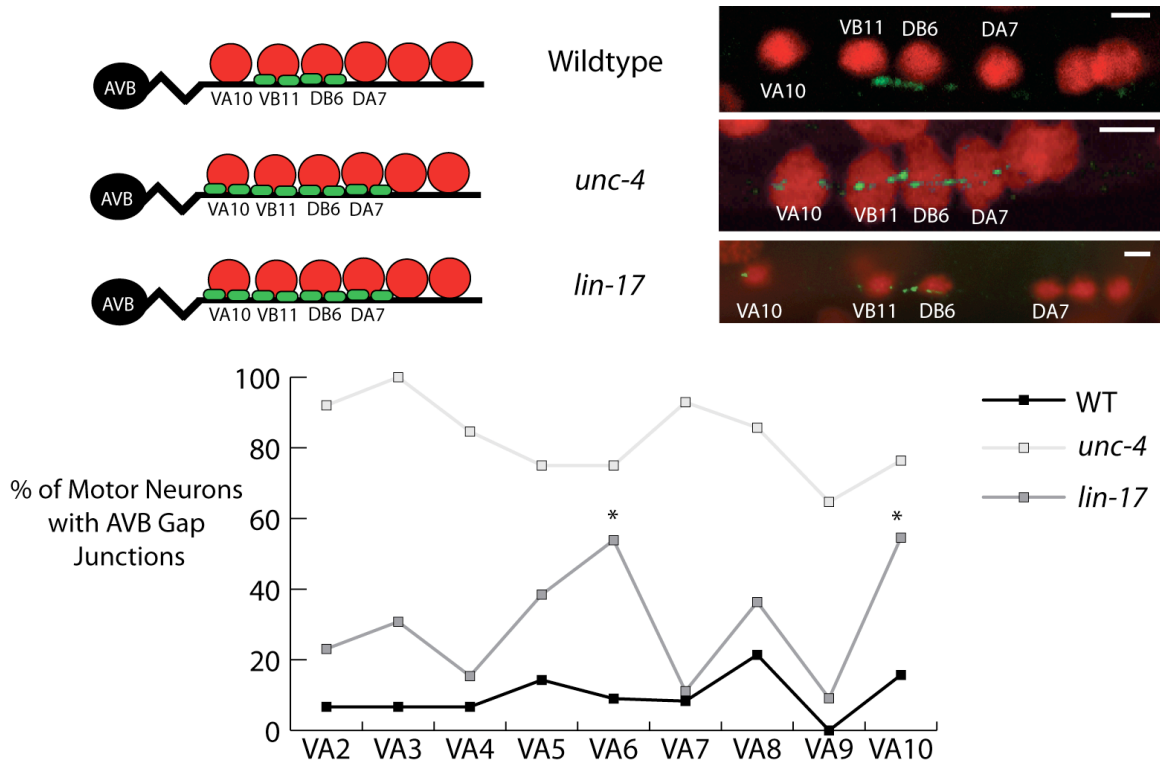
Figure 2.7. LIN-17/Frz inhibits miswiring of VA motor neurons with AVB gap junctions.

A. Posterior region of ventral nerve cord showing AVB gap junctions (green puncta) with motor neuron soma (red filled circles) B. Confocal image of *lin-17* mutant showing ectopic AVB gap junction (green puncta) on VA10 soma of DAPI-stained motor neurons (red). Lateral view of adult, anterior to left, ventral down. Scale bar is 5 um. Aberrant AVB to VA gap junctions are observed on VA6 and VA10 in a *lin-17(n671)* mutant in comparison to a wildtype background. Wildtype and *unc-4(e120)* results shown here are also depicted in Figure 2.6. n > 10 for each VA motor neuron. p values were calculated by Fisher's exact test for comparison of *lin-17* vs wildtype results. * p < 0.05.

l(Klassen and Shen 2007; Von Stetina et al. 2007b) (Table 2.1) and a *plin-17::LIN-17::GFP* transgenic line also shows expression in VAs (data not shown). Finally, a 3kb promoter *wdEx611[mom-5::GFP]* fusion is expressed in several ventral cord motor neurons including VAs (Figure 2.8). These results suggest that the Frizzled receptors MOM-5, MIG-1 and LIN-17 may be constitutively expressed in wildtype VA motor neurons. (We have not verified the expression pattern of LIN-18/Ryk.) However, microarray results have shown that both the *mom-5* and *mig-1* transcripts are significantly upregulated in VA motor neurons when the *unc-4* pathway is disabled by an *unc-37*/Groucho mutant (Von Stetina et al. 2007b) (Table 2.1). This finding requires confirmation (see Discussion) but offers the intriguing possibility that *unc-4* effectively quells the VA motor neurons response to EGL-20/Wnt by preventing MOM-5 and MIG-1 levels from exceeding a critical threshold.

UNC-4 Antagonizes a canonical Wnt signaling pathway.

Wnt signaling pathways are generally classified as either canonical or non-canonical. In *C. elegans*, canonical signaling involves the transcription factor β-catenin, BAR-1. In this pathway, Wnt signaling stabilizes BAR-1 by inhibiting the activity of a so-called "destruction complex" that includes the conserved proteins Axin, GSK3β, and Casein Kinase Iα. In the absence of a Wnt signal, the destruction complex phosphorylates cytosolic β-catenin, leading to its degradation. Thus, if BAR-1/β-catenin functions in a canonical pathway to
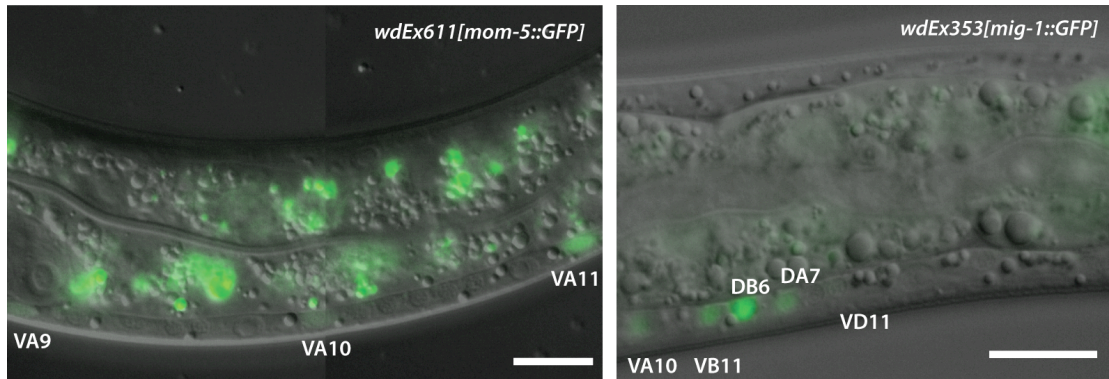
Figure 2.8. Frizzled Receptors are expressed in VA motor neurons.

Two GFP reporters to *wdEx611[mom-5::GFP]* and *wdEx353[mig-1::GFP]* show GFP expression in VA motor neurons. L2 animals are shown. Scale bar is 5 microns.

Wnt Receptors	Microarray Data			GFP reporters	
	[1,2]DA	[3,4] WT VA	[5]unc-37 VA	Transgenics	VA
mom-5	EG	EG	1.8X	mom-5::GFP	Yes
mig-1	EG	1.6X	1.8X	mig-1::GFP	Yes
lin-17	1.7X	ND	ND	lin-17::GFP	Yes
cfz-2	ND	EG	ND	?	
lin-18	ND	ND	ND	?	
cam-1	EG	EG	ND	?	

[1]1471-2164-6-42-s7.xls
[2]1471-2164-6-42-s9.xls
[3]gb-2007-8-7-r135-s13.xls
[4]gb-2007-8-7-r135-s4.xls
[5]unc-37 up anno 071806 no dups no DA cat.xls

Table 2.1. Microarray results suggest Wnt receptors are expressed in A-class motor neurons and are regulated by UNC-4.

Frizzled receptors *mom-5* and *mig-1* are detected in VA and DA motor neurons. by both microarray results and GFP reporters. *mom-5* and *mig-1* transcripts are also upregulated in *unc-37* mutant animals, suggesting that *unc-4* functions to regulate the expression, and thus sensitivity of VA motor neurons to a Wnt signal. *lin-17* mRNA is detected in DA motor neurons, but is not in VAs, however, our GFP reporter data suggests that *lin-17* is expressed in VA motor neurons.

Footnotes refer to file names of microarray data sets showing relative expression levels of Wnt receptors in DA/VA motor neurons. EG refers to "expressed genes" that are detected but not enriched (Fox et al. 2005a; Von Stetina et al. 2007a).

promote VA miswiring, then a loss-of-function *bar-1* mutation should suppress this defect. We observe weak suppression of *unc-37(e262)* in the tapping assay (Figure 2.9B) but not *unc-4* mutants (Figure 2.9D is not statistically significant $p > 0.05$). One explanation for this ambiguous result is that *bar-1* mutant animals are Unc possibly due to a required function in another motor neuron class (Vashlishan et al. 2008) and are thus difficult to score in our movement assay.

To resolve this question, we performed four additional experiments to test the requirement of the destruction complex in the Unc-4 phenotype. In *C. elegans*, genetic ablation of *pry-1*/Axin effectively over-activates canonical Wnt signaling by preventing degradation of BAR-1/β-catenin. It follows that if PRY-1/Axin negatively regulates EGL-20/Wnt-dependent signaling in VA motor neurons, then a *pry-1* mutation should constitutively activate this pathway. We tested this idea by exploiting the temperature sensitive *unc-4(ts)* allele which is capable of wildtype backward locomotion at the permissive temperature of 16°C. *pry-1* animals also show normal movement at this temperature. Backward locomotion is strongly impaired, however, in the *pry-1; unc-4(ts)* double mutant (Figure 2.10A). This synthetic Unc-4 phenotype is consistent with a model in which both *unc-4* and *pry-1* function as negative regulators of a Wnt pathway that leads to VA miswiring (Figure 2.10).

In the second experiment to test the role of the destruction complex in the VA miswiring defect, we treated animals with LiCl to inhibit GSK3β activity and thus hyperactivate canonical Wnt signaling. As shown in Figure 2.10A, treatment of wildtype animals induces a strong backward movement defect. This LiCl-
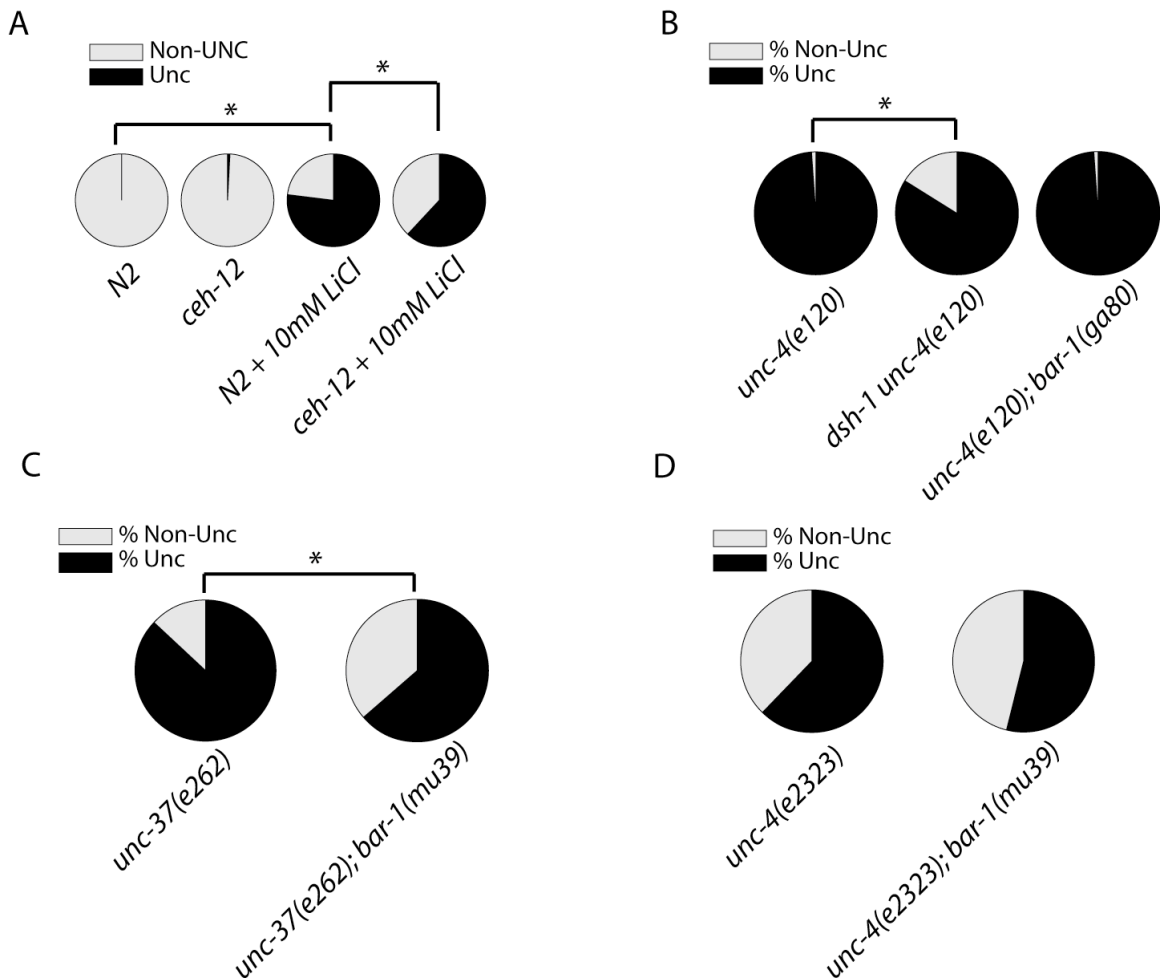
Figure 2.9. Inhibition of intracellular canonical Wnt signaling suggests EGL-20 functions via a canonical mechanism.

A. Lithium is a potent GSK3β inhibitor. N2 and *ceh-12* mutant animals have normal backward locomotion. Treatment of a synchronized population of L1/L2 animals with 10 mM LiCl induces a backward Unc phenotype. Mutations in *ceh-12* partially attenuate the backward Unc phenotype. Results shown are the sum of three individual experimental replicates. B. Mutants in the intracellular effector protein *dsh-1* rescues *unc-4(e120)*. B + D. *bar-1*/β-catenin mutations suppress *unc-37(e262)* but not alleles of *unc-4(e120, e2323)*. * p > 0.05 using Fisher's Exact Test.
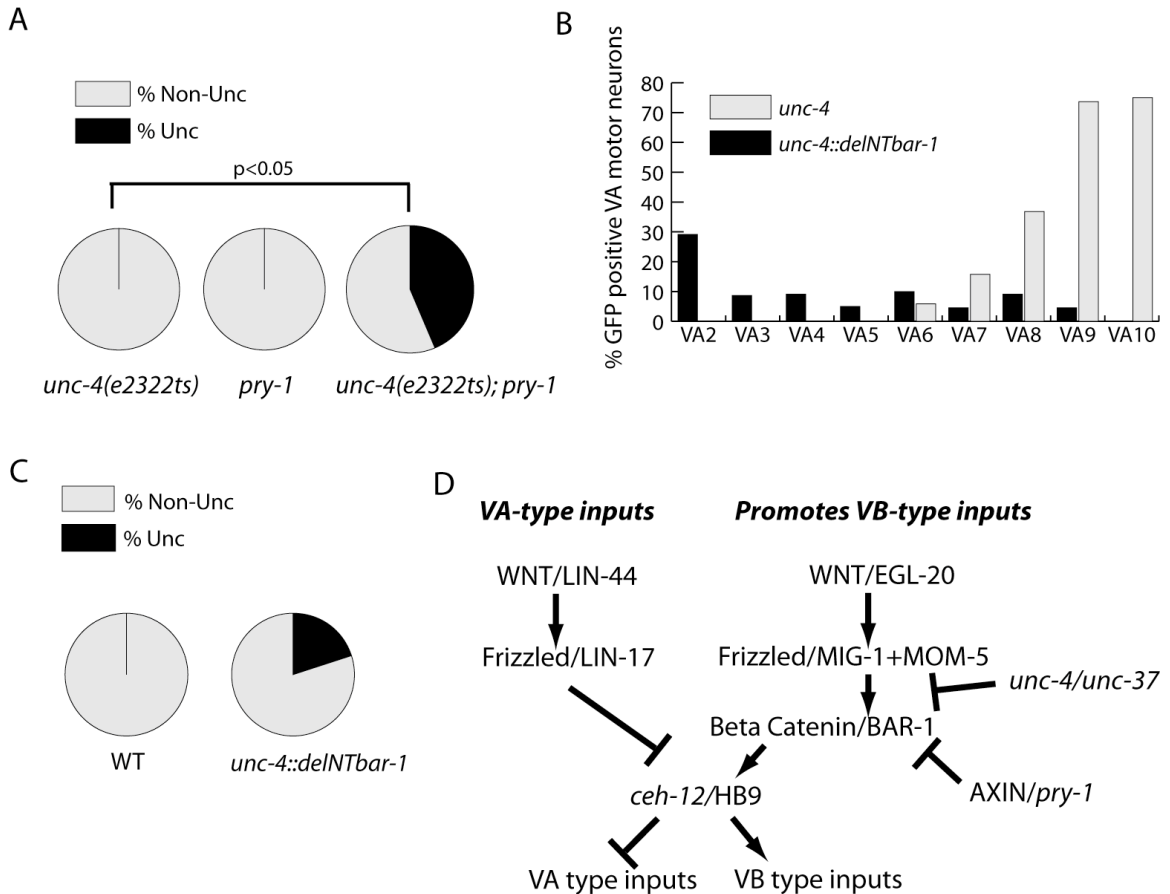
Figure 2.10. Canonical wnt pathway components, PRY-1/Axin and BAR-1/β catenin regulate *ceh-12* expression and VA motor circuit function.

A. A mutation in the Axin homolog *pry-1* enhances the Unc-4 phenotype of temperature sensitive allele, *unc-4(e2322ts)* at permissive temperature (16°C). Backward movement was scored in the tapping assay as either Unc (no backing) or non-Unc (detectable backward movement) (see Methods). (n > 50 * p < 0.05 Fisher's exact test). B. Expression of constitutively active β-catenin/BAR-1 in wildtype VA motor neurons induces ectopic *ceh-12::GFP*. VA expression of *ceh-12::GFP* in *unc-4(e120)* is also depicted in Figure 2.1. The extrachromosomal array *wdEx636*[*unc-4*::delNT-BAR-1] induces ectopic *ceh-12::GFP* in VA motor neurons. C. *wdEx636* induces an Unc-4 phenotype at low frequency. D. Proposed model: LIN-44/WNT signaling and UNC-4 antagonize a canonical Wnt signaling pathway that promotes *ceh-12* expression and the miswiring of VA motor neurons with VB-type inputs.

induced Unc-4 phenotype is attenuated in a *ceh-12* null mutant, a result

predicted by a model in which VA miswiring depends on activation of *ceh-12*

expression by canonical Wnt signaling.

If inhibition of the destruction complex by either the *pry-1*/Axin mutation or

by LiCl treatment, prevents degradation of BAR-1/β-catenin, then a constitutively

active BAR-1/β-catenin protein should produce a similar phenotypic effect. In our

third experiment, we tested this prediction with ΔNT-BAR-1, a truncated β-catenin

protein lacking N-terminal phosphorylation sites that trigger Axin/GSK3-mediated

degradation (Gleason et al. 2002a). Selective expression of ΔNT-BAR-1 in A-

class motor neurons results in an Unc-4-like movement defect resembling that

produced by CEH-12/HB9 overexpression (Figure 2.10C) (Von Stetina et al.

2007b). Moreover, the *punc-4::*ΔNT-BAR-1 transgene also induces ectopic *ceh-*

12::GFP expression in VA motor neurons in which wildtype *unc-4* function is

intact (Figure 2.10B). In summary, activation of a canonical Wnt signaling

pathway by three independent approaches *pry-1*/Axin mutation, LiCl-treatment,

and constitutively active BAR-1/β-catenin. phenocopies Unc-4 and therefore

supports a model in which UNC-4 antagonizes a canonical Wnt signaling

pathway to prevent *ceh-12*/HB9 expression and VA miswiring.

In a final experiment, we utilized the canonical Wnt-pathway inhibitor,

pyrvinium, to correlate activity of the destruction complex with the Unc-4

phenotype. As described in Chapter 4, experiments performed by Curtis Thorne

in Ethan Lee's lab have shown that pyrvinium interacts with Casein Kinase 1α to

Pyrvinium suppresses Unc-4 movement defect
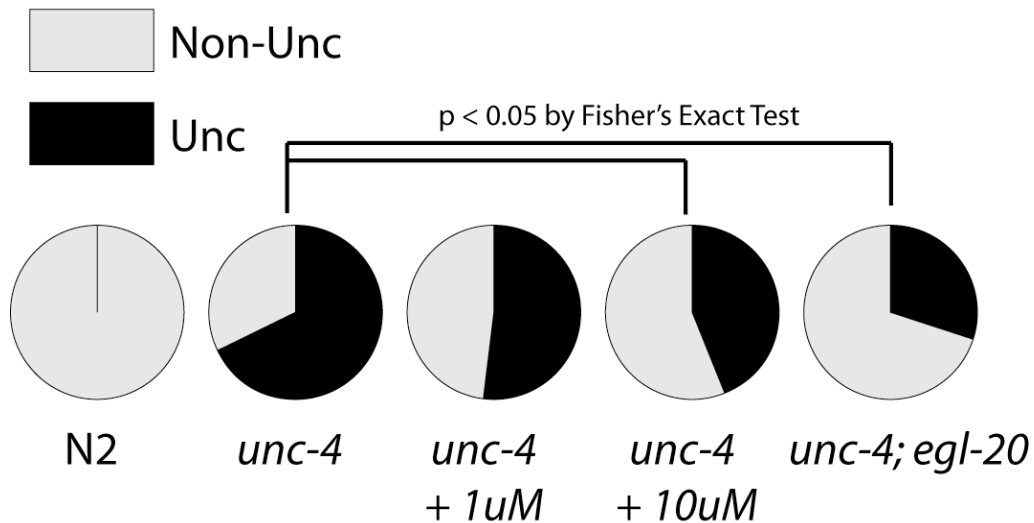
Figure 2.11. Pyrvinium suppresses the unc-4 movement defect in _unc-4(e2322ts)_ animals at 23°C.

Treatment of _unc-4(e2322ts)_ animals with the Caesin Kinase Iα activator, pyrvinium, suppresses the Unc-4 backward movement defect in a dose dependant manner. Results shown are derived from two replicate experiments. _unc-4(ts); egl-20(n585)_ tapping assay result shown for comparison.

activate the destruction complex and downregulate β-catenin. Experiments that I

performed (Chapter 4) have confirmed that pyrvinium inhibits other

developmental processes (neuroblast migration, vulval morphogenesis) in *C.*

elegans that depend on canonical Wnt signaling (Thorne et al., submitted). We

tested the hypothesis that *unc-4* antagonizes a canonical Wnt pathway by

activating CK1α with pyrvinium. As shown in Figure 11, pyrvinium treatment

suppresses the Unc-4 movement defect of the *unc-4(ts)* hypomorphic allele.

Taken together, our results provide strong support for the hypothesis that UNC-4

preserves VA type synaptic inputs by antagonizing an EGL-20/Wnt dependent

canonical signaling pathway.

DISCUSSION

This chapter describes the discovery that Wnt signaling controls the

specificity of motor neuron inputs in the *C. elegans* ventral nerve cord. Our

findings underscore the conserved role of Wnt in patterning neural connections

and provide a potentially new model for how this evolutionarily ancient cue can

regulate synaptic specificity. For these studies, we exploited a simple, well-

defined circuit in which sister VA and VB motor neurons are connected to

separate sets of pre-synaptic interneurons. We propose a model in which UNC-4

preserves normal VA motor neuron inputs by preventing VAs from responding to

a local EGL-20/Wnt cue, possibly by repressing transcription of specific frizzled

receptors, MOM-5 and MIG-1; in *unc-4* mutants, a canonical Wnt signaling

pathway is activated to drive expression of the VB gene, CEH-12/HB9, and the consequent rewiring of VA motor neurons with VB-type inputs. A more complex role for Wnt signaling in this model is revealed by our discovery of a separate pathway, involving a distinct Wnt ligand (LIN-44) and frizzled receptor (LIN-17), that antagonizes *ceh-12*/HB9 expression. Thus, our results have revealed competing pathways that drive the creation of alternative sets of specific connections in a functional motor circuit. The strong conservation of the transcription factors and Wnt signaling components that regulate these events suggests that similar mechanisms may also control regional wiring specificity in more complex nervous systems.

UNC-4 may control the sensitivity of VA motor neurons to an EGL-20/Wnt signal.

Our genetic evidence indicates that UNC-4 antagonizes a canonical Wnt signaling pathway that is activated by EGL-20/Wnt. VA motor neurons located in the posterior ventral nerve cord in a region near EGL-20/Wnt expressing cells in the *C. elegans* tail region are uniquely responsive to EGL-20 in *unc-4* mutants. This finding indicates that one important function of UNC-4 is to prevent this subset of posterior VAs from responding to a local Wnt cue. Because similar effects are observed for a mutant that disables the transcriptional co-repressor protein, UNC-37/Groucho, it seems likely that the critical role of UNC-4 is to block expression of specific target genes. The de-repression of *ceh-12*/HB9 in these posterior *unc-4* mutant VA motor neurons is a clear indication of this possibility. We also have results from a microarray experiment that are consistent with the

alternative possibility that UNC-4 prevents VA motor neurons from responding to EGL-20/Wnt by blocking transcription of the frizzled receptors *mom-5* and *mig-1*. However, experiments with promoter-GFP reporter genes for *mig-1* and *mom-5* did not detect de-repression in either *unc-4* or *unc-37* mutants (data not shown). In the future, it will be important to resolve this question. We have recently established a collaboration with Rik Korswagen (Hubrecht Institute, The Netherlands) who has developed a new, *in situ* hybridization method based on FISH technology that could answer this question by directly measuring endogenous *mom-5* and *mig-1* transcript levels in the VAs in wildtype and *unc-4* mutant animals.

Connectivity experiments suggest an anterior source of EGL-20/Wnt.

Our model should also account for the surprising finding that the motor neuron VA2, which is located at the anterior end of the ventral nerve cord, appears to be as responsive to EGL-20/Wnt as VA motor neurons at the posterior end of the nerve cord. This conclusion is based on our finding that loss of function mutations in either *egl-20* or its presumptive frizzled receptor, *mig-1*, suppress Unc-4 miswiring (gap junctions with AVB) of VA2 as well as that of VA9 and VA10 (Figure 2.6). This result suggests that VA2 is unusually responsive to the distal EGL-20 cue originating with posterior cells or that another local, anterior source of EGL-20 is involved. A similar hypothesis has been proposed to explain the effect of LIN-44, which is also highly expressed in the tail, on vulval development in the midbody region. In that case, a hypothesized *lin-44*/Wnt

88

signal expressed in the nearby anchor cell is necessary for coordinating asymmetric cell divisions (Green et al. 2008).

EGL-20 activates a canonical Wnt signaling pathway.

Our genetic and pharmacological results demonstrating roles for the destruction complex and for BAR-1/β-catenin in the Unc-4 miswiring phenotype, strongly suggest that EGL-20/Wnt activates a canonical Wnt signaling pathway. This assumption is based on the observation that the destruction complex and BAR-1 are exclusively employed by canonical Wnt signaling pathways in *C. elegans.* Additional evidence in support of this hypothesis is our finding, reported in Chapter 3, that mutations in *pop-1*/TCF, were isolated as weak suppressors of the Unc-4 movement defect. This genetic epistasis result is consistent with a canonical signaling model in which BAR-1/β-catenin activates POP-1/TCF to promote transcription of *ceh-12*/HB9. The *ceh-12* promoter contains a consensus POP-1/TCF binding site but biochemical experiments are needed to determine if POP-1 function is required in this pathway *in vivo*. It will also be interesting to explore the mechanism whereby the Ryk receptor, LIN-18, contributes to readout of the EGL-20/Wnt signaling cascade. Finally, our results show that a separate Wnt signaling pathway activated by LIN-44/Wnt and LIN-17/Frz oppose the EGL-20-dependent signaling. The downstream elements of the *lin-44/lin-17* pathway are unclear. One possible model is suggested by recent reports of a non-canonical pathway responsible for asymmetric neuroblast divisions. (Bertrand and Hobert 2009; Hingwing et al. 2009) In these studies, the β-catenins *sys-1*

and *wrm-1* interact with the POP-1/TCF to specify cell fate. A high SYS-1:POP-1 ratio in the nucleus produces an anterior neuron fate whereas a low SYS-1:POP-1 ratio results in a posterior neuron fate. In this context, LIN-44/LIN-17 signaling could be promoting an A-class wiring phenotype independently of *unc-4*, by enhancing an anterior neuronal fate through the β-catenin asymmetry pathway. Future experiments are needed to explore this model.

***unc-4* controls gap junction specificity by modulating Wnt signaling.**

Our results indicate that *unc-4* controls gap junction specificity by modulating the output of two distinct Wnt signaling pathways in VA motor neurons. Normally, *lin-17*/Frizzled functions in VA motorneurons and acts in parallel to *unc-4* to antagonize *ceh-12* expression and inputs from AVB. UNC-4 performs this function by antagonizing the sensitivity of VA motor neurons to a posterior EGL-20/Wnt signal, hypothetically by controlling the expression of the Frizzled receptors *mom-5* and *mig-1* in VA motor neurons. Once VA motor neurons become sensitized, EGL-20 activates a canonical Wnt pathway to turn on *ceh-12* and VAs receive ectopic inputs from AVB.

One hypothesis suggests that the choice between AVB versus AVA inputs may be due to the relative location gap junction proteins are positioned on the cell body. AVB makes connections directly with cell soma of motor neurons whereas AVA makes gap junctions with neuronal processes. This subcellular compartmentalization may be play a role in the specification of these particular inputs. Wnt signaling has been previously shown to regulate neuromuscular

90

junction location via compartmentalization. In the dorsal projecting motor neuron, DA9, pre-synaptic components are restricted to the dorsal, longitudinal process where DA9 normally makes neuromuscular junctions onto dorsal muscles (Klassen and Shen 2007). The dorsal projecting process, where LIN-17 is expressed is devoid of pre-synaptic components. Loss of *lin-17*/Frizzled results an expansion of pre-synaptic domain into the former location of LIN-17 expression. Thus, LIN-17 is restricting the pre-syanptic domain and compartmentalizing this neuron. Since Wnt signaling has been shown to control the subcellular compartmentalization of pre-syaptic components, it is also possible that it may have a similar effect on gap junction proteins.   If this is the case, it may be possible to miswire a VA motor neuron by targeting the post-synaptic gap junction components to a different subcellular domain.

Conclusions.

This study, and recently reported results from other laboratories, indicate that synaptic specificity may be regulated by non-cell autonomous cues that do not originate with the synaptic partner neurons (Klassen and Shen 2007; Poon et al. 2008; Pecho-Vrieseling et al. 2009). Here, we show that two different exogenous Wnt signals trigger transduction pathways that operate within a common cytoplasm to promote opposite patterns of synaptic inputs. Our results indicate that UNC-4 functions to bias one outcome versus the other. It is interesting to note, however, that the necessity for this UNC-4 activity is limited to a subset of VA motor neurons that are responsive to EGL-20. Other VAs, which

are also miswired in *unc-4* mutants, must therefore depend on additional cell-specific *unc-4* regulated pathways. Genetic experiments described in the Chapter 3 were designed to identify genes in these additional *unc-4*-regulated pathways.

Strain	% Unc	% Non-Unc
WT	0	100
unc-4(e2320)	98	2
unc-4(e120)	99	1
ceh-12(gk391); unc-4(e120)	54	46
ceh-12(gk391); unc-4(e2320)	58	42
dsh-1 unc-4(e120)	84	16
unc-4(e120); egl-20(n585)	87	13
unc-4(e2320); egl-20(n585)	46	54
ceh-12(gk391); unc-4(e120); egl-20(n585)	65	35
ceh-12(gk391); unc-4(e2320); egl-20(n585)	69	31
unc-4(e2320); bar-1(mu39)	99	1
unc-4(e120); bar-1(ga80)	99	1
unc-4(e120); egl-20(n585); bar-1	99	1
unc-4(e120); dpy-20 wdEx636	100	0
mig-1(e1787) mom-5(ne12)/Ht2	12	88
mig-1(e1787) mom-5(ne12)/Ht2; unc-4(e120)	90	10
dpy-20 wdEx636	20	80
ceh-12(gk391); dpy-20 wdEx636	40	60
lin-17 lin-44 MT4705	4	96
lin-17 lin-44; unc-4(e120)	94	6
egl-20(n585)	36	64
egl-20(n585); bar-1(mu39)	7	93
unc-37(e262)	87	13
unc-37(e262); bar-1(mu39)	64	36
unc-37(e262); egl-20(n585)	70	30
unc-4(e2323)	63	38
ceh-12(gk391); unc-4(e2323)	6	94
unc-4(e2323); egl-20(n585)	13	87
unc-4(e2323); bar-1(mu39)	54	46
unc-4(e2323); dpy-20 wdEx636	74	26

at 23 C

unc-4(e2322ts)	80	20
unc-4(e2322ts); egl-20(n585)	22	78
unc-4(e2322ts); bar-1(ga80)	81	19
unc-4(e2322ts); bar-1(mu39)	69	31
unc-4(e2322ts); egl-20(n585)	29	71

at 23 C

WT	0	100
unc-4(ts)	80	20
unc-4(ts);egl-20	26	74
unc-4(ts);lin-44	70	30
unc-4(ts);mig-1	42	58
unc-4(ts);mom-5(or57)	67	33
unc-4(ts);lin-17	90	10
unc-4(ts) dsh-1	29	71
unc-4(ts);bar-1(ga80)	42	58
unc-4(ts);pop-1	22	78

at 16C

unc-4(e2322ts)	0	100
lin-17	10	90
unc-4(e2322ts); lin-17	55	45
pry-1	0	100
unc-4(e1222ts);pry-1	38	62
unc-4(e2322ts)	0	100
lin-17	10	90
unc-4(e2322ts); lin-17	55	45
pry-1	0	100
unc-4(e1222ts);pry-1	38	62
N2	0	100
ceh-12	1	99
N2 + 10mM LiCl	77	23
ceh-12 + 10mM LiCl	62	38

Table 2.2. Compilation of Tapping Assay Data.

Percentages of Unc versus Non-Unc animals in each genetic background tested are listed here. n >50 for each geneotype tested.

CHAPTER III

GENETIC SCREENS IDENTIFY NEW UNC-4 SUPPRESSOR LOCI THAT FUNCTION THROUGH PATHWAYS IN PARALLEL TO CEH-12 TO REGULATE SYNAPTIC CHOICE

INTRODUCTION

Coordinated movement depends on the creation of specific connections in the motor circuit. Interneurons that enter the axial nerve cord synapse with selected motor neuron targets to establish functional circuits. Guidance cues and receptors that steer interneurons to their destinations have been identified but much less is known about how neurons choose synaptic partners.

Recent work has revealed that target recognition may depend on local, extracellular cues. For example, studies of the Drosophila neuromuscular junction have implicated the diffusible morphogen Wnt in targeting the appropriate muscle for innervation (Inaki et al. 2007). Differential microarray experiments identified Wnt4 as a local repulsive cue that prevents motor neurons destined for muscle M12 from innervating M13 (Inaki et al. 2007). In this case, motor neurons that innervate M13 are intrinsically insensitive to Wnt4 whereas motor neurons that innervate M12 are repelled (Inaki et al. 2007). A similar role for a repulsive cue has been observed in the developing vertebrate spinal cord. Central synaptic connections between selected pools of motor and sensory neurons are altered by changing the PlexinD1-SemaE3 signaling system (Pecho-Vrieseling et al. 2009). In the wild type animal, sensory afferents from a specific

muscle synapse with relay neurons which in turn connect with motor neurons that innervate the same muscle. However, genetic ablation of either the Sema3e ligand or its receptor Plexnd1 results in the inappropriate targeting of sensory afferents to motor neurons (Pecho-Vrieseling et al. 2009). This result suggests that Sema3e-Plexnd1 signaling prevents the creation of direct inputs from sensory neurons to motor neurons in this circuit (Pecho-Vrieseling et al. 2009).

Chapter 2 described experiments that characterize how UNC-4 regulates *ceh-12* expression to control motor neuron inputs. Our previous data suggest that UNC-4 regulates multiple pathways, which function in parallel to *ceh-12,* to specify inputs to VA motor neurons. In an effort to identify genes that function in these parallel pathways, we utilized a sensitized genetic screen to isolate mutations that suppress the Unc-4 backward movement defect. This idea is based on the observation that mutations that disable *ceh-12* or its upstream *egl-20*/Wnt signaling pathway partially restore backward locomotion to an *unc-4* mutant. Thus, we reasoned that mutations in *unc-4*-regulated genes functioning in parallel pathways should also result in Unc-4 suppression. (Figure 3.1) Our approach has uncovered 16 independent complementation groups with a Blr (Backward Locomotion Restored) phenotype. These *blr* loci include components of the *egl-20*/Wnt pathway in addition to genes that antagonize *unc-4* dependent wiring in anterior VA motor neurons. Future molecular analysis of these loci should reveal genes with key roles in synaptic choice.

My contribution to this project was to oversee the project goals, perform the genetic screens, outcross the *blr* mutants, complete restriction endonuclease single nucleotide polymorphism ('SNIP' SNP) mapping experiments, construct genetic strains, perform movement assays, and use GFP markers to score gap junction and chemical synaptic inputs to VA motor neurons. I have been fortunate to work with several additional individuals who have also contributed to this project. Of particular note, this work was performed in collaboration with Rachel Skelton, who assisted with outcrossing, mapping, and complementation tests for *blr* mutations. Rachel also scored the gap junctions for *wd83* and *wd95*. Dan Ruley, an undergraduate from the College of Wooster, performed many of the SNIP SNP PCR gels. Zhaoying Xu, an undergraduate from Grinnell College, characterized *wd88* by verifying the mapping results for *wd88*, constructing strains with *wd88*, and assisting with *wd88* gap junction scoring. Skye Baccus, an undergraduate from Vanderbilt, verified SNIP SNP mapping data for *wd76* and constructed strains with *wd87*. Kristy Hamilton, a Vanderbilt undergraduate, worked on *wd95* with Rachel. Ian Boothby, a high school senior at Hume-Fogg, created strains with multiple *blr* mutations and assisted with validating previous results.
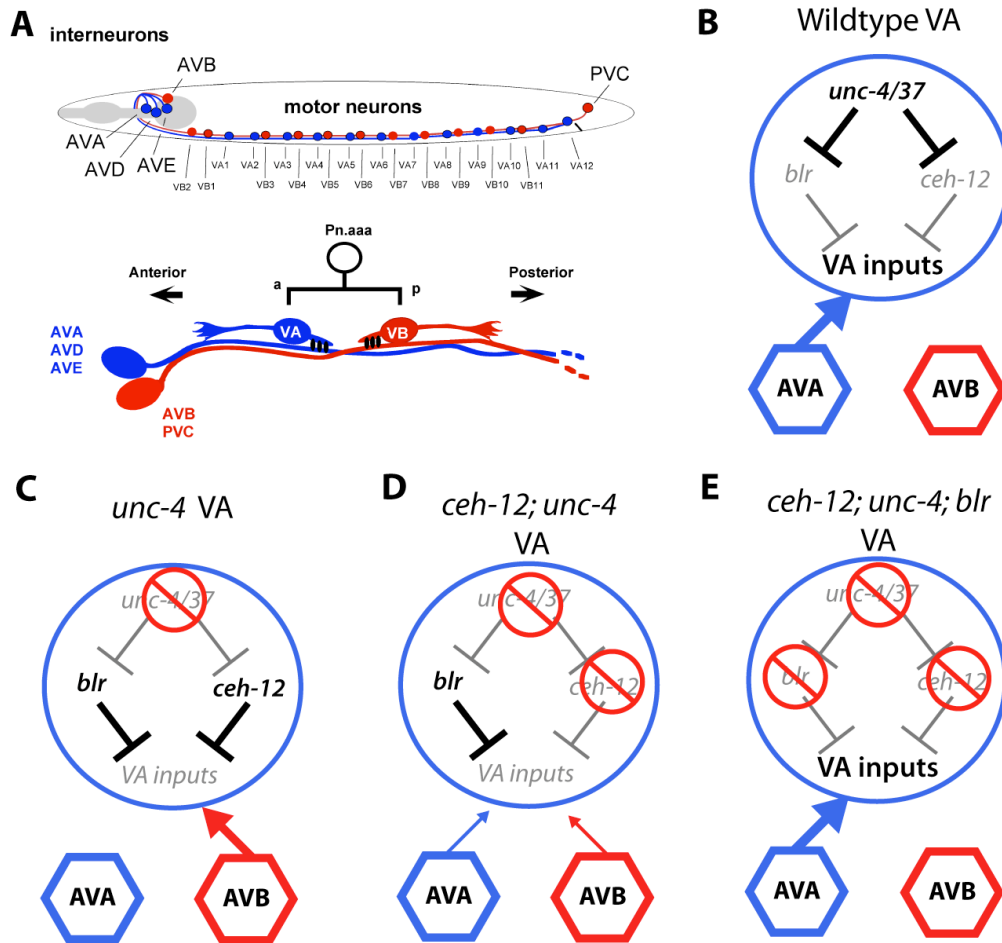
Figure 3.1. UNC-4 controls multiple, parallel pathways to specify VA inputs.

A. The postembryonic VA and VB motor neurons arise from a common progenitor and receive inputs from different sets of command interneurons. VAs receive inputs from interneurons (AVA, AVD, AVE) that drive **backward** locomotion and VB motor neurons are connected to interneurons (AVB, PVC) that control **forward** movement. B. UNC-4 functions with UNC-37 to repress VB genes. C. Mutations in *unc-4/37* cause de-repression of at least two targets, including the VB gene *ceh-12/*Hb9. D. Mutations in *ceh-12*, cause the partial loss of gap junction inputs from the forward circuit, improving locomotion. E. Mutations in both downstream pathways depicted in this schematic should restore backward locomotion.

MATERIALS AND METHODS

Culture of *C. elegans*.

Nematodes were cultured according to previously established protocols (Brenner 1974). Nematodes were cultured on NGM plates inoculated with OP50-1 or Na22 *E. coli* strains.   The N2 strain was used as a wildtype reference and all mutant lines were derived from the N2 background. Strains used in this work were obtained from the Caneorhabditis Genetics Center (CGC) (University of Minnesota), K. Shen (Stanford), and J. Shaw (University of Minnesota).

Strains used in this work include, *ceh-12(gk391); unc-4(e2322ts, e2323, e120, e1220, wd1); unc-37(e262); unc-24(e138); lin-17(n671); mig-1(e1787)* (Brenner 1974; Miller et al. 1993a; Maloof et al. 1999; Von Stetina et al. 2007a) *blr-1(wd76); blr-2(wd77, wd86); blr-3(wd82); pop-1(wd92, wd97, wd99); mig-1(wd96, wd89, wd100); blr-5(wd84); blr-8(wd87, wd98); blr-9(wd88); unc-37(wd85); blr-11(wd90); blr-12(wd91); blr-15(wd95); blr-19(wd101); blr-20(wd102), blr-21(wd103)* (This work).

Strains used in genetic crosses include: *euIs82a[unc-129::GFP; dpy-20+]* (I), *juIs76[unc-25::GFP; lin-15+]* (II), *rhIs2[glr-1::GFP]* (III), *ayIs2[egl-15::GFP]* (IV), *mIs11[myo-2::GFP, pes-10::GFP, gut::GFP]* (IV), *ccIs9753[myo-2::GFP]* (V), *oyIs44[odr-1::RFP]* (V), *oxIs12[unc-47::GFP]* (X). The GRASP stain, [TV1477 (*wyEx1914[unc-4::NLG-1::spGFP1-10, flp-18::NLG-1::spGFP11, flp-18::mCherry::rab-3, odr-1::DsRed2]*)] and UNC-7::GFP strain (EH578 [*punc-*

7::UNC-7S:GFP, *col-19*::GFP]) were generously provided by K. Shen (Stanford) and J. Shaw (U. Minnesota), respectively.

Chromosomal deficiencies used in this study include: *mDF10/nT1* (-0.3 to 0.075), *mDF4/nT1* (-0.8 to 2.167), *dpy-13 ama-1 mDF8/nT1* (0.9 to 2.45), *mDF9/nT1* (-0.969 to 2.15), *eDF19/dpy-20 unc-24*, and *nDF41/bli-6 egl-19 unc-24* (1.65 to 3.37). (CGC)

Hypochloride treatment

Age-synchronous populations of worms were isolated using hypochloride treatment. A confluent plate of gravid adult worms were washed into a 50mL conical tube using water. Worms were pelleted using a low-speed spin in a clinical centrifuge and the supernatant aspirated to remove suspended bactera. A hypochloride solution (7.5mL water, 2mL bleach, 0.5mL 10N NaOH) was added to approximately 1 mL of worms and mixed by inversion, causing the gravid adults to rupture and release their eggs. This was monitored using a drop of solution containing the worms under a stereo-dissecting microscope. Once ~50% of the adults lysed, the tube was filled with M9 to stop the reaction. Isolated eggs were washed with M9 three times to remove residual bleach, and transferred to a new tube. Isolated eggs were placed on a new 100mm NGM OP50^{-1} plate and incubated at 20°C.

Isolation of Unc-4 suppressor mutations.

Pilot Screen

Recessive *unc-4* suppressor mutations were isolated using two genetic screens: first, a pilot screen of 5,000 haploid genomes, and second, a 'stuck screen' of 40,000 haploid genomes.

The pilot screen was conducted using the sensitized strain, *ceh-12(gk391); unc-4(wd1)*. In this case, the double mutant strain is unable to execute a full backward sinusoidal wave but has significantly greater mobility than the *unc-4(wd1)* mutant alone (Table 3.2). Animals were synchronized by hypochlorite treatment and mutagenized with 0.05M ethyl methansulfonate (EMS) during the L4 larval stage (Brenner 1974). 100-200 animals were placed on 100mm NGM plates, inoculated with E. coli OP50-1, and grown at 20°C overnight to recover from mutagenesis. P0 animals were picked, 5 at a time, to individual NGM OP50-1 plates and grown at 20C for 3-4 days. F1 progeny were then picked onto individual NGM OP50-1 plates at a density of 3 F1s/plate. F2 animals were screened for backward locomotion in response to head touch. Mutations that resulted in suppression of the Unc-4 backward locomotion defect were labeled as *blr* loci for *B*ackward *l*ocomotion *r*estored for their ability to suppress the Unc-4 backward locomotion phenotype. New *blr* mutants were transferred to individual NGM OP50-1 plates for self fertilization. F3 progeny were re-examined to confirm backward locomotion. Two independent *blr* alleles (*wd76, wd77*) were isolated from the progeny of 5,000 F1 animals.

'Stuck' screen

To increase the throughput of our Unc-4 suppression screen, we adopted a second genetic background, NC25[*unc-4(e2322ts); unc-24(e138)*], in which animals are unable to execute either forward or backward locomotion (Miller et al. 1993a) (Figure 3.2). This synthetic "stuck" phenotype results from the combined effects of the *unc-4* (unable to crawl backward), and *unc-24* (uncoordinated forward movement) mutants. In previous work from this laboratory, dominant Unc-4 suppressors with improved backward locomotion were isolated as F1 progeny that could traverse a 100mm plate to reach a patch of bacteria (food). We reasoned that a similar approach could be utilized to isolate F2 recessive suppressors of *unc-4(ts)*. To test this idea, we performed an experiment, to determine whether *ceh-12(0)* could be detected in this assay. NC25 animals were "raced" overnight versus *ceh-12; unc-4(ts); unc-24(e138)* worms at 25°C. The *ceh-12; unc-4(ts); unc-24* mutant worms were able to chemotax to the food whereas the NC25 "stuck" mutants did not. Based on this result, we concluded that our genetic screen had the potential to discover recessive mutations that partially rescue the *unc-4* defect.

unc-24(0); unc-4(ts)

'STUCK'

EMS   F2

unc-24(0); unc-4(ts); blr

Unc-4 suppressed

Mutagenized Stuck Worms

Supressed worms can move to food

100mm Race Plate
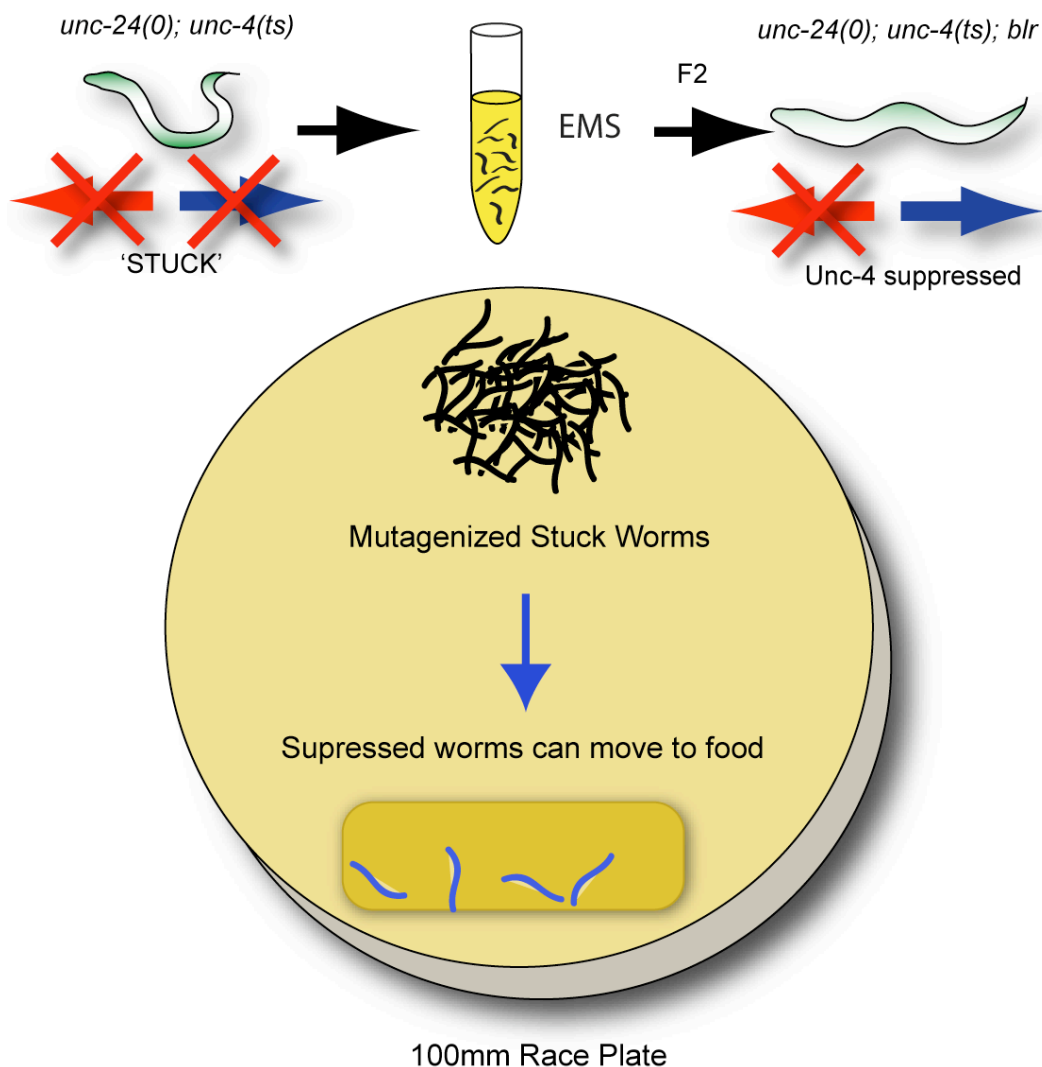
Figure 3.2. Methodology for stuck screen.

unc-4; unc-24 double mutants are defective in both forward and backward locomotion. P0 animals were mutagenized with EMS and grown to the F2 generation.   To identify suppressors of the Unc-4 backward locomotion defect, worms were 'raced' along a chemotaxis gradient to isolate worms with enhanced locomotion. We isolated strains that were suppressed for both forward (*unc-24* suppressors) and backward locomotion (*unc-4* suppressors). Unc-4 suppressed worms were identified from the 'winners' of this race by tapping each candidate on the head to stimulate backward locomotion. Unc-24 suppressors were discarded.

The "stuck" suppression genetic screen was performed as previously described (Miller et al. 1993b), with minor modifications. NC25 animals were synchronized by hypochlorite treatment, and mutagenized with 0.05M EMS during the L4 larval stage. P0 animals were placed on 150mm, plates seeded with Na22 *E. coli* bacteria, and grown at 25°C (25 P0 animals per plate) until F2 animals were largely L2 to L4 larve. F2 progeny were collected by rinsing with M9 buffer and washed 3-4 times by low speed centrifugation to remove bacteria. The number of F2 animals was estimated by placing a drop (~50μL) on a glass slide and counting under a stereo-dissecting microscope. A total of 10^6 F2 animals were screened or ~20,000 F1s (assuming ~50 F2 progeny/F1) for ~40,000 haploid genomes.

To initiate the screen, washed F2 animals were placed on one side of a 100mm NGM plate opposite a small patch of food (OP50-1) (Figure 3.2) and incubated overnight at 25°C. Animals in the bacterial patch were tapped on the head with the tip of a platinum wire to confirm enhanced backward locomotion. Candidate *blr* mutants were then picked individually to 60mm NGM OP50-1 plates for self-fertilization. 50 independent *blr* mutant strains were isolated from this screen. Unc-24 suppressor mutations (i.e. restored forward locomotion) were also identified in this screen but were discarded.

Outcrossing of *blr* mutants.

All crosses were performed at 25°C, unless otherwise stated. All Blr strains were outcrossed from the mutagenized NC25 genetic background by

104

mating with *unc-4(e2322ts)* males (previously grown at the permissive

temperature of 16°C). Unc-4 cross-progeny hermaphrodites (*unc-4(ts)/unc-4(ts);*

unc-24/+; *blr/+*) were picked from this mating and allowed to self-fertilize. Blr,

non-Unc-24, animals were recovered from the next generation and picked for

selfing until homozygous for *unc-24*(+). Most *blr* mutants segregated in the F2

generation at a 1:3 Blr/non-Blr frequency, indicating that they were recessive

mutations. In the case of the dominant *blr* mutation (*wd85*), all outcrossed F1

animals were Blr and segregated 3:1 Blr/non-Blr. In contrast, a subset of

suppressor strains did not segregate 1:3 Blr/non-Blr animals in the F2 generation

in, but rare Blr animals were discovered as F2s. These were recognized as

potential synthetic Unc-4 suppressors, with more than one mutation occurring in

a single animal. All mutations characterized in this study have been outcrossed,

$\geq$ 10x.

Blr mutant phenotype classification.

Outcrossed *blr* mutants were classified into four groups based on a

qualitative assessment of the strength of *unc-4(ts)* suppression at 25°C. Class I

mutations were well-suppressed, appearing almost wildtype in an *unc-4(e2322ts)*

background (Figure 3.3). Class II were less suppressed than Class I, but could

execute backward movement (Figure 3.3). Class III mutants required significant

prodding, but would execute at least 2 full backward body bends (Figure 3.3).

Class IV — *unc-4; unc-24; wd95*

Class III — *wd83; unc-4; unc-24*

Class II — *wd89; unc-4; unc-24*

Class I — *wd85; unc-4; unc-24*

ceh-12 — *ceh-12; unc-4; unc-24*

"Stuck" — *unc-4; unc-24*
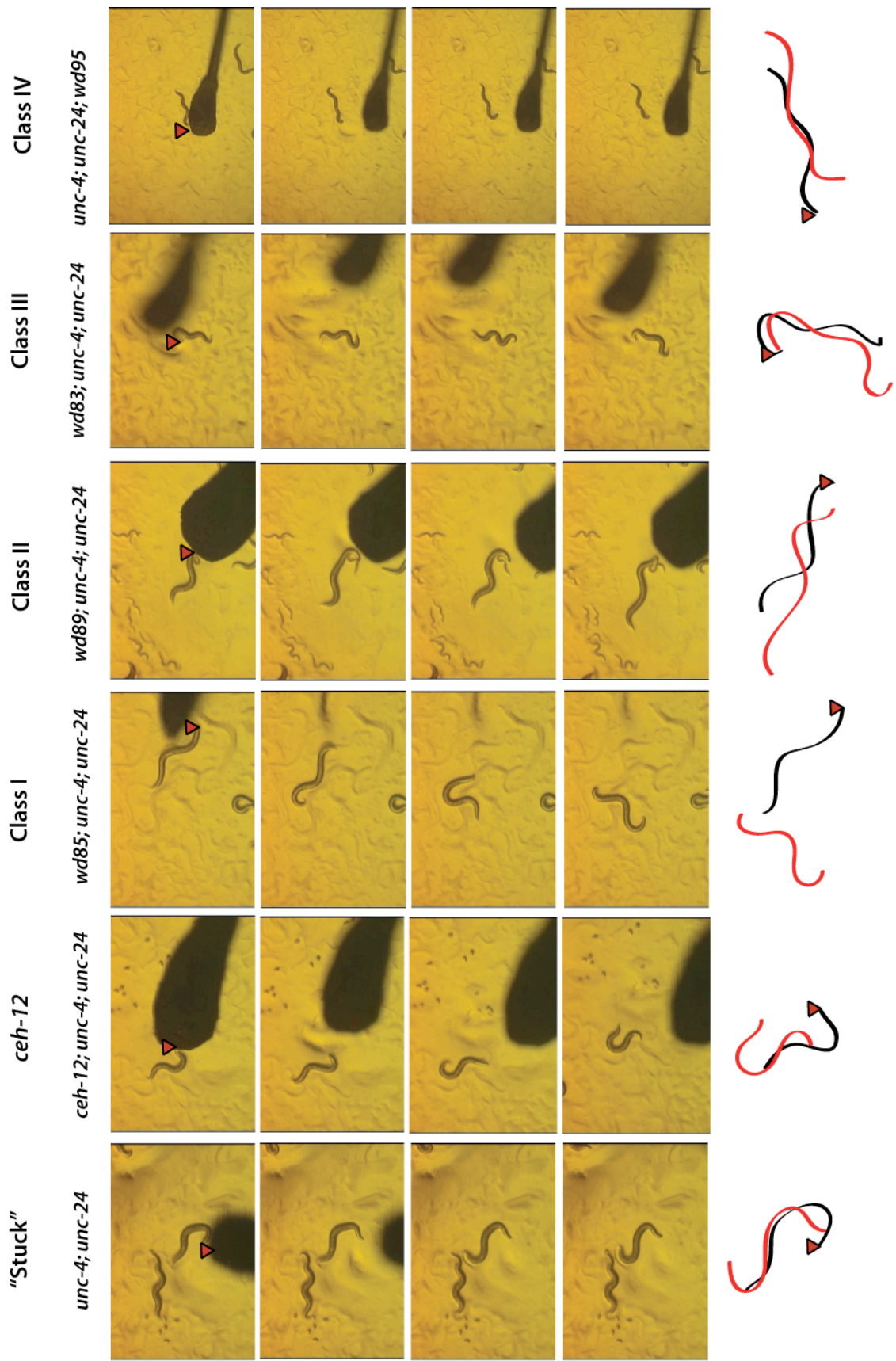
Figure 3.9. *blr* **mutants suppress** *unc-4(ts); unc-24* **"Stuck" animals.**

blr mutations exhibit a wide range Unc-4 suppression. Pannels are displayed from left to right from Class I to Class IV according to decreasing strength of Unc-4 suppression. *Top:* Genotype of animals is shown for comparison. *Middle:* pannels from movies. Animals were tapped on the head (Red triangle) to stimulate backward locomotion. *Bottom:* Overlayed, central spinal traces from the first and last video frame. Relative degree of locomotion can be assessed from these traces.

Class IV mutants show improved movement in comparison to NC25 but were typically limited to a single backward body bend (Figure 3.3).

Mapping and complementation.

The SNIP SNP mapping protocol was used to map *blr* alleles (Davis et al. 2005). Due to weak suppression of the *unc-4(ts)* allele conferred by the class III and class IV mutations, these mutations were mapped at 23°C in order to lower the threshold for Unc-4 suppression. Class I and II mutations were mapped at 25C (Figure 3.4). To initiate SNIP SNP mapping, the original, suppressed 'stuck' strain (e.g., *blr-3; unc-4(ts); unc-24*) was crossed with Hawaiian males (CB4856). F1 animals were allowed to self-fertilize at 25C and Unc-4, non-Blr F2 animals, (*unc-4(ts); blr/+; unc-24/+*) were isolated. For each strain, > 40 individual F3 Blr animals are picked to individual plates and allowed to lay eggs overnight.   F3 adults from each individual plate were combined into a single tube containing 20μL of lysis buffer (50mM KCl, 10mM Tris pH 8.3, 2.5mM MgCl$_2$, 0.45% IGEPAL CA-630, 0.45% Tween 20, 0.01% gelatin, 60μg/mL proteinase K), and frozen at –80°C for bulk segragate analysis (Davis et al. 2005). 10μL of DNA from pooled F3 animals was used for a PCR master mix containing 424μL water, 52μL 10X PCR buffer (10x: 22.5 mM MgCl$_2$, 500mM Tris-HCl, 140 mM (NH$_4$)$_2$SO$_4$, pH 9.2 at 25C), 10.4 μL 10mM dNTPs, and 3.12 μL Go-Taq (Promega). A control master mix was made using 50 wildtype, N2 animals. Each master mix was pipetted into alternating 8-lane rows of a 96 well plate. A
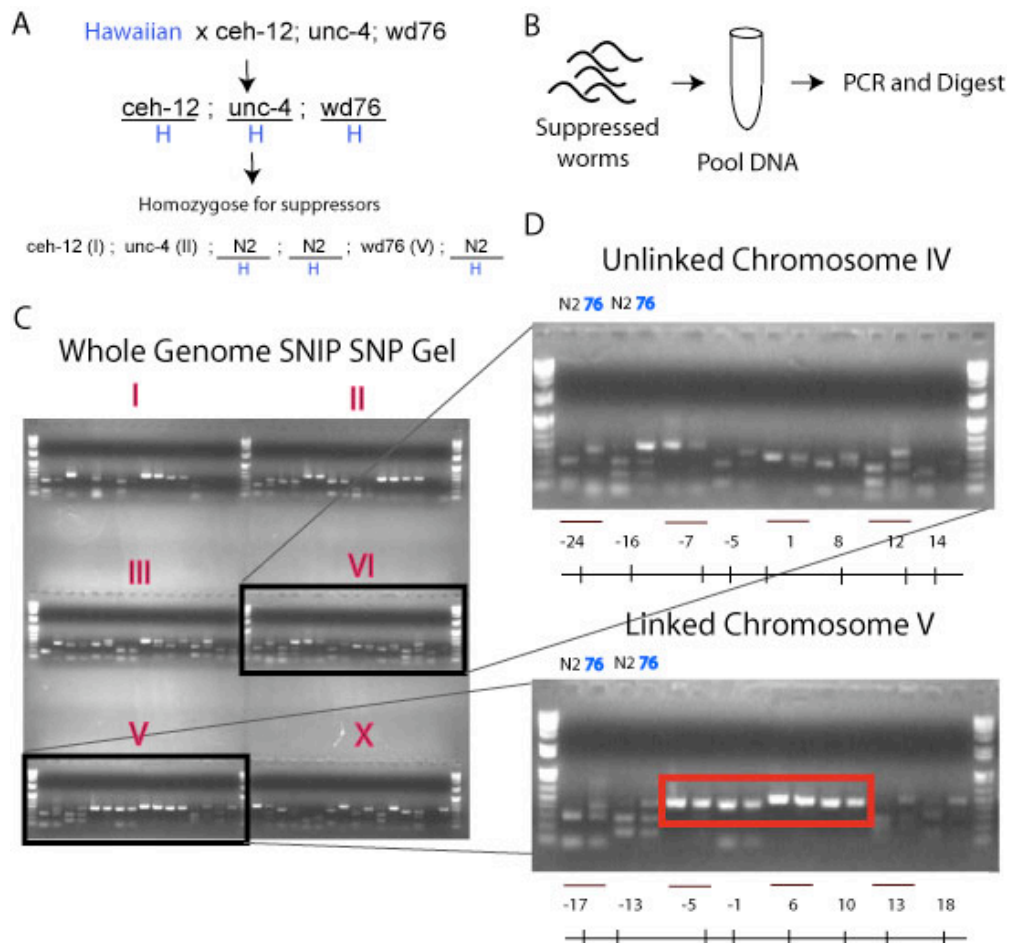
Figure 3.4. SNIP SNP mapping strategy.

A mapping strain containing suppressor mutations are crossed with Hawaiian males (CB4856), which contain different SNPs along the length of their genome. Worms are then homozygosed for unc-4, then suppressor mutations. B. Suppressed worms are pooled and used as template for PCR reactions that flank SNPs. These SNPs can be distinguished between the Bristol and Hawaiian Geneotypes by using the restriction endonuclease DraI. C. PCR reactions are performed in a 96 well format on both the template bulk segregate DNA from the previous genetic step, as well as a control DNA containing only Bristol DNA. This allows a direct comparison between the different SNPs. D. Comparison between an Unlinked chromosome and linked chromosome. Because the mutagenesis was performed in the Bristol strain, and we are selecting for these mutations, the local area of a chromosome containing the suppressor mutation will segregate with a majority of Bristol SNPs. Thus, these locations will appear to be Bristol on a gel. Unlinked chromosomes will segregate 50% Bristol and 50% Hawaiian, and will appear unlinked.

pin-replicator was used to add primers from a 96-well template (96 well plate) of 10μM for each primer pair. For each of the 6 chromosomes, 8 individual SNPs were compared by DraI restriction endonuclease digestion. PCR reactions were performed using the following conditions: 2 minutes at 94°C, 35x (15s 94°C, 45s 60°C, 1 min 72°C), 5 min 72°C, 4°C. Digestion was performed by adding 6μL to each well of the Master mix (4.15μL water, 1.6μL 10x NEB Buffer 3 (New England Biolabs), 0.25μL DraI) and incubation at 37°C at the minimum of 4 hours. Digested PCR products were loaded onto a 1.5% agarose gel by alternating lanes with N2 and *blr* DNA. This arrangement placed the N2 control PCR reaction immediately adjacent to the *blr* PCR reaction for each corresponding SNP there by allowing rapid visual inspection of the gel to identify adjacent *blr* mutant lanes with predominant Bristol (N2) SNPs and thus the chromosomal interval for the mapped *blr* allele. Individual plates containing the F4 progeny of these animals were numbered and grown to confluency. These plates were washed off with water into 1.5mL microcentrifuge tubes and pelleted at 3,000 rpm in a clinical centrifuge. Supernatant was removed and washed 3x times with water to remove residual bacteria. Animals were pelleted and 30μL of worm pellet was placed into concentrated 4x lysis buffer. PCR was performed as above, but 5μL of each primer pair (100μM), for an individual SNP, was added to the master mix instead of DNA. DNA template from the 96-well plate was pin-replicated into the plate containing the master mixes. Each SNIP (8 in total) for a single chromosome was examined using this method. This technique allowed us to isolate a specific interval using positional information conferred by Hawaiian

and Bristol SNPs. Using this technique, we have outcrossed and mapped 22 independent *blr* mutations.

Isolation of synthetic Blr mutations.

The genetic screen isolated two strains that contained mutations which function together to confer a synthetic Blr phenotype with *unc-4(e2322ts)*. The mutations *wd90* and *wd91* were first isolated within a single Class I suppressor strain. We noticed that upon outcrossing of this strain into a *unc-4(e2322ts)*, the suppressor did not segregate with a 3:1 non-Blr to Blr ratio; Blr worms showed up in the F2 generation at a much lower frequency. We suspected that this strain contained mutations in multiple loci that conferred a synthetic Blr phenotype onto *unc-4(ts)*. To test this model, we mapped these mutations using our SINP SNP protocol, however, we searched within the F3 generation (*unc-4(ts); blr*/Hawaiian; *blr*/Hawaiian) to find rare, Blr worms, in order to be certain that these mutations are recovered as homozygotes. Examination of the F4 progeny confirmed Blr phenotype in the isolated strains and thus suggested the *blr* mutations were homozygous. Our SNIP SNP results clearly showed linkage to two chromosomes, V and X (*wd90* and *wd91*), which is highly suggestive of a synthetic Blr phenotype conferred by two independent mutations. Similar results were obtained for the mutations *wd101* and *wd102* which were originally isolated as a single Class II Blr strain. These mutations mapped to chromosomes I (*wd101*) and III (*wd102*).   Due to the difficulty of working with a synthetic Blr

111

phenotype, these mutations (*wd90, wd91, wd101, wd102*) were not characterized further for this analysis.

Deficiency experiments.

SNIP SNP mapping data placed *wd77* near *dpy-13* on chromosome IV. Chromosomal deficiencies (large chromosomal deletions) were used to confirm these results and to establish physical boundaries flanking *wd77*. To perform the deficiency mapping, *egl-15::GFP* males were mated with *ceh-12; unc-4(wd1)* animals producing *ceh-12/+; unc-4(wd1)/+; egl-15::GFP/+* males, which were mated with *nT1*/Df. This mating generated the strains: (*ceh-12* or +)/+; (*unc-4(wd1)* or +)/+; (*nT1* or Df)/(*egl-15::GFP* or +). In order to homozygose the balancer and deficiency, GFP+ males and hermaphrodites from this mating (either *nT1/egl-15::GFP* or Df/*egl-15::GFP*) were mated back into each other and viable, non-GFP progeny (*nT1*/Df) were picked. A low frequency of viable, non-GFP animals from this mating, (1/16) would contain both a *ceh-12* mutation and an *unc-4* mutation. These animals were identified by PCR (*ceh-12*) and visual inspection of the F2 generation (*unc-4*). From this mating, the final strain *ceh-12; unc-4(wd1); nT1*/Df was achieved. *ceh-12; unc-25::GFP* II; *egl-15::GFP* IV males were mated with *ceh-12; unc-4(wd1); nT1*/Df to produce *ceh-12; unc-4/unc-25::GFP; egl-15::GFP/*Df males which were then mated with *ceh-12; unc-4; blr-2(wd77)*. The resulting non-GFP F1 progeny (*ceh-12; unc-4; wd77 / (Df or nT1)* were tapped on the head with a metal pick to determine if they were *Blr*. (50% of non-GFP progeny should be Df/*blr* whereas 50% should be nT1/*blr*). To control

against the possibility of assaying self-progeny from *ceh-12; unc-4; wd77*, we

assayed only male animals, which should represent cross progeny (Males occur

at a frequency of ~50% in male/hermaprodite matings, whereas they occur at a

frequency of ~0.1% in hermaprodite self-fertilization)*.* Results were (failure to

complement *wd77* shown in **bold**) ***mDF10*** (-0.3 to 0.075), ***mDF4*** (-0.8 to 2.167),

dpy-13 ama-1 mDF8 (0.9 to 2.45), ***mDF9*** (-0.969 to 2.15), *eDF19*, and *nDF41*

(1.65 to 3.37) (Figure 3.5).
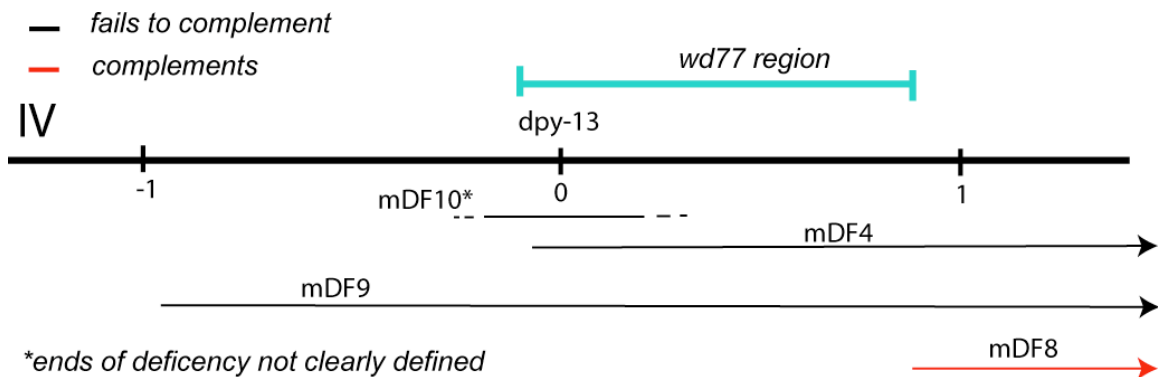
Figure 3.5. *wd77* is likely a loss of function mutation and is near *dpy-13* on chromosome IV.

Complementation tests using chromosomal deficiencies near *dpy-13* on chromosome IV suggest *wd77* is located within a 1-megabase region on this chromosome. No obvious candidate Wnt pathway genes lie within this region. *wd77* fails to complement multiple deficiencies that cover this region suggesting that *wd77* likely represents a loss of function allele.

Complementation tests.

Complementation tests were performed to identify allelic mutations. Mutations that mapped to a specific chromosome were crossed with each other using the following genetic strategy: *unc-4(e2322ts)* males (grown at 16°C), were mated with a *unc-4(ts); blr-A* hermaphrodites, and grown at 16°C to generate F1 *unc-4(ts); blr-A/+* males. These *unc-4(ts); blr-A/+* males were mated with a *unc-4(ts); blr-B* strain, generating 50% progeny *unc-4(ts); blr-A/blr-B*, and 50% *unc-4(ts); +/blr-B*. Weak Blr alleles (Class III, IV) were performed in duplicate and independently scored for complementation by two blinded observers (JS and Rachel Skelton). Discrepancies were resolved by additional complementation experiments. This method resulted in the identification of 16 different complementation groups involving 22 independent suppressor mutations.

Genetic tests.

Outcrossing of suppressor mutations

Blr alleles were outcrossed into a N2 background using an integrated GFP reporter *in trans* to the *blr* mutation. *unc-4(ts); blr* animals were crossed with males homozygous for a GFP reporter integrated on the same chromosome as the *blr* mutation. GFP+ cross-progeny were allowed to self-fertilize and F2 non-Unc, non-GFP animals were picked in successive generations to isolate a homozygous Blr strain that did not segregate Unc-4. *unc-4(ts)* males were crossed back into the *blr* strain to confirm the presence of the *blr* mutation. Only

115

one mutation showed an Unc phenotype on its own; *blr-2(wd77),* displays a loopy, backward Unc trait. This loopy Unc phenotype, however, did not interfere with *blr-2(wd77)* animals ability to complete sinusoidal locomotory waves that promote backward movement.

Construction of strains containing multiple mutations

All crosses were performed at 23°C, unless otherwise stated. Integrated GFP reporters were used in genetic crosses to mark the chromosome *in trans* to selected mutants: *euIs82a[unc-129::GFP; dpy-20+]* (I), *juIs76[unc-25::GFP; lin-15+]* (II), *rhIs2[glr-1::GFP]* (III), *ayIs2[egl-15::GFP]* (IV), *mIs11[myo-2::GFP, pes-10::GFP, gut::GFP]* (IV), *ccIs9753[myo-2::GFP]* (V), *oyIs44[odr-1::RFP]* (V), *oxIs12[unc-47::GFP]* (X). The deletion allele of *ceh-12(gk391)* was verified by PCR as previously described (Von Stetina et al. 2007b).

Quantification of the blr phenotype

A movement assay was used to detect effects of specific *blr* mutants on unc-4-dependent backward locomotion (Von Stetina et al. 2007b). The experimenter was blinded to genotype to avoid bias. For each genotype, $\geq$ 50 L4-young adult animals (at 23°C, unless otherwise noted) were tapped a single time on the head with the tip of a platinum wire. Backward movement was scored as either **Unc** (coiled instantly with no net backward movement) or as **Non-Unc** (detectable backward movement of posterior region or entire body). Statistical tests of differential effects on backward locomotion were performed using the Fisher's Exact Test.

Anti-GFP immunostaining to detect AVB gap junctions with ventral cord motor neurons.

The chromosomal integrant NC1694 (*wdIs54*[*punc-7*::UNC-7S:GFP, *col-19*::GFP] *unc-7*(*e5*) X) was generated by gamma irradiation (4000 Rads) (Mello et al. 1991) of EH578 (Starich et al. 2009a) and 10X backcrossed into the wildtype N2 strain. Standard methods were used to cross *wdIs54* into other genetic backgrounds (Brenner 1974). Embryos were obtained by hypochlorite treatment and allowed to hatch overnight in M9 buffer. The resultant growth-arrested L1 animals were applied to bacterial feeding plates and gap junctions staining scored in the late L4 larval stage. AVB gap junctions with ventral cord motor neurons were detected by anti-GFP immunostaining as previously described (Von Stetina et al. 2007a). Motor neuron soma with adjacent UNC-7S::GFP marked puncta (AVB gap junctions) were scored in the region of the ventral nerve cord between VA2 and VA11. [VA2-VA11, VB3-VB11, DA2-DA7, DB3-DB7, DD2-DD5, VD3-VD11, AS2-AS10, and VC1-VC6]. At least 10 neurons at each position for each motor neuron class were observed for a given genotype and assigned a score of gap junction 'present' or 'absent'. The experimenter was blinded to genotype to rule out bias. A Fisher's exact test was used to estimate statistically significant differences ($p < 0.05$) for the presence versus absence of UNC-7S::GFP puncta for each individual neuron for each genotype (e.g. VA2 of wildtype was compared to VA2 of *unc-4*).

GRASP (GFP Reconstitution Across Synaptic Partners).

GRASP (split-GFP) experiments were performed using the TV1477 (*wyEx1914[unc-4::NLG-1::spGFP1-10, flp-18::NLG-1::spGFP11, flp-18::mCherry::rab-3, odr-1::DsRed2]*) generously provided by K. Shen (Stanford). The split-GFP signal appears as discrete puncta, which corresponds to specific chemical synapses between AVA and A-class (DA, VA) motor neurons in the ventral nerve cord. To limit quenching by exciting light, GFP puncta were scored within specific zones: Zone 1, VA2-VA4; Zone 2, VA5-VA6; Zone 3, VA7-VA8; Zone 4, VA9, VA10. Scoring was limited to animals showing expression of the co-selectable marker *odr-1::DsRed2* in the head and split-GFP puncta adjacent to VA11, which is not miswired in *unc-4* mutants (White et al. 1992a). The experimenter was blinded to genotype to rule out bias. To score each animal, the 100x objective lens positioned over each zone using DIC optics within the plane of the ventral nerve cord before exposing the region to GFP exciting light and quickly noting the presence or absence of GFP puncta.

RESULTS

A pilot mutant screen for Unc-4 suppressor genes that function in parallel to *ceh-12*/HB9.

Previous work in the Miller lab showed that the *unc-4* target gene, *ceh-12*/HB9, is selectively de-repressed in posterior VA motor neurons in *unc-4* mutants to induce miswiring with VB-type inputs. The functional role of *ceh-12*/HB9 was confirmed by a genetic epistasis experiments in which *ceh-12* loss-

of-function mutants suppress the formation of ectopic VB-type gap junctions with the command interneuron AVB. This role of *ceh-12* is limited to VA motor neurons in the posterior ventral nerve cord which therefore suggests that *unc-4* must regulate (i.e., repress) at least one additional target that functions in parallel to *ceh-12* in anterior VAs (Figure 3.1) (Von Stetina et al. 2007a). This model is also consistent with the finding that *ceh-12* affords only weak suppression of the backward movement defect of an *unc-4(0)* allele, presumably due to the restoration of normal inputs only to posterior VAs. We reasoned that a mutation in an anterior VA target should enhance *ceh-12* suppression and therefore should be detectable as a *"blr"* (*b*ackward *l*ocomotion *r*estored) mutant with significantly improved backward movement in comparison to the *ceh-12(0); unc-4(0)* parent strain. This reasoning provided the rationale for an initial pilot screen for *blr* alleles. Hermaphrodites that were mutant for both *ceh-12* and *unc-4* null alleles [*ceh-12(gk391); unc-4(wd1)*] were mutagenized with EMS. F2 progeny of ~5,000 F1 animals were examined in a clonal screen for improved backward locomotion. Two recessive *blr* alleles, *wd76* and *wd77,* were identified. (A detailed phenotypic characterization of these alleles is provided below). Genetic mapping (see below) and complementation tests confirmed that *wd76* and *wd77* affect different genes and thus that the screen was not saturated. The pilot screen was labor intensive, however, and prompted us to develop a more efficient strategy for isolating additional *blr* mutations.

Isolation of recessive Unc-4 suppressor mutants from a synthetic Unc phenotype.

As noted above, *ceh-12(0)* is a weak suppressor of *unc-4* null alleles; *ceh-12(0);unc-4(0)* double mutant animals are capable of initiating sinusoidal waves (i.e., wiggling the tail) but are unable to sustain backward locomotion (see Methods). In contrast, *ceh-12(0)* double mutants with *unc-4* hypomorphic alleles show a robust Blr phenotype with strong backward movement. For example, 96% of animals that are mutant for *ceh-12* and the temperature sensitive allele, *unc-4(e2322ts)*, show virtually wildtype backward locomotion at restrictive temperature (25°C) (Table 3.2). We reasoned therefore, that an independent mutation in a pathway acting in parallel to *ceh-12* (e.g., to regulate inputs to anterior VA motor neurons) should also afford strong suppression of *unc-4(e2322ts)*. This prediction was confirmed by our finding that the *wd76* and *wd77* *blr* alleles isolated as *ceh-12* enhancers of Unc-4 suppression, also restore backward locomotion to *unc-4(ts)* at 25°C (Table 3.1). To enhance detection of new potential *blr* alleles, we utilized an allele of *unc-24*, which blocks forward locomotion. This combination of *unc-4* and *unc-24* mutations results in a synthetic "Stuck" phenotype in which *unc-4(ts); unc-24(0)* animals are unable to crawl either forward or backward. In this genetic background, however, *ceh-12(0)* animals can move sufficiently well to traverse a 100 mm plate and reach a patch of bacterial food in an overnight test (data not shown) whereas the majority of "Stuck" animals are immobilized. This approach effectively selects for candidate Blr mutants (i.e. F2 progeny that reach the bacterial patch) and therefore avoids the necessity of testing each F2 animal individually for improved backward

120

movement as in the pilot screen. The *unc-4; unc-24* stuck strain was previously utilized in the Miller lab to isolate dominant F1 suppressor alleles of *unc-37*/Groucho (Miller et al. 1993b). The *unc-37(d)* allele isolated in the earlier screen corresponds to an UNC-37 missense mutation that restores physical interaction with mutant UNC-4 protein (Pflugrad et al. 1997b; Winnier et al. 1999). In this case, we screened F2 animals to search for potential recessive loss-of-function *blr* alleles. With this approach, we tested ~10^6 F2 animals to identify > 50 *blr* mutants. Blr alleles were initially grouped in four broad categories based on a qualitative estimate of the strength of Unc-4 suppression (Table 3.1). Outcrossing recovered 22 independent *blr* alleles that map to 16 different complementation groups (see Methods). A selected group of these *blr* alleles is characterized in detail below.

Blr mutations correspond to Wnt pathway genes.

We noticed that a group of six alleles with comparable Blr phenotypes mapped to the left arm of chromosome I in the vicinity of the Wnt pathway genes *mig-1*/Frizzled and *pop-1*/TCF. Independent experiments in the Miller lab have established that ectopic *ceh-12* expression in posterior VAs depends on an EGL-20/Wnt signal emanating from nearby cells in the tail (Chapter 2). This model is supported by genetic epistasis experiments showing that *egl-20* displays a strong Blr phenotype as a double mutant with *unc-4(ts)*. Moreover, *egl-20* does not enhance the Blr trait of *ceh-12* in combination with *unc-4(0)* alleles. Additional
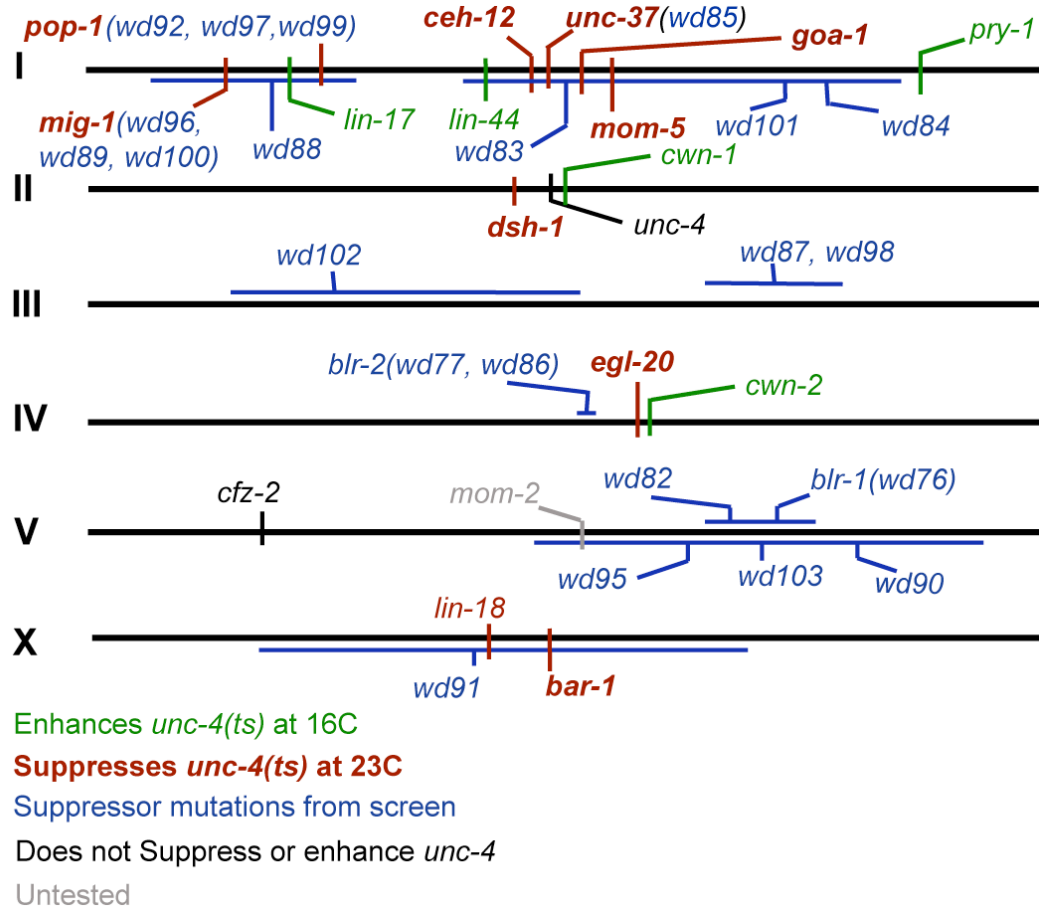
Figure 3.6. Map of suppressor mutants identified in genetic screen.

We have mapped 22 suppressor mutants to locations on the *C. elegans* genome, resulting in a total of 16 complementation groups. Two of these complementation groups fail to complement known components of the Wnt signaling pathway (*pop-1* and *mig-1*). Other Wnt pathway loci and genetic interactions with *unc-4* are indictaed.

Degree of *unc-4(e2322ts)* suppression	Mutation
Class I	*wd85, (wd90, wd91)*
Class II	**wd76***, *wd89, wd98, wd104, (wd101, wd102)*
Class III	**wd77***, ***wd82, wd83, wd87, wd88**, *wd93, wd94, wd96*
Class IV	*wd84, wd92,* **wd95**, *wd86, wd97, wd99, wd100, wd103*

Table 3.1. Degree of *unc-4* suppressor activity of mutations in *unc-4(e2322ts)* background.

Unc-4 suppressor mutations were initially classified according to suppressor strength. Class IV mutations were extremely weak, and required significant prodding in order to complete a sinusoidal backward movement whereas Class I mutations were almost wildtype at 25°C. Alleles in **boldface** are characterized in this study. * Indicates alleles identified in pilot screen. () Synthetic Unc-4 suppressor mutations isolated in same strain. See methods.

genetic tests established that the Wnt receptor encoding gene *mig-1*/Frz

functions downstream of *egl-20* to activate *ceh-12* expression in posterior VAs

(Chapter 2). Complementation tests confirmed that *blr* alleles, *wd89, wd96* and

wd100 are *mig-1* alleles. As homozygotes, *wd89, wd96* and *wd100*, show a

similar extent of Unc-4 suppression as the canonical loss-of-function allele *mig-

1(e1787)*. Additional genetic experiments revealed that *blr* alleles *wd92, wd97*

and *wd99* fail to complement *pop-1(hu9)*. This result is consistent with a model in

which *pop-1*/TCF functions downstream of MIG-1/Frz in a canonical Wnt

signaling pathway to drive *ceh-12* expression (Chapter 2). In addition to

providing independent confirmation of the role of Wnt signaling in *ceh-12*

expression, these results also show that our Blr mutant screens were capable of

detecting *bona fide* suppressors of the Unc-4 defect.

Genetic test for *blr* alleles that function in parallel to *ceh-12*.

blr alleles affecting genes that function in parallel to *ceh-12* are predicted

to satisfy three conditions: (1) Phenocopy *ceh-12* suppression of hypomorphic

unc-4 alleles; (2) Enhance *ceh-12* suppression of *unc-4(0)* alleles; (3) Suppress

the appearance of ectopic AVB gap junctions with anterior, but not posterior,

VAs. These criteria were evaluated for six independent *blr* mutations (*wd76,

wd77, wd82, wd87, wd88, wd95*) (Figure 3.6) each one representing a different

complementation group.

blr mutations rescue the Unc-4 backward locomotion defect in _unc-4_ hypomorphic alleles.

We tested the first condition using two different hypomorphic alleles of _unc-4_, _e2322ts_ and _e2323_. The temperature sensitive allele _unc-4(e2322ts)_, corresponds to a L to F amino acid substitution in the DNA-binding homeodomain. Although ectopic _ceh-12_ expression is limited to posterior VA motor neurons in _unc-4(ts)_ mutant animals, _ceh-12(0)_ strongly suppresses the _unc-4(ts)_ backward movement defect. In contrast, _ceh-12(0)_ results in weak suppression of _unc-4_ null alleles (Table 3.2). One explanation for this disparity is that the UNC-4(ts) protein retains residual transcriptional repressor activity. In this scenario, UNC-4 target genes functioning in anterior VAs are partially repressed in _unc-4(ts)_ animals such that the loss of _ceh-12_ activity in posterior VAs elevates overall VA activity above a critical threshold that restores backward movement (Von Stetina et al. 2007b). All of the blr alleles (_wd76, wd77, wd82, wd87, wd88, wd95_) suppress _unc-4(ts)_. The _e2323_ mutation corresponds to an R to Q amino acid substitution that disrupts physical interaction with UNC-37/Groucho and thus perturbs repression of _unc-4_ target genes (Winnier et al. 1999). In this case, only three of the six _blr_ alleles tested (_wd77, wd87, wd95_) suppress _unc-4(e2323)_ and in each instance, _ceh-12(0)_ displays a stronger suppressor phenotype. We attribute these results to the potentially distinct molecular effects of these mutations on _unc-4_ pathway function.

Table 3.2.

	Percentage Unc	Percentage Suppressed	p < 0.05
WT	0	100	
unc-4(e2320)	98	2	
unc-4(e120)	99	1	
ceh-12(gk391); unc-4(e120)	**54**	**46**	*
ceh-12(gk391); unc-4(e2320)	**58**	**42**	*
ceh-12(gk391); unc-4(wd1)	**62**	**38**	*
unc-37(e262)	87	13	
WT	0	100	
blr-2(wd77)	0	100	
blr-1(wd76)	0	100	
blr-9(wd88)	0	100	
blr-8(wd87)	2	98	
blr-3(wd82)	0	100	
blr-15(wd95)	0	100	
ceh-12(gk391)	0	100	
ceh-12(gk391); blr-2(wd77)	0	100	
ceh-12(gk391); blr-1(wd76)	2	98	
ceh-12(gk391); blr-8(wd87)	0	100	
ceh-12(gk391); blr-3(wd82)	0	100	
unc-4(e2323)	63	38	
unc-4(e2323); blr-2(wd77)	**23**	**77**	*
unc-4(e2323); blr-1(wd76)	50	50	
blr-9(wd88); unc-4(e2323)	62	38	
unc-4(e2323); blr-8(wd87)	**28**	**72**	*
unc-4(e2323); blr-3(wd82)	64	36	
unc-4(e2323); blr-15(wd95)	**20**	**80**	*
unc-4(e2320)	98	2	
unc-4(e2320); blr-2(wd77)	99	1	
unc-4(e2320); blr-1(wd76)	100	0	
blr-9(wd88); unc-4(e2320)	100	0	
unc-4(e2320); blr-3(wd82)	96	4	
unc-4(e120)	99	1	
unc-4(e120); blr-2(wd77)	100	0	
blr-9(wd88); unc-4(e120)	94	6	
unc-4(e120); blr-8(wd87)	**80**	**20**	*
unc-4(e120); blr-3(wd82)	96	4	
unc-4(e120); blr-15(wd95)	**64**	**36**	*

ceh-12(gk391); unc-4(e2320)	58	42	
ceh-12(gk391); unc-4(e2320); blr-2(wd77)	**96**	**4**	*
ceh-12(gk391); unc-4(e2320); blr-1(wd76)	46	54	
ceh-12(gk391); unc-4(e2320); blr-8(wd87)	51	49	
ceh-12(gk391); unc-4(e2320); blr-3(wd82)	**38**	**62**	*
ceh-12(gk391); unc-4(wd1)	62	38	
ceh-12(gk391); unc-4(wd1); blr-2(wd77)	**86**	**14**	*
ceh-12(gk391); unc-4(wd1); blr-1(wd76)	**24**	**76**	*
ceh-12(gk391); unc-4(e120)	54	46	
ceh-12(gk391); unc-4(e120); blr-15(wd95)	**16**	**84**	*
ceh-12(gk391); unc-4(e120); blr-1(wd76)	**1**	**99**	*
ceh-12(gk391); unc-4(e120); blr-3(wd82)	**16**	**84**	*
unc-37(e262)	87	13	
ceh-12(gk391) unc-37(e262)	**49**	**51**	*
unc-37(e262); blr-2(wd77)	**94**	**6**	*
unc-37(e262); blr-2(wd76)	80	20	
unc-4(e120); blr-8(wd87)	80	20	
blr-9(wd88); unc-4(e120); blr-8(wd87)	82	18	
unc-4(e2320); egl-20(n585)	46	54	
blr-9(wd88); unc-4(e2320); egl-20(n585)	**96**	**4**	*

Table 3.2: Genetic results of *blr* mutants on Unc-4 suppression.

Table of genetic suppressor mutations and their effect on the restoration of *unc-4* backward movement. Mutations in *wd82, wd76, wd95, wd77*, function in parallel to *ceh-12*. *wd87* mutants do not appear to enhance *ceh-12* suppression of Unc-4. **Boldface and *** indicates statistical significance ($p < 0.05$ from control strain by Fisher's Exact Test). Control strain is listed as first strain in each group, except for the first group listed which compares *ceh-12* suppression of individual *unc-4* alleles. n > 50 for all strains listed.

Table 3.3. Genetic evidence for *blr* gene function in parallel to *ceh-12*		
blr alleles	Enhance *ceh-12* suppression of Unc-4 movement	Suppress AVB gap junctions with anterior VA motor neurons
wd76	yes (*wd1, e120*)	yes (VA3, VA6, VA7)
wd77	no	no (VA10)
wd82	yes (*e2320, e120*)	yes (VA5, VA6)
wd87	no*	yes (VA2-4, VA8)
wd88	ND	yes (VA2, VA3, VA5, VA8)
wd95	yes (*e120*)	yes (VA3, VA6, VA7)
* *wd87* fails to enhance *ceh-12* suppression of *unc-4(e2320)* but was not tested against *ceh-12; unc-4(e120)*.		

Table 3.3. Genetic evidence for *blr* gene function in parallel to *ceh-12*.

This table summarizes the data presented in Table 3.2. Four suppressor alleles (*wd76, wd77, wd82,* and *wd95*) enhance suppression of *ceh-12* in at least one *unc-4(0)* allele. Two of these alleles (*wd76, wd95*) also suppress ectopic inputs from AVB in *unc-4(e120)*. Note about *wd77*: tapping assay results show that *wd77* seems to antagonize *ceh-12* suppression of *unc-4* although *wd77* was originally isolated in a genetic screen in the *ceh-12; unc-4(wd1)* background as an enhancer of *ceh-12*.

A subset of blr mutations enhance *ceh-12* suppression of *unc-4(0).*

Our results showing that *blr* alleles suppress *unc-4* hypomorphic mutations are consistent with the alternative possibilities that the *blr* mutations disrupt genes that function either in the *ceh-12* pathway or in parallel. To distinguish between these models, we tested these *blr* alleles for enhancement of *ceh-12(0)* suppression of *unc-4(0)* mutants and thus evidence for function in a parallel pathway. (*wd88* was not tested in this assay because of linkage to *ceh-12* on chromosome I).

Experiments with three different *unc-4* null mutations detected three recessive *blr* alleles (*wd76, wd82, wd95*) that enhance *ceh-12* suppression of Unc-4: all three alleles, *wd76, wd82,* and *wd95,* enhance suppression of *ceh-12; unc-4(e120)*; one allele, *wd76*, enhances suppression in the *ceh-12; unc-4(wd1)* background (Table 3.2, 3.3); one allele, *wd82*, enhances backward locomotion of *ceh-12; unc-4(e2320)*. All three of these *unc-4* alleles are predicted nulls: *e120* frame shifts the translational reading frame in the conserved C-terminal UNC-37/Groucho domain; *wd1* is a large deletion that removes the *unc-4* gene and upstream regions; *e2320* deletes exons encoding the UNC-4 homeodomain and disrupts the reading frame. The reasons for the different genetic interactions of these *unc-4* alleles with *ceh-12* and *blr* mutants are unclear. For example, *wd76* enhances *ceh-12* suppression of *unc-4(e120)* and *unc-4(wd1)* but has no effect on *ceh-12; unc-4(e2320)*. In any case, the observed enhancement of the *ceh-12* Blr phenotype in at least one of these *unc-4(0)* genetic backgrounds is

consistent with the proposal that three of these *blr* genes, *wd76, wd82,* and

wd95, function in parallel to *ceh-12*.

blr mutations suppress the Unc-4 miswiring defect of specific VA motor neurons.

VA motor neurons are miswired with gap junctions from AVB interneurons

in *unc-4* mutants (White et al. 1992b; Von Stetina et al. 2007b). In wild type

animals, gap junctions with AVB are normally reserved for B-class motor neurons

(DB and VB)(White et al. 1976b). We have previously shown that *ceh-12*

expression is limited to posterior VAs in *unc-4* mutants and that *ceh-12* functions

in this subset of VA motor neurons to promote the creation of gap junctions with

AVB (Von Stetina et al. 2007b). Thus, mutations in *blr* genes from pathways in

parallel to *ceh-12* are predicted to eliminate AVB gap junctions with anterior VAs.

We tested this idea by assaying *blr* alleles for suppression of the Unc-4 AVB gap

junction defect. For these experiments, we utilized an UNC-7S::GFP marker (see

Methods) that co-localizes with AVB gap junctions in the ventral nerve cord as

discrete GFP-stained puncta adjacent to the cell soma of motor neuron partners

(Von Stetina et al. 2007b; Starich et al. 2009b).

The results of this assay confirmed that *blr* alleles *wd76* and *wd95* are

likely to affect genes that function in parallel to *ceh-12*. In both cases, the

creation of AVB gap junctions with anterior *unc-4* mutant VA motor neurons is

suppressed. For example, all VA motor neurons scored in this assay (VA2-VA10)

show ectopic UNC-7S::GFP puncta in the reference allele, *unc-4(e120)* (Figure

3.7). However, in the double mutant *unc-4(e120); blr-15(wd95)*, AVB gap
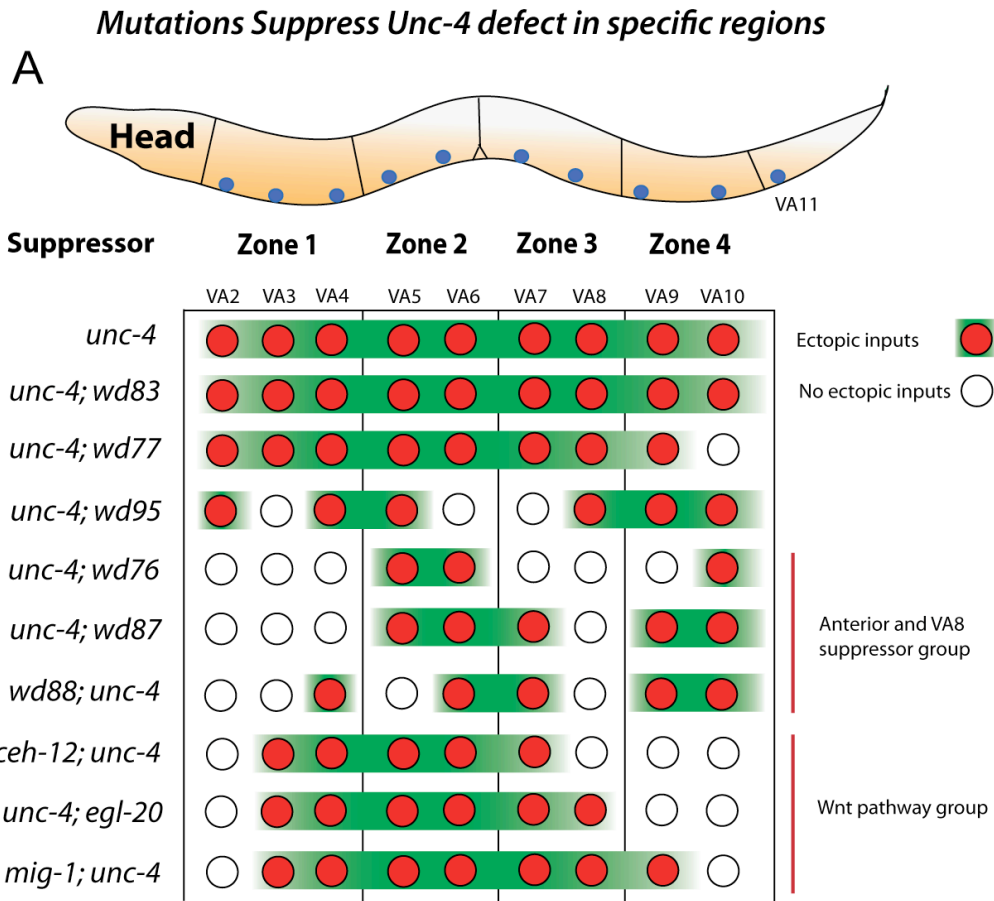
Figure 3.7. *blr* mutants suppress the *unc-4* AVB to VA gap junction miswiring defect for specific VA motor neurons.

blr mutants suppress ectopic AVB to VA gap junction connections onto specific VA motor neurons in *unc-4* mutants. Ectopic AVB gap junction connections (red circles) represent statistically significant differences in wiring (p < 0.05, Fisher's Exact Test) when the frequency of AVB gap junction connections in *blr; unc-4(e120)* double mutants versus *unc-4(e120)*. *wd76, wd87,* and *wd88* suppress ectopic gap junction connections in a similar subset of motor neurons (VA2-4, VA8) and may function in a common pathway. *wd95* suppresses ectopic connections only in VA6 and VA7, suggesting it may represent a different signaling pathway. *ceh-12, egl-20,* and *mig-1*, mutations function in a common pathway and suppress gap junctions in VA2, VA9, and VA10.

131

junctions are observed at a significantly lower frequency for VA3, VA6 and VA7.

Similarly, *wd76* suppresses the AVB gap junction defect for VA2-VA4 and VA7-

VA9. These results are consistent with the finding above that *wd76* and *wd95*

enhance *ceh-12* suppression of the *unc-4(e120)* backward movement defect

(Table 3.3).

Surprisingly *wd87* did not enhance *ceh-12* suppression of *unc-4(e2320)* in

the tapping assay (Table 3.3); *wd87* does suppress the AVB gap junction defect

for anterior VA motor neurons (VA2-4, VA8) in the null allele *unc-4(e120)* and

therefore is also likely to function in parallel to *ceh-12*. Similarly, *wd88*, which was

not tested as a *ceh-12* enhancer of backward movement (see above), effectively

reduces ectopic AVB gap junctions for VA motor neurons in which *ceh-12* does

not function (i.e. VA3, VA5, VA8) and therefore is likely to regulate the specificity

of VA inputs to these cells. The effects of *wd87* and *wd88* on a common set of

VA motor neurons, led us to hypothesize that these two mutations may affect

genes that function in the same pathway. In order to test this hypothesis, we

created the strain *blr-9(wd88); unc-4(e120); blr-8(wd87).* Based on the

assumption that *wd88* and *wd87* are null alleles, our hypothesis suggests that if

these two mutations function in parallel pathways, then these mutations are likely

to have a synergistic function and *wd88* mutations will enhance *wd87*

suppression of the Unc-4 backward movement defect in *unc-4(e120).* If these

mutations function in a common pathway, however, our hypothesis suggests that

wd88 will not enhance *wd87* suppression of *unc-4(e120).* In the tapping assay,

blr-9(wd88); unc-4(e120); blr-8(wd87) animals were no more suppressed than

the *unc-4(e120); blr-8(wd87)* mutant alone (Table 3.2). This result is consistent with the finding that *wd87* and *wd88* suppress the AVB gap junction defect in an overlapping set of VA motor neurons (VA2, VA3, VA8) and could function in a common pathway.

We note that *wd77* specifically suppresses the AVB gap junction defect for VA10 but not for more anterior VAs (Figure 3.7). This result was surprising because *ceh-12* also functions in VA10 and the isolation of *blr-2(wd77)* in the pilot Unc-4 suppressor screen suggests that *wd77* enhances *ceh-12* suppression of Unc-4 movement (Table 3.3). We note, however, that the tapping assay failed to confirm that the outcrossed *wd77* allele enhances *ceh-12* suppression of Unc-4. We attribute this discrepancy a potential synthetic Blr phenotype for the original *wd77* isolate and that one of the suppressor loci was lost during outcrossing. Together these results suggest that *ceh-12* and *blr-2(wd77)* may function in the same pathway to regulate the specificity of interneuron gap junctions with VA10. This model could be tested by asking if *wd77* affects *ceh-12::GFP* expression.

We note that *wd82*, which enhances *ceh-12* suppression of Unc-4 movement (Table 3.3), was not tested for suppression of the AVB gap junction defect. Evidence for parallel roles for *blr* genes in VA motor neuron connectivity is also supported by our finding of two synthetic *blr* strains that depend on the simultaneous occurrence of mutations in separate loci (see Methods). In summary, these assays identified alleles from five different *blr* loci (*wd76, wd82, wd87, wd88, wd95*) that suppress the AVB to VA gap junction defect in anterior

VA motor neurons and thus are likely to affect genes that function in parallel to *ceh-12*.

As a positive control for these experiments, we confirmed that *ceh-12* suppresses the AVB gap junction defect for posterior VAs as previously reported (Von Stetina et al. 2007b) (Figure 3.7). We also observe *ceh-12(0)* suppression of AVB gap junctions with VA2 at the anterior end of the ventral nerve cord although a *ceh-12::GFP* reporter is exclusively expressed in posterior VAs in *unc-4* mutants (Von Stetina et al. 2007b). However, here we note that mutations in Wnt pathway genes, *egl-20*/Wnt and *mig-1*/Frz, that are required for ectopic expression of *ceh-12::GFP* in posterior VAs, also suppress the AVB gap junction miswiring defect in VA2. These results strongly suggest that the endogenous *ceh-12* gene must be expressed in VA2 in *unc-4* mutants and that this effect depends on Wnt signaling. A role for Wnt signaling in VA2 is surprising because EGL-20 is reported to be exclusively expressed in cells in the tail region that are posterior to VA10 (Coudreuse et al. 2006). Either VA2 is particularly sensitive to this remote *egl-20*/Wnt cue or EGL-20 is also expressed in anterior cells that have not been previously detected.

blr mutants restore AVA to VA chemical synaptic inputs.

GFP Reconstitution Across Synaptic Partners (GRASP) was recently developed as an assay for detecting specific synapses between two individual neurons (Feinberg et al. 2008). GRASP relies on split-GFP technology in which two halves of GFP are tagged with the NRG-1/Neuroligan protein, which

localizes to pre and post-synaptic domains, and expressed in two different neurons. These NRG-1::GFP-fragments then interact trans-synaptically to reconstitute a complete fluorescent GFP protein at sites of synaptic contact between the NRG-1::GFP-expressing neurons.

Expression of the *flp-18::NLG-1::spGFP11* in AVA and the *unc-4::NLG-1::spGFP1-10* in VA motor neurons produces discrete GFP puncta in the ventral nerve cord that correspond to AVA synapses with A-class motor neurons; a subset of GRASP GFP puncta are eliminated in *unc-4* mutants (Feinberg et al. 2008) as predicted by EM studies showing that AVA synapses with VA motor neurons (VA2-VA10) are absent in *unc-4* mutant animals (White et al, 1986). I used this strain to ask if *blr* alleles restore AVA to VA synapses as double mutants with *unc-4*. As shown in Figure 3.8, GRASP puncta are largely undetectable in L4 stage *unc-4(ts)* animals (grown at 25°C). In contrast, *unc-4(ts)* animals at the L1 larval stage showed significantly more GRASP staining. This result suggests that *unc-4* function is required for maintaining AVA to VA synapses but is not necessary for the initial establishment of these connections. This finding is consistent with temperature shift experiments with the *unc-4(ts)* allele showing that *unc-4* function is required during the L2 and L3 stages (Miller et al. 1992). However, it will be important to replicate this GRASP experiment with an *unc-4* null allele to determine if initial AVA to VA synapses are a consequence of residual UNC-4 function in the *unc-4(ts)* allele. A comparison of these findings for the *unc-4(ts)* allele to GRASP results for *blr* alleles, *wd76* and *wd77*, detected significantly more GRASP GFP puncta in the *wd76; unc-4(ts)*
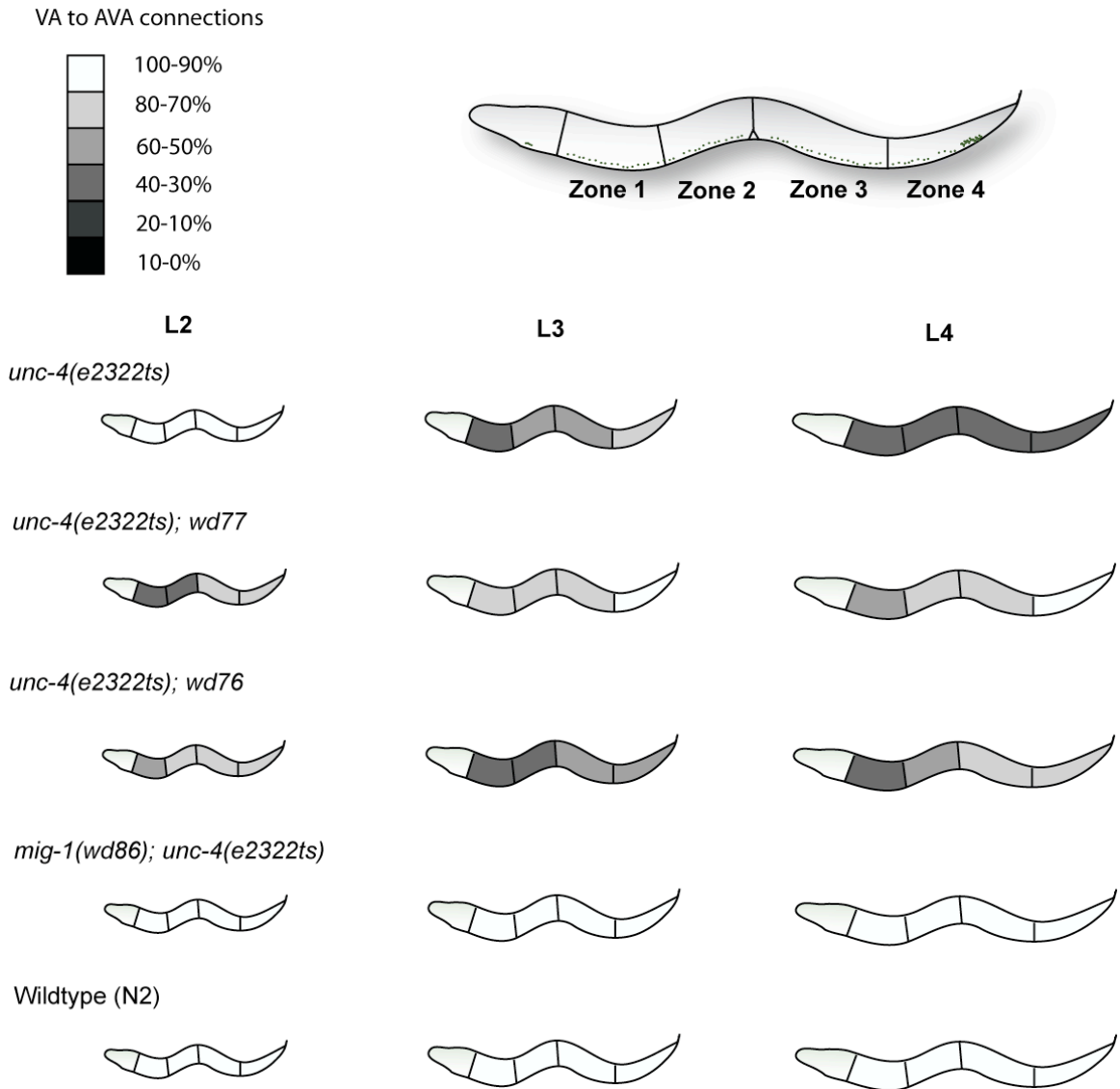
Figure 3.8. *blr* mutants restore AVA to VA wiring in *unc-4* mutants.

GRASP GFP puncta corresponding to AVA to A-class synapses were scored in four distinct zones along the A/P body axis (see Figure 3.7). AVA-A-class synapses progressively declined from L2 animals as the worms aged. Very few GFP puncta were detected in L4 *unc-4(e2322ts)*. Note strains restoration of AVA-A-class synapses in posterior Zone 4 for *wd77* and a detectable increase in GRASP puncta for *wd76*. *mig-1(wd86)* resulted in strong restoration of AVA-VA synapses throughout the VNC.

and *wd77;unc-4(ts)* doubles than in *unc-4(ts)* alone. Restoration of GRASP

puncta was more pronounced in L4 than for L1 animals but some suppression

was detected at all larval stages examined. The *mig-1(wd86)* allele results in

restoration of GRASP puncta throughout the ventral cord. This result is surprising

given our findings that *mig-1* is selectively required for miswiring of posterior VAs

with AVB gap junctions. Additional tests with genes that function in the EGL-

20/Wnt pathway (Chapter 2) are needed to confirm this result.

blr alleles induce miswiring of selected VA motor neurons.

As noted above, mutations in *ceh-12* and in selected *blr* genes suppress

the creation of AVB gap junctions with specific VA motor neurons. These results

suggest that the wildtype *blr* gene products promote the AVB miswiring defect in

unc-4 mutants. We were therefore surprised to detect evidence that some of the

blr genes in fact adopt the opposite role in other VA motor neurons of inhibiting

the creation of AVB gap junctions (Figure 3.9). For this assay, we examined the

potential effects of *blr* mutations on VA inputs in a wildtype background. For

example, *wd95* suppresses AVB gap junction inputs with VA3, VA6 and VA7 in

unc-4(e120) but appears to induce miswiring of VA9 in *unc-4(+)* animals. The

differential effects of *wd87* are even more striking; in this case, we observed

suppression of AVB gap junctions with VA2-4 and VA8 in *unc-4(e120)* (Figure

3.7) as opposed to the imposition of ectopic AVB gap junctions with VA4-6, VA9

and VA10 in the wildtype (Figure 3.9). These results suggest that genetic circuits

controlling gap junction specificity may differ significantly among members of the

VA motor class with a given gene adopting a positive role in one VA and the opposite and negative function in another. To test this idea, we examined AVB gap junction inputs to VAs in a *lin-17*/Frz mutant. As described in Chapter 2, *lin-17* encodes a member of the frizzled class of Wnt receptors that antagonizes expression of *ceh-12* and the consequent miswiring of VA motor neurons. This model is consistent with our finding that a subset of VAs (VA6 and VA10) are miswired with AVB inputs in the *lin-17* mutant alone; this result is consistent with a mild backward Unc phenotype displayed by *unc-17* mutants and with our finding that the *unc-17* allele does not suppress AVB gap junctions for other VAs in an *unc-4* mutant. In contrast, *mig-1*/Frz mutants do suppress the creation of AVB gap junctions with selected VAs (VA2 and VA10) (Figure 3.9) as predicted from the role of MIG-1 as a frizzled receptor that mediates EGL-20/Wnt-dependent expression of *ceh-12* (Figures 2.1 and 2.2 in Chapter 2). Here, our results showing that the *mig-1* mutation results in ectopic AVB inputs to VA5 and VA6, have also revealed that MIG-1/Frizzled could function in these specific VAs to antagonize the imposition of VB type inputs. These results suggest that MIG-1 functions in one subset of VA motor neurons in concert with LIN-17 to preserve VA type inputs but acts in other VAs to oppose the LIN-17 pathway. Finally, we note the interesting finding that *wd77, wd83, wd87* and *wd95* result in ectopic AVB gap junctions with VA11 (Figure 3.9), one of three VA motor neurons (VA2, VA11, VA12) that is not miswired in *unc-4* mutants (White et al. 1992a). These results underscore the likelihood that *blr* alleles isolated in our screen could have roles in synaptic choice that are independent of *unc-4* function.

Mutations have regional effects on normal VA wiring
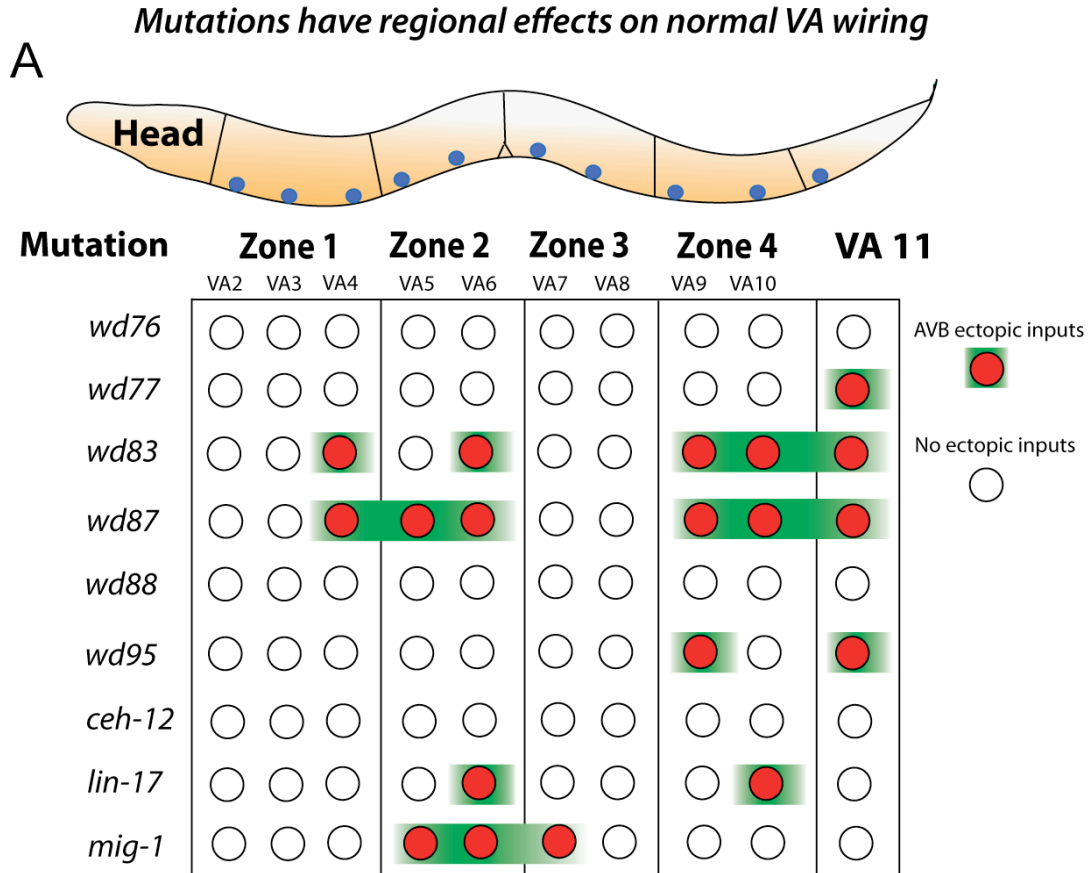
Figure 3.9. *blr* **mutants prevent AVB to VA gap junctions in wildtype VAs.**

blr genes and Wnt signaling components function in wildtype VAs to prevent ectopic AVB to VA gap junction connections. Ectopic AVB gap junction connections (red circles) represent statistically significant differences in wiring (p < 0.05, Fisher's Exact Test) when the frequency of AVB gap junction connections in *blr* mutants versus wildtype. Mutations in *wd77, wd83, wd87,* and *wd95*, all result in ectopic AVB to VA11 gap junctions.

blr-9(wd88) antagonizes Unc-4 suppression by egl-20.

blr-9(wd88) displays interesting genetic properties: (1) wd88 suppresses unc-4(ts) but not other unc-4 alleles; (2) wd88 suppression of unc-4(ts) is synthetically enhanced by mutations in unc-24; (3) wd88 antagonizes egl-20 suppression of unc-4(e120). The reasons for these genetic results are unclear. Of particular note are results showing that wd88 is strong suppressor of the AVB to VB gap junction defect in anterior unc-4 mutant VA motor neurons (Figure 3.7) suggesting that wd88 could function in parallel to ceh-12. If this model is correct, then wd88 would be expected to enhance Unc-4 suppression by a mutation in egl-20/Wnt since wildtype egl-20 function is required for ectopic ceh-12 expression in unc-4 mutant VAs. (Linkage of wd88 to ceh-12 on chromosome I prevented construction of a wd88 ceh-12 double.) Surprisingly, the combination of wd88 with egl-20 did not improve backward locomotion of the null allele unc-4(e120). This result stands in contrast to other blr alleles (wd76 and wd95) that suppress AVB gap junctions with anterior VAs (Figure 3.7) and also enhance ceh-12 suppression of Unc-4 (Table 3.2, 3.3). We conclude that wd88 may function in a common pathway with egl-20, due to the fact that wd88 does not enhance egl-20 suppression of unc-4(0). It is also possible that wd88 is a hypomorphic mutation, and therefore, may have only a limited effect on suppression of the movement phenotype.

DISCUSSION

One of the fundamental problems in neurobiology is to understand how neurons select synaptic targets. Our evidence indicates that this decision can be controlled by neuron-specific gene expression. In the nematode, *C. elegans*, the UNC-4 transcription factor is selectively expressed in VA motor neurons to block expression of downstream genes that result in an alternative pattern of presynaptic inputs that is normally restricted to VB class motor neurons. One of these UNC-4 target genes, *ceh-12*, which is normally expressed in VB motor neurons, is also ectopically expressed in a subset of posterior VA motor neurons in *unc-4* mutants. One consequence of ectopic CEH-12 expression in posterior VAs is the adoption of inappropriate gap junctions with AVB. Ectopic AVB miswiring in anterior VA motor neurons, however, is not dependant upon ectopic *ceh-12* expression, suggesting the involvement of additional pathways that function, in parallel to *ceh-12,* to promote ectopic AVB inputs to anterior VAs. The work described in this chapter uses a genetic screen, based on this model, to identify mutations in genes that function in parallel to *ceh-12* to regulate VA motor neuron input specificity. We report the isolation of 22 independent Unc-4 suppressor or *blr* (backward locomotion restored) alleles mapping to 16 complementation groups. We describe detailed phenotypic characterization of six of these Unc-4 suppressors mutations that identify at least three *blr* loci that function in parallel to *ceh-12*.

We examined ectopic AVB to VA gap junctions in *unc-4* mutant animals to determine if these *blr* loci promoted ectopic AVB to VA gap junction connections. *ceh-12* mutations rescue the ectopic AVB gap junction defect in posterior *unc-4* mutant VA motor neurons (VA8, VA9, VA10). We found that five *blr* alleles (*wd77, wd76, wd87, wd88, wd95*) also suppress ectopic AVB gap junctions with anterior VAs. Three *blr* alleles *(wd76, wd87, wd88)* suppress AVB to VA gap junction within the same group of anterior motor neurons (VA2, VA3, and VA8) (Figure 3.7). This observation is consistent with the genetic result showing that *wd87* and *wd88* do not enhance each other's Blr trait and therefore could function in a common pathway. (Figure 3.7, Table 3.2) *wd76* stands apart as the only allele in this group that enhances *ceh-12* suppression of Unc-4 and therefore is likely to function in parallel to *ceh-12.* This model predicts that the *wd76, ceh-12* double mutant will suppress the AVB gap junction defect in both posterior (*ceh-12* pathway) and anterior (*wd76*) pathways. Whether *wd76* functions in the *wd87-wd88* pathway can be determined by examining double mutants for enhanced Unc-4 suppression. *wd95* appears to suppress the ectopic gap junction defect in VA3 and in the midbody VA motor neurons, VA6 and VA7) (Figure 3.7). This result is consistent with the finding that *wd95* enhances *ceh-12* suppression of the Unc-4 backward movement defect and therefore supports the model in which *wd95* affects a gene that functions in parallel to *ceh-12*.

Our genetic screens also identified a mutation in at least one new gene that likely functions in the *ceh-12* pathway. Although *blr-2(wd77)* was isolated in a screen designed to detect recessive enhancers of *ceh-12,* retesting of the

outcrossed *wd77* allele did not confirm enhancement of the *ceh-12* Blr

phenotype. This result is consistent with the independent observation that the

outcrossed *wd77* allele suppresses the AVB gap junction defect for a posterior

VA motor neuron (VA10) in which *ceh-12* functions but does not suppress this

Unc-4 trait in anterior VAs (Figure 3.7). One explanation for this result is that

wd77 affects a gene that functions in the EGL-20/Wnt pathway. This possibility

can be tested by determining if *wd77* suppresses ectopic *ceh-12::GFP*

expression in *unc-4* mutants. It is interesting to note, however, that no previously

identified Wnt pathway gene maps to the *wd77* interval. An alternative and

exciting possibility is that *wd77* affects a gene that functions downstream of *ceh-12*.

Our gap junction data also predicts that because *wd95* and *wd76* seem to

suppress wiring defects in different neurons, it is possible that these two

mutations may genetically enhance suppression of *unc-4(0)*. This hypothesis

can be tested by the creation of double and triple mutant strains (e.g. *unc-4(e120); wd76; wd95*) with these *blr* mutations.

We have described an unusual *blr* mutation, *wd88*, that is enhanced by

mutations in *unc-24*. *unc-24* encodes a stomatin protein and mutants show a

jerky, forward movement defect. A similar phenotype is displayed by mutations

in the stomatin gene, *unc-1* and in the innexin genes, *unc-7* and *unc-9*. The

UNC-1 protein co-localizes with UNC-9 and physiological measurements are

consistent with a model in which UNC-1 regulates the activity of UNC-9/innexin

gap junction channels (Chen et al. 2007a). These results point to a likely role for

these genes (*unc-24, unc-1, unc-7* and *unc-9*) in gap junction assembly or function in the forward locomotory circuit involving AVB and B-class motor neurons. It will be interesting to determine if mutations in *unc-7*, *unc-9* and *unc-1* also enhance the Blr phenotype of *wd88*. This result would be consistent with model in which *wd88* functions in parallel to these forward Unc genes. Perhaps, in this scenario, the forward Unc genes contribute to VA miswiring in *unc-4* mutants (e.g. ectopic AVB gap junctions) such that this defect is strongly suppressed in double mutants with *wd88*.

Preliminary results obtained with the GRASP split-GFP synaptic marker indicate that mutations in *blr* alleles can restore AVA to VA synapses in an *unc-4* mutant. Although these results require confirmation with a recently generated GRASP marker with significantly brighter GFP fluorescence (R. Skelton, personal communication), the result showing that *wd77* suppresses both the gap junction (AVB-VB) and chemical synaptic (AVA-VA) *unc-4* defects in posterior VAs (zone 4) (Figure 3.7) is promising.

Our results show that *ceh-12* and other *blr* genes identified in this work function to promote the creation of VB type inputs (AVB gap junctions) to VA motor neurons. We did not detect, however, a role for any of these *blr* genes, including *ceh-12*, in the formation of AVB gap junctions with VB motor neurons. This result is consistent with a model in which *blr* genes share redundant functions in VB motor neurons but not when ectopically activated to drive the creation of AVB gap junctions with VAs. This model could be tested by examining

the effects of double mutants of *ceh-12* and *blr* genes on AVB gap junctions with VB motor neurons.

Future experiments will focus on the molecular identification of *blr* genetic loci by genome re-sequening with high throughput Illumina technology (Sarin et al. 2008). These results are expected to provide a foundation for a detailed cell biological analysis of the mechanism of synaptic choice in this motor circuit.

CHAPTER IV

PYRVINIUM, A SMALL MOLECULE INHIBITOR OF CASEIN KINASE Iα, FUNCTIONS IN C. ELEGANS TO BLOCK MULTIPLE WNT SIGNALING PATHWAYS.

The following section describes experiments conducted in collaboration with Curtis Thorne in the laboratory of Ethan Lee, MD, PhD at Vanderbilt University in the Department of Cell and Developmental Biology. Curtis performed a chemical screen using Xenopus egg extracts and identified pyrvinium, an FDA-approved drug, as a potent inhibitor of canonical Wnt signaling. Pyrvinium functions through a novel mechanism, acting as an activator of the destruction complex protein Caesin Kinase Iα (CKIα). The goal of the collaboration was to determine if this newly discovered small molecule inhibitor of the Wnt signaling pathway, pyrvinium, blocks canonical Wnt signaling in *C. elegans*. The following chapter details experiments designed to test this hypothesis.

I performed all *C. elegans* experiments described in this section. Curtis Thorne in Ethan Lee's lab performed the initial chemical genetics screen. The section discussing the chemical screen is paraphrased from the recent paper (Thorne et al. 2010, *submitted*) on this work.

INTRODUCTION

A critical step in the canonical Wnt signaling pathway is the degradation of β-catenin via the destruction complex. This complex, consisting of Axin, GSK3, CKIα, and APC, keeps cytosolic levels of β-catenin low. Upon Wnt activation, the destruction complex is blocked, increasing intracellular levels of the effector protein, β-catenin and simultaneously degrading the scaffold Axin.

Mutations in the destruction complex component APC were identified as the culprit in a familial form of colon cancer, and increased cytosolic levels of β-catenin have been linked to epithelial cell transformation (Nakamura et al. 1991). Over 80% of sporadic cases of colon cancer are attributed to a mutation in APC, and 10% are caused by a gain of function mutation in β-catenin. Thus, spurious activation of the Wnt pathway is strongly liked to tumorogenesis. In an effort to identify potential compounds for the treatment of colon cancer, the Lee laboratory utilized a cytoplasmic Wnt signaling pathway, reconstituted from Xenopus egg extracts, to screen a small molecule library for inhibitors of an activated pathway. Pyrvinium, an FDA approved drug, was identified as a small molecule activator of the destruction complex component Caesin Kinase Iα.

Pyrvinium is an antihelminthic compound that is FDA approved for the treatment of *Enterobius vermicularis,* commonly known as pinworms. Pinworms are one of the oldest known human pathogens, having been detected in fossilized human feces dating from around 7837 BCE (Fry and Moore 1969), and continue to plague modern industrialized societies (Downey et al. 2008). Aristotle

(384-322 BCE) is said to have discussed pinworms and their associated malady in his writings (Horne 2002). Transmission occurs via a fecal-oral route and presents clinically as a mild gastritis, prurtis ani, and/or restless sleeping, however most affected individuals show no clinical symptoms (Feldman M 2006; Downey et al. 2008). Pyrvinium, first FDA-approved in 1955 for the treatment of pinworms, has been phased out of use in the United States by more potent and broad-spectrum antihielmenthics. One reason for its low potency may be due to its limited solubility in aqueous solutions. In addition, pyrvinium does not cross the intestinal epithelium and 90% of ingested drug is excreted in feces (Yu et al. 2008). These characteristics, although limiting for pinworm treatment, can be desirable for the treatment of other intraluminal parasites such as *Cryptosporidium parvum* (Downey et al. 2008). Despite over 50 years of use, the mechanism of action of pyrvinium against these parasites remains unknown (Downey et al. 2008).

Here, I describe experiments designed to characterize the effects of pyrvinium on the canonical Wnt signaling pathway in the free-living, soil nematode, *C. elegans*. We find that pyrvinium treatment phenocopies inhibition of the canonical Wnt signaling pathway in three developmental contexts: Vulval morphogeneisis, neuroblast migration, and the *unc-4* pathway. In addition, I describe the effects of pyrvinium on the non-canonical asymmetric pathway in the early embryo. Finally, I propose a hypothetical chemical genetic screen designed to identify regulators of *kin-19*/CKIα in *C. elegans*.

MATERIALS AND METHODS

C. elegans strains.

Nematodes were cultured according to standard practices (Brenner 1974). This work utilized the following alleles: *mat-2(ax102)* (CGC), *pop-1(hu9); mnIs32[mec-7::GFP]* (G. Garriga), *unc-4(e2322ts)* (Miller et al. 1992). All nematodes were cultured on standard NGM plates inoculated with OP50^{-1} *E. coli*, unless otherwise stated.

Pyrvinium treatment of *C. elegans*.

Pyrvinium was prepared using the pamoate salt. (Generous donation from Lee lab – sigma) Pyrvinium pamoate is blood-red in color and fluoresces under yellow light. Pyrvinium is very hydrophobic and is only weakly soluble in water. *Unc-4 assay:* Pyrvinium was mixed to a maximum concentration of 100μM in soybean oil (CVS pharmacy) and applied directly to the surface of the plate in question. This has been used previously to treat *C. elegans* with naphthalene (Kokel et al. 2006). Pyrvinium was found to be only partially soluble in mineral oil, as un-dissolved crystals of pyrvinium were seen upon inspection under 10x magnification. However, centrifugation of the pyrvinium/soybean oil mixture removed crystals but not the fluorescence. In addition, a visual inspection of treated worms showed red fluorescence indicative of ingested pyrvinium.

Experimental results were compared between pyrvinium-treated animals and vehicle controls. Adult worms of the requisite geneotype for each experiment were placed onto treatment plates, and their F1 progeny were used for data

collection. Treatment of Adult worms ensured that all progeny scored would have been exposed to pyrvinium during their entire life cycle. 3-4 adult worms were placed on each pyrvinium treatment plate and vehicle control plate. Worms were scored as L4 to young adults for each experiment.

Vulval morphology assay

Pyrvinium pamoate was dissolved in 95% ethanol to a final concentration of 1mM. 100uL of 1mM ethanol/pyrvinium mixture was added to 10mL of NGM media immediately prior to pouring plates. Final concentration of ethanol in plate was 1%, which is below threshold for biological activity. This mixture resulted in a final concentration of 10uM per plate. Experimental results were compared between pyrvinium treated animals and vehicle controls. Adult worms of the requisite geneotype for each experiment were placed onto treatment plates, and their F1 progeny were used for data collection. Treatment of Adult worms ensured that all progeny scored would have been exposed to pyrvinium during their entire life cycle. 3-4 adult worms were placed on each pyrvinium treatment plate and vehicle control plate. Worms were scored as L4 to young adults for each experiment.

mat-2 lethality and Q cell migration assays

DMSO plates were created using the same procedure as ethanol plates. Experimental results were compared between pyrvinium treated animals and vehicle controls. Experimental results were compared between pyrvinium treated animals and vehicle controls. Adult worms of the requisite geneotype for each experiment were placed onto treatment plates, and their F1 progeny were used

for data collection. Treatment of Adult worms ensured that all progeny scored would have been exposed to pyrvinium during their entire life cycle. 3-4 adult worms were placed on each pyrvinium treatment plate and vehicle control plate. Worms were scored as L4 to young adults for each experiment.

Data collection.

Unc-4 locomotion

We assayed unc-4 locomotion as previously described (Chapter 2 and 3). Animals were treated with pyrvinium/soybean oil mixture and incubated at 23C for 3 days and then their backward movement was quantified.

Vulval development

Pyrvinium's effect on vulval development was scored for visual defects at 100x magnification under DIC light microscopy using a Ziess Axioplan microscope, retrofitted with a CCD camera and OpenLab software. Visual defects observed ranged from abnormal morphology to protrouding vulva (pvl). All animals were scored by picking individual, adult animals onto glass slides. Slides were prepared with a 2% agarose pad, and worms were anesthetized using a 0.1% tricane and 0.1% tetramisole mixture. Slides were scored blind to geneotype and treatment paridigm.

Egg retention in the uterus was ascertained from this population by counting the number of eggs directly visualized under these conditions.

RNAi.

RNA interference was conducted using the feeding method (Kamath et al. 2001). Worms were fed bacteria expressing double stranded RNA from the Arringer library. dsRNA expression in *E. coli* was induced using a β-lactose induction protocol. (Protocol from Eric Lambie) (www.genetics.wustl.edu/tslab/Protocols/Lactose_RNAi_Plates.htm) 1L of NGM plates were supplemented with 20mL of 20% sterile filtered β-lactose in water. Pyrvinium/DMSO was added after supplementation with β-lactose and before plates were poured. *E. coli* colonies were picked from a toothpick stab of the Ahringer library. A single colony was used to inoculate a 2 mL culture, grown overnight at 37°C with 10μL of 100mg/mL ampicillian in a 15 mL falcon tube. The overnight culture was diluted 1:100 in LB/AMP and grown at 37°C, with shaking, for 6 hours. 200μL of LB/AMP/*E. coli* mixture was plated on each plate, allowed to dry, and incubated at room temperature for 4 days before using.

mat-2 experiments.

4 adult worms of requisite genotype were placed on each plate and allowed to lay eggs for 48 hours at the indicated temperature. All adult worms were then removed, and plates grown for 24-72 hours (depending on temperature) at the same temperature as the previous step. This step was necessary to control against a developmental delay induced by low temperature conditions and pyrvinium treatment by allowing all surviving eggs to hatch. Total Live progeny vs. dead (unhatched) eggs were counted on each plate.

Experiments were conducted in duplicate. Fisher's exact test was used for all statistical analysis.

Q neuroblast migration.

Q neuroblast migration was scored using the marker *mec-7::GFP*. *mec-7::GFP* is expressed in the six touch receptor neurons AVM, PVM, ALML, ALMR, PVML, and PVMR. I used the neurons ALML/R and PVML/R as positional markers, which are not sensitive to a Wnt signal. Treated animals were isolated and the AVM and PVM cell bodies were scored under a fluorescent stereo dissecting scope under a GFP filter according to their relative positions along the AP axis. Abnormal migration was scored as positive in an animal if PVM had migrated past the midbody position of ALML/R.

RESULTS

A *Xenopus* extract screen identifies pyrvinium as a potent small molecule inhibitor of the canonical Wnt pathway

The canonical Wnt signaling pathway is kept inactive by the constitutive phosphorylation and degradation of β-catenin by the destruction complex. Normal intracellular signaling levels of Axin, a scaffold protein for the destruction complex, are kept high. Upon treatment with LRP6ICD, a section of the intracellular domain of LRP6 that activates the Wnt pathway, β-catenin and Axin levels display an inverse relationship: the destruction complex is directly blocked

by LRP6ICD binding to GSK3 and Axin is eventually degraded (by an unknown mechanism), allowing β-catenin levels to increase its intracellularly (Cselenyi et al. 2008). This relationship underlies the general mechanism present in this signaling pathway.

Recent work in Ethan Lee's lab developed a specific assay in which Xenopus egg extracts is used as an *in vitro* model to study the cytoplasmic components of canonical Wnt signaling. (Figure 4.1A) Treatment of cytosolic Xenopus egg extracts with the LRP6ICD induces robust activation of the pathway. *in vitro,* translated fluorescent proteins (Axin-Renila luciferase and β-catenin-Firefly-Luciferase) were added to the extracts, allowing bimodal monitoring of the pathway's activation state (Cselenyi et al. 2008). Activation is detected by a coincident decreased activity of Axin-Renilla luciferase versus an enhanced activity of β-catenin-firefly luciferase. This bimodal assay allowed for a high-throughput screen of chemical modulators of the Wnt signaling pathway, under which active compounds (inhibitors of the pathway) would be expected to increase the ratio of renilla(Axin) versus firefly(β-catenin) luciferase activity, thus reversing the ratio.

The primary screen using this system identified 20 candidate molecules (both activators and inhibitors) that modulated the β-catenin/Axin ratio at least 3 standard deviations from the mean. (Figure 4.1B) Pyrvinium pamoate was the most potent inhibitor of this pathway. (Figure 4.1C)
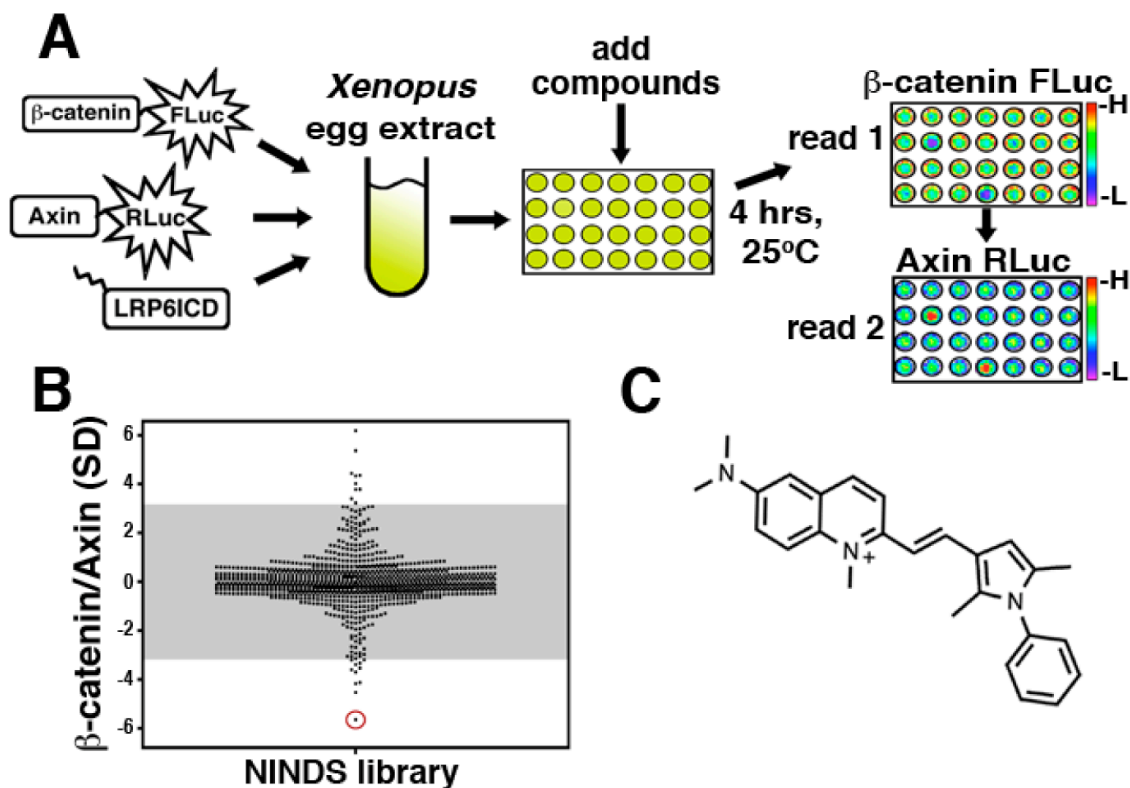
Figure 4.1. Xenopus egg extract screen identifies pyrvinium as a potent inhibitor of canonical Wnt signaling.

A. Diagram of high-throughput screen. Xenopus egg extract contains exogenous Axin-renilla and β-catenin-firefly luciferase tagged proteins. Wnt signaling is activated by addition of exogenous LRP6ICD. Chemicals from chemical libraries are added to activated extract in 384-well plates and incubated for 4 hours at 25°C. Renilla and firefly-luciferase levels are examined individually and quantified relative to controls. High and low luciferase levels are shown as indicated. B. Normalized scatter plot of Axin and Renilla luciferase levels for FDA approved compounds examined within this screen. Both activators and inhibitors are shown. Shaded region represents levels less than 3 standard deviations from the mean. Pyrvinium, a potent inhibitor is circled in red. C. Chemical structure of pyrvinium. (Adapted from Thorne, et al. submitted)

Pyrvinium functions via a conserved mechanism across phyla.

In order to determine if pyrvinium interacts with a conserved component and functions as an inhibitor of the canonical Wnt signaling pathway, Curtis tested pyrvinium for the inhibitory effects on the canonical Wnt pathway in several different model organisms. One of the classical examples of ectopic Wnt signaling is the induction of a primary axis duplication. Injection of Wnt3a induces a duplicate axis in Xenopus through a canonical Wnt signaling mechanism. Treatment with pyrvinium blocks formation of the Wnt3a induced secondary axis and confirms that pyrvinium inhibits a Wnt signaling, *in vivo*. In the fruitfly, *Drosophila*, Wingless signaling helps pattern the denticle-banded cuticle. Injection of pyrvinium disrupts denticle banding in *Drosophila* embryos. This result confirms that pyrvinium treatment blocks Wnt signaling in *Drosophila* and that the target of pyrvinium may be conserved. In human cell culture, nuclear β-catenin accumulation is characteristic of an activated Wnt signaling pathway. Pyrvinium blocks Wnt3 induced nuclear β-catenin accumulation in human cell culture, suggesting that the target of this pathway is also conserved in humans. These experiments were performed in the Lee laboratory (Thorne, et al. *submitted*).

Pyrvinium blocks Q cell migration in *C. elegans*.

To determine if the target of pyrvinium is conserved in *C. elegans*, I asked if pyrvinium would perturb Q cell migration, which is regulated by canonical Wnt signaling (Ch'ng et al. 2003). The QL and QR neuroblasts are born embryonically

at the same time and migrate from their initial positions about an hour after the animal hatches. The neuron QL, and its descendents, activate expression of the hox gene *mab-5*, and migrate towards the posterior of the animal, whereas the QR interneuron does not express *mab-5* and migrates toward the anterior.

QL responds directly to an EGL-20 Wnt signal from the posterior, signals through *lin-17* and *mig-1*/Frizzled and *bar-1*/β-catenin to induce MAB-5/HOX expression (Maloof et al. 1999). The expression of *mab-5* causes the QL daughter cell to migrate towards the posterior. Mutations that affect positive regulators of canonical Wnt signaling (e.g. *bar-1*/β-catenin, *pop-1*/TCF, *egl-20*/Wnt), cause the QL cell to reverse direction and migrate towards the anterior (Maloof et al. 1999). Mutations in negative regulators of Wnt signaling, such as *pry-1*/Axin mutants, cause the QR daughter cell to express *mab-5*, and migrate towards the posterior. Mutations in the destruction complex like *pry-1*/Axin, cause an intracellular rise in β-catenin that activates Wnt signaling in the QR cell, which normally does not respond to Wnt. Thus, I reasoned that Q-cell migration would serve as a sensitive assay for detecting pyrvinium dependant inhibition of Wnt signaling.

C. elegans has a cuticle which is impermeable to many types of pharmacological agents (Lewis et al. 1980a; Lewis et al. 1980b). We reasoned that this may prevent pyrvinium from reaching the neuroblasts at a significant concentration. Therefore, a sensitized genetic background may be necessary to see the effects of pyrvinium. We used a hypomorphic allele in *pop-1*/TCF to
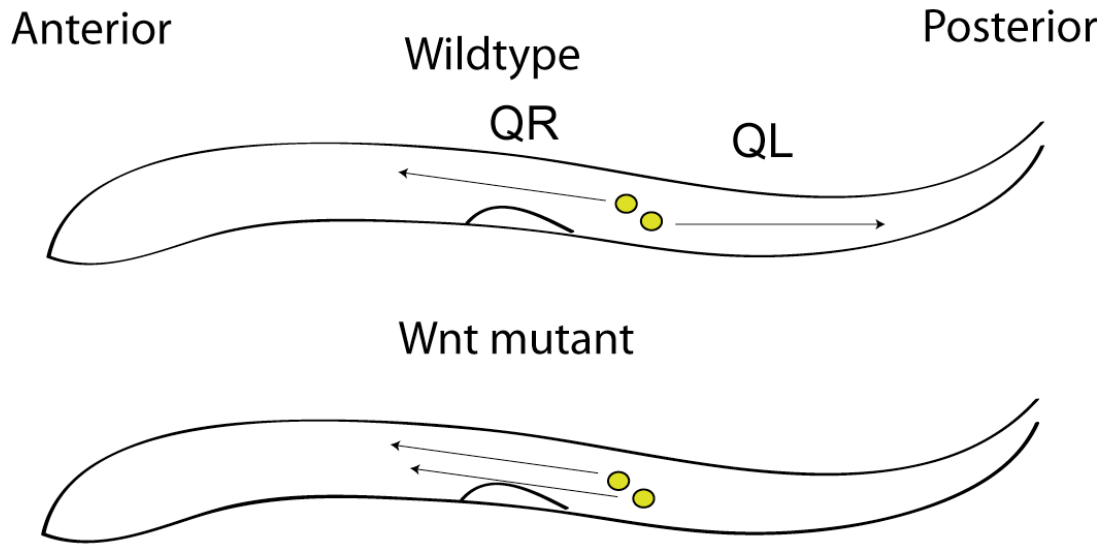
mec-7::GFP	Vehicle	% Abnormal	n
pop-1(hy)	0.1% DMSO	58	50
pop-1 + 1uM	0.1% DMSO	70	50
pop-1 + 10uM	0.1% DMSO	78	50
pop-1 + 100uM	0.1% DMSO	84	50

Figure 4.2. Pyrvinium treatment results in abnormal Q cell migration.

Q cell progeny migrate in opposite directions depending on their response to a posterior Wnt signal. Mutations that block canonical Wnt signaling cause both Q cell progeny to migrate toward the anterior. Hypomorphic mutations in *pop-1*/TCF cause an incompletely penetrant migration phenotype. Pyrvinium treatment enhances *pop-1*-disrupted Q cell migration.

sensitize the genetic background to pyrvinium. Figure 4.2 shows that treatment

of *pop-1(hu9); mnIs32[mec-7::GFP]* animals with pyrvinium results in a dose

dependant increase in the number of anteriorly displaced QL neuroblast progeny.

For example, treatment of *pop-1* with 100μM pyrvinium increases the number of

displaced QL progeny from 58 to 84%. (Figure 4.2) This inhibition of posterior

migration is presumably due to the loss of activated canonical Wnt signaling in

the QL neuroblast.

Pyrvinium blocks vulval development in *C. elegans.*

Vulval development depends on multiple interacting Wnt signaling

pathways (Green et al. 2008). Mutations in the β-catenin homolog, *bar-1*, display

a range of vulval morphology defects (Eisenmann and Kim 2000; Gleason et al.

2006). Thus, we hypothesized that vulval morphogenesis should be disrupted by

pyrvinium if it targets Wnt signaling in this tissue.

Pyrvinium treatment produces a broad array of vulval morphology defects.

Ranging from protrouding vulva (pvl) to vulvaless (vul) phenotypes. In adult

animals, these vulval defects occurred approximately ~30% of the time after

treatment with 10μM pyrvinium. (Figure 4.3) To confirm these results, we asked

if animals also displayed an egg retention phenotype (Egl), which is consistent

with a disrupted vulval epithelium. Pyrvinium-treated animals had a statistically

significant (p >0.0005) increase in the number of eggs retained in the vulva

compared to vehicle controls.   Wildtype animals averaged 9.9 eggs/worm

whereas pyrvinium treated worms had 12.9 eggs/animal. We conclude from

A

WT

B

10uM pyrvinium

C

Abnormal Vulval Morphology

	Vehicle	Abnormal	n
WT	0.1% EtOH	0%	30
WT + 10uM	0.1% EtOH	33%	30

D

Egg Retention in the Uterus

	Vehicle	Ave # Eggs	n
WT	0.1% EtOH	$9.9 + 3.9$	65
WT + 10uM	0.1% EtOH	$12.9 + 4.3$	65

$p > 0.0005$
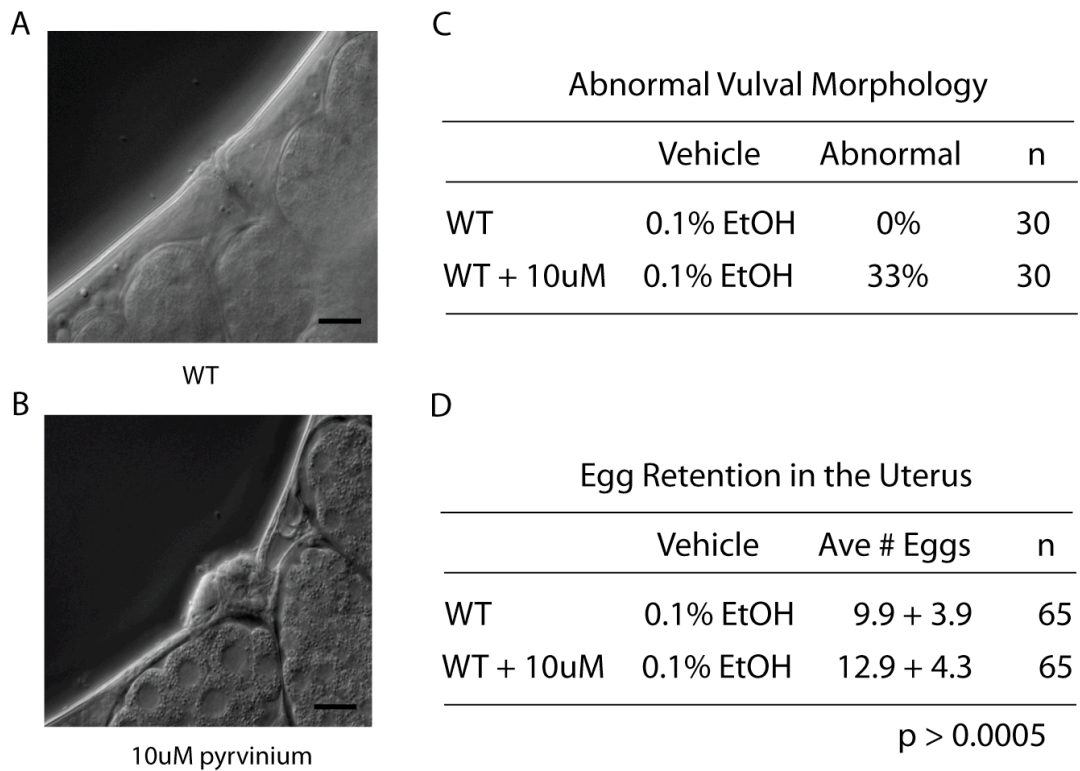
Figure 4.3. Pyrvinium disrupts vulval morphology in *C. elegans*.

A. Normal vulval morphology (vehicle) B. Protrouding vulva (Pvl) on $10 \mu M$ treated pyrvinium plates. C. One third of pyrvinium treated animals have disrupted vulval morphology. D. Pyrvinium treatment results in egg (embryo) retention in the uterus, a trait that is consistent with disrupted vulval function.

these results that pyrvinium phenocopies Wnt signaling mutants by disrupting vulval morphogenesis and development.

Pyrvinium suppresses the Unc-4 backward movement defect.

We have shown that UNC-4 antagonizes a Wnt signaling pathway to inhibit the expression of the VB gene, *ceh-12*. (Chapter 2) I have hypothesized that *ceh-12* expression depends on a canonical Wnt signaling pathway and therefore should be inhibited by treatment with pyrvinium. In this assay, the repression of *ceh-12* expression was motivated by assessing a related behavioral phenotype. As described in Chapter 2, Wnt dependent expression of *ceh-12* in VA class motor neurons results in a backward movement defect caused by the miswiring of VAs with VB motor neuron-type inputs. Mutations in Wnt pathway genes block VA expression of *ceh-12* and the concurrent backward movement phenotype. Thus, we reasoned that pyrvinium should also suppress Unc-4 movement if its target is required for *ceh-12* expression. (Figure 2.1)

To test this hypothesis, *unc-4(e2322ts)* animals were treated with two concentrations of pyrvinium at the threshold temperature of 23C. As shown in Figure 4.4, Pyrvinium showed dose dependant suppression of the Unc-4 backward movement defect. This result provides additional conformation that the pyrvinium target is conserved and that it functions in a canonical Wnt signaling pathway.
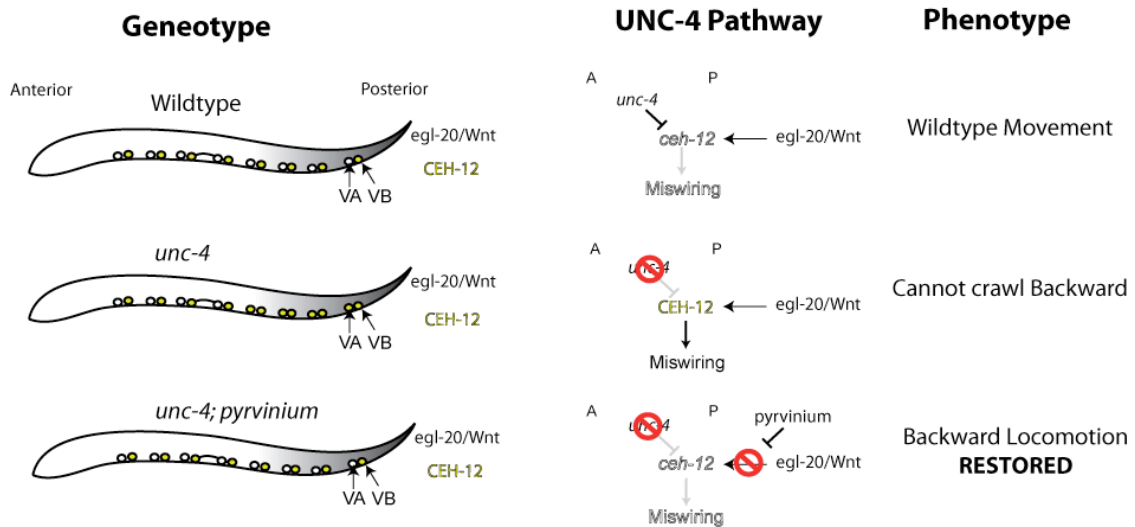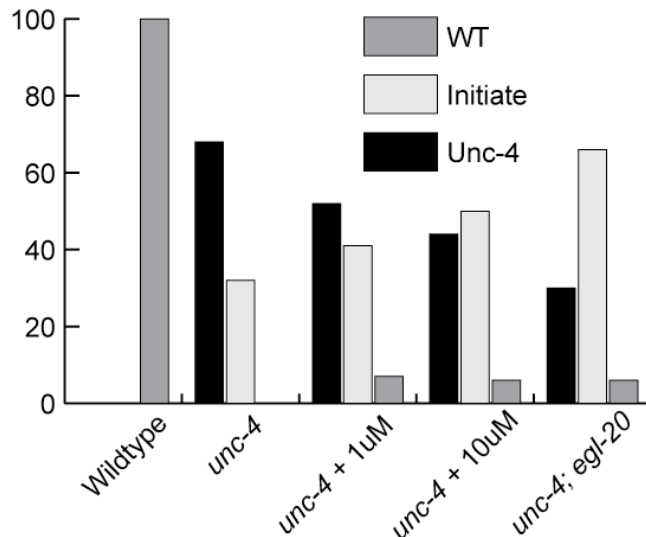
Figure 4.4. Pyrvinium suppresses the Unc-4 backward movement defect.
A. UNC-4 normally functions to prevent an EGL-20/Wnt dependent signaling pathway from activating expression of *ceh-12*/HB9 in posterior VAs and disrupted backward movement. Blocking a canonical Wnt signaling, via pyrvinium, should rescue the backward movement defect. B. Inactivation of Wnt signals quells *ceh-12* expression and restores backward locomotion. Treatment of an *unc-4* hypomorphic mutant rescues backward movement in a dose dependant manner.

162

Pyrvinium induces a synthetic lethal phenotype in *C. elegans* embryos.

Experiments performed in the Lee laboratory established that pyrvinium is the only known small molecule that can suppress an adenomatous polyposis coli (APC) mutation (SW480 cells) that is responsible for the familial form of colon cancer. To determine if this function of pyrvinium is also conserved in *C. elegans*, I obtained a mutant in the *apc-1/mat-2* gene from the Caneorhabditis Genetics Center. Upon treatment of *mat-2(ax102)* worms with pyrvinium I observed a highly penetrant synthetic lethal phenotype. (Table 4.1) This result was initially surprising since the model of pyrvinium action predicted the opposite result; i.e suppression of the *apc-1/mat-2* phenotype. I then realized that *apc-1/mat-2* in *C. elegans* actually encodes a conserved subunit of the Anaphase Promoting Complex or Cyclosome (APC/C) (a.k.a. Apc1 in *S. cerevisiae*) and not the homolog of adenomatous polyposis coli (APC) (which is *apr-1* in *C. elegans*). This fortuitous discovery also provided evidence of the inhibition of Wnt signaling by pyrvinium.

mat-2 null mutants are embryonic lethal (Golden et al. 2000). For our studies, we used a hypomorphic allele, *mat-2(ax102)*, that is temperature sensitive. For example, ~80% of the progeny of a *mat-2(ax102)* hermaphrodite are viable at 15°C; viability declines to ~20% at 20°C (Table 4.1). Treatment with 100 μM pyrvinium at either 15°C or 20°C consistently reduced viability of *mat-2* embryos to ~5% (Table 4.1). Wildtype (N2) *C. elegans* embryos are unaffected by pyrvinium alone or by carrier (DMSO). These results indicate that pyrvinium induces a synthetic lethal phenotype in combination with *mat-2(ax102ts)* allele.

Pyrvinium Induces a Synthetic Lethal Phenotype with *mat-2 (ax102)*

	[Pyrvinium] μM	% Viable	P-value (vs DMSO)
15°C	DMSO	78.9	
	10	72.7	0.089
	100	4.2	2.9E-36
20°C	DMSO	21.3	
	10	7.4	0.00015
	100	5.0	0.00012

Table 4.1. Pyrvinium Induces a Synthetic Lethal Phenotype with *mat-2 (ax102).*

Pyrvinium induces synthetic lethality with the of the APC/C mutant *mat-2(ax102)* at both permissive (15°C) and non-permissive (20°C) temperature. P-values were determined using Fisher's exact test.

RNAi of *pop-1/TCF* Confers Increased Lethality to *mat-2*

RNAi clone	N2 % live	*mat-2* % live	P-value N2 vs *mat-2*	P-value (vs EV)
Empty Vector	69.6	10.0	6.65E-29	
bar-1	100.0	11.0	3.18E-86	0.457
pop-1 (clone 1)	4.0	0.8	0.011	3.29E-06
pop-1 (clone 2)	3.3	0.0	0.004	9.22E-07

Table 4.2. RNAi of *pop-1/TCF* Confers Increased Lethality to *mat-2.*

An RNAi assay tested the hypothesis that knockdown of a wnt signaling component critical for early embryonic development would enhance *mat-2* lethality. *bar-1* (one of several β-catenin genes) is not involved in early embryonic development and represents a Wnt pathway control. RNAi of *pop-1(TCF/LEF)* enhanced lethality in the *mat-2* genotype vs wildtype (N2) control. The experimenter was blind to genotype and to the identity of RNAi clones. *P-values* were determined using Fisher's exact test.

Wnt signaling is required for early embryonic development in *C. elegans*. The combined defects in Wnt signaling and the APC/C pathway could account for the synthetic lethality of pyrvinium with the *mat-2* mutant. This model predicts that genetic ablation of other components of the early embryonic Wnt pathway should also result in lethality in combination with *mat-2*. To test this idea, we use RNAi for knockdown of the TCF-LEF transcription factor, POP-1, an essential component of the early embryonic Wnt signaling pathway in *C. elegans* (Rocheleau et al. 1997). As shown in Table 4.2, RNAi of *pop-1* produces an almost fully penetrant lethal phenotype in combination with *mat-2*. [Although RNAi of *pop-1* alone induces lethality, penetrance is significantly enhanced by *mat-2* ($p < 0.004$-0.01).] As a control, we used RNAi to deplete *bar-1*/β-catenin, which is not required for Wnt dependant signaling in the early embryo (Rocheleau et al. 1997). No significant difference was found with *bar-1* RNAi versus empty vector control plates. These results are consistent with one hypothesis that inhibition of Wnt signaling by pyrvinium is responsible for the enhanced lethality of the *mat-2* phenotype in early embryos. This fortuitious discovery also suggested a genetic strategy to identify *C. elegans* genes that mediate the effects of pyrvinium treatment (see below).

DISCUSSION

A small molecule inhibitor of the Wnt signaling pathway is currently lacking as a research tool (Clevers 2006). A small molecule inhibitor also has the

potential to revolutionize the treatment of β-catenin-derived tumors. Experiments

performed in the Lee laboratory established that the FDA-approved drug,

pyrvinium is a potent, small molecule inhibitor of canonical Wnt signaling. My

work has now confirmed that pyrvinium phenocopies Wnt signaling pathway

mutants in *C. elegans* and therefore is likely to target a conserved Wnt signaling

pathway component.

Biochemical assays performed in the Lee lab have now established that

pyrvinium targets Casein Kinase Iα, a conserved component of the destruction

complex. These results indicate that pyrvinium functions as an activator,

enhancing the activity of CKIα. Phosphorylation of β-catenin by CKIα acts as a

priming step for GSK3-dependant phosphorylation of β-catenin and subsequent

degradation by the ubiquitin-proteosome pathway. Overactivation of CKIα would

inhibit the pathway by ectopically phosphorylating β-catenin and inducing the

destruction complex to function more effectively.

In *C. elegans*, the homolog of CKIα, *kin-19*, functions in vulval morphology

and early embryonic development (Peters et al. 1999; Walston et al. 2004;

Gleason et al. 2006). As discussed in the introduction of this thesis, the

patterning of the EMS blastomere is dependant upon a Wnt signal. Previous

studies have shown that *kin-19* RNAi blocked endoderm development in early

embryonic development, which phenocopies a mutant in the downstream

transcription factor *pop-1*/TCF. This effect was enhanced in the presence of

another component of the destruction complex, *apr-1*/APC, which is consistent

with its role as a positive effecter in the non-canonical β-catenin asymmetry pathway.

Future Directions.

In experiments to measure the effects of pyrvinium on *C. elegans* embryonic development, we discovered that pyrvinium treatment of animals with a weak mutation in the apc-1 subunit of the Anaphase Promoting Complex/Cyclosome (*mat-2*) results in a highly penetrant synthetic lethal phenotype. Synthetic lethality may arise from convergent roles of CKIα/Wnt signaling and APC/C function in early embryonic development (Rappleye et al. 2002; Nakamura et al. 2005; Huang et al. 2007). Weak *mat-2* alleles (e.g. *mat-2(ax102)* used in this study) result in early embryonic anterior/posterior polarity defects (Rappleye et al. 2002). APC/C function is required for PAR-2 localization to the posterior membrane of the 1-cell stage and subsequent asymmetric division (Rappleye et al. 2002). In *C. elegans*, the Wnt pathway contributes to the polarization of the ABar blastomere by differentially regulating the placement of its duplicated centrosomes (Walston et al. 2004). Significantly, *kin-19*/CKIα regulates both the Wnt/β-catenin pathway and a separate spindle orientation pathway. Thus, it is likely that defects in A-P patterning, present at a basal level in *mat-2(ax102)* animals, is exacerbated by the combined effects of pyrvinium on Wnt signaling (inhibition) and CKIα (activation).

The *mat-2* synthetic lethality with pyrvinium affords a powerful strategy for detecting "suppressor" mutant hits in the CKIα/Wnt pathway. Mutants that block

pyrvinium activity (e.g. mutations in CKIα, protein targets of CKIα in the Wnt pathway, or regulators of CKIα activity) should rescue lethality. Strong selection for suppressor mutants (i.e. viability) should allow high-throughput screens with the capacity to reveal these classes of CKIα/Wnt pathway gene mutations.

The genetic screen (Figure 4.5) is designed to detect rare suppressors of pyrvinium-dependent lethality. Initially, we will screen for dominant suppressors. For example, a mutation that prevents pyrvinium binding to 50% of available CKIα could be detected as a haplo-insufficient dominant suppressor; this model assumes that only one copy of the wildtype CKIα gene would reduce the potency of pyrvinium at the selection threshold and therefore restore essential CKIα/Wnt signaling in the embryo. A mutation with such a highly specific effect, however, is likely to be rare because of the dual requirement of blocking pyrvinium-mediated CKIα activity but not other essential functions (RNAi of *kin-19* is lethal). Earlier genetic screens in the Miller lab have detected site-specific and allele-specific dominant suppressor mutations in *C. elegans* at a frequency of 10^{-5} per F1 progeny (Miller et al. 1993a). Our screen is designed to detect pyrvinium-resistant (i.e. viable) mutations at a similar low frequency.
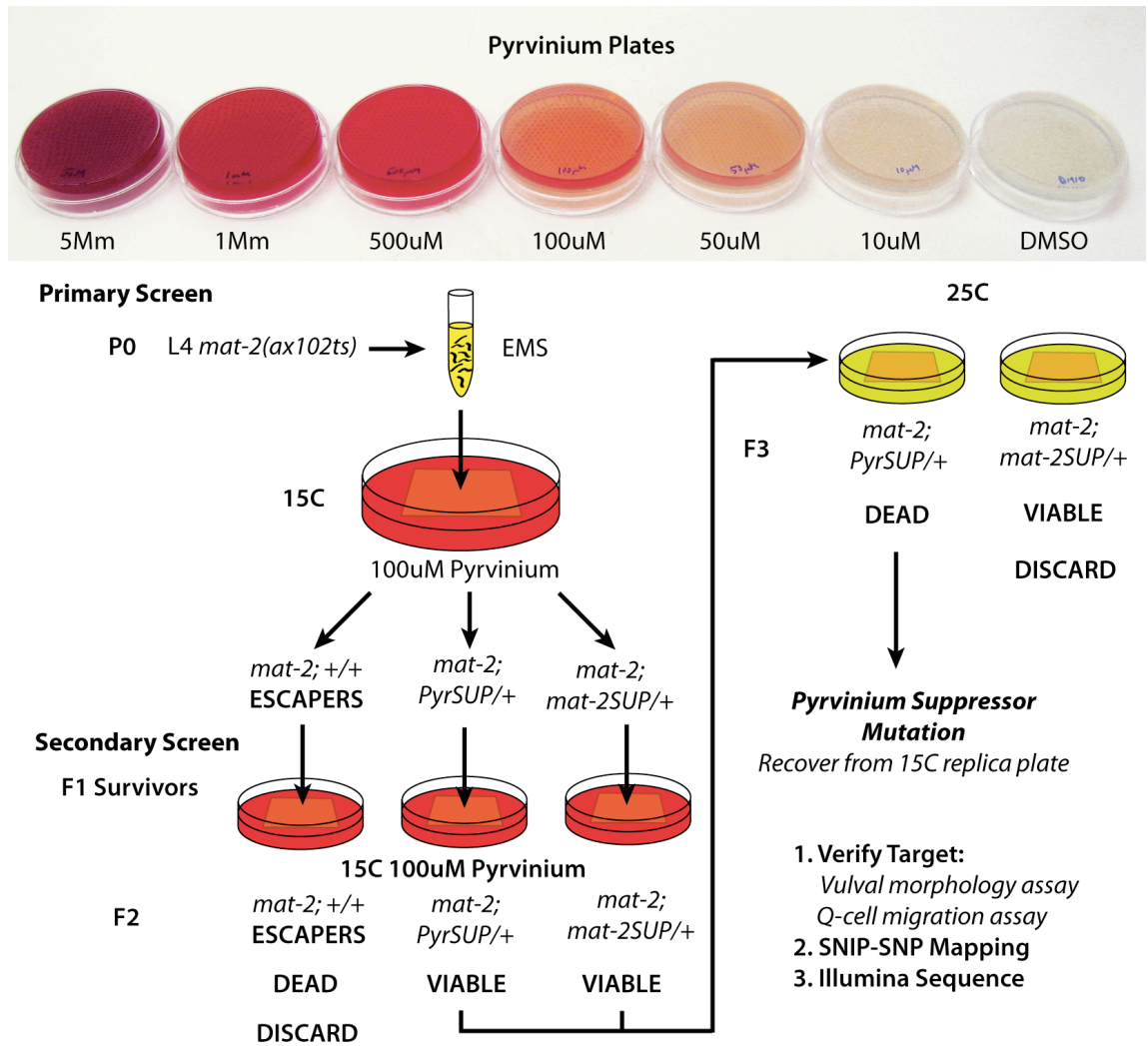
Figure 4.5. Hypothetical genetic screen for *kin-19* regulators.

Genetic screen to isolate suppressor mutations in pyrvinium target. TOP: Pyrvinium in NGM plates. Primary Screen: Mutagenized animals are cultured on 15 C pyrvinium plates. Secondary Screen: Escapers (~5% of progeny) produce few F2 progeny and are discarded. Mat-2 suppressors (*mat-2SUP*) are viable at 25°C and are discarded. Authentic pyrvinium suppressor (PyrSUP) mutants (viable at 15°C, lethal at 25°C) are recovered from 15°C replica plates.

170

CHAPTER V

GENERAL DISCUSSION AND FUTURE DIRECTIONS

It is clear from work done by others and the experiments contained within this document, that environmental cues play a large role in shaping neuronal connections within a developing circuit. Its possible that it is the concentration of long-range cues, as well as local guidepost signals, create a specific environment whereby a single neuron responds to these cues in an either pro- or anti- synaptogenic manner. This hypothesis offers an alternative model to the idea that specific connections are coordinated exclusively by signals between synaptic partners. Our work, does not exclude the possibility of interaction between two neurons but points to additional roles for external signals during the process of synaptic choice.

Wnt signaling is critical for proper synaptogenesis.

As described in Chapter I, local Wnt signals are critical cues for the development of pre- and post-synaptic structures and Wnt has been shown to regulate the formation of chemical synapses in a wide array of model organisms. Both β-catenin and non-β-catenin-dependant mechanisms have been shown to promote or inhibit synapogenesis. Furthermore, there is evidence of antagonism between Wnt signaling pathways in multiple different organisms for the development of non-neural tissues and in synaptogenesis. Key developmental

events in both neurons and in other tissues may be controlled by Wnt signaling pathways that antagonize each other.

Chapter 2 describes results that are consistent with a model in which UNC-4/37 modulates the sensitivity of VA motor neurons to two antagonistic Wnt signaling pathways. One pathway functions by promoting the creation of inappropriate, ectopic VB-type inputs to VA motor neurons. In this pathway, EGL-20/Wnt promotes expression of *ceh-12/*HB9, in posterior VA motor neurons. Our evidence indicates that downstream signaling depends on the cytoplasmic components of a canonical Wnt pathway. *unc-4* limits the sensitivity of VA neurons to EGL-20/Wnt presumably by repressing the expression of the Frizzled receptors MIG-1 and MOM-5. A different Wnt pathway, involving LIN-44/Wnt and LIN-17/Frizzled functions to antagonize VB-like inputs onto VA motor neurons, potentially via a non-canonical Wnt pathway mechanism. Our evidence indicates that LIN-44/LIN-17 represses *ceh-12* expression but the mechanism of this effect and how it antagonizes EGL-20/MOM-5 dependent activation of *ceh-12* expression is not understood.

Chapter 3 describes genetic screens designed to identify pathways in parallel to *ceh-12*/HB9 to regulate VA motor neuron inputs. Genetic analysis of the mutations isolated in these screens identified at least three genes (*blr-1, blr-3,* and *blr-15*) that are likely to function in parallel to *ceh-12.* First, these *blr* alleles suppress *unc-4* hypomorphic mutations as would be expected for genes that act in opposition to the *unc-4* pathway. Second, these *blr* mutations enhance *ceh-12* suppression of *unc-4(0)* alleles, indicating their likely function in

a parallel pathway to *ceh-12*. Third, *blr-15(wd95)* and *blr-1(wd76)* suppress the

ectopic AVB to VA gap junction inputs in anterior regions that are not rescued by

mutations in *ceh-12*; this result suggests that the pathways regulated by *blr-1* and

blr-15 may function in these anterior VA motor neurons to promote VB wiring.

Chapter 4 describes experiments to test the potency of the CKIα inhibitor,

pyrvinium, on Wnt signaling in *C. elegans*. These experiments confirmed that

pyrvinium phenocopies genetic mutants of canonical Wnt pathway components

in multiple different *C. elegans* tissues. Furthermore, pyrvinium is able to

suppress the Unc-4 phenotype, lending additional support to our proposal that

unc-4 antagonizes a canonical Wnt pathway. This result also suggests that CKIα

may play a role downstream of *unc-4*. On the basis of these experiments, we

conclude that pyrvinium blocks canonical Wnt signaling in *C. elegans*. Chapter 4

also describes a fortuitous result, which led to the design of a genetic screen that

exploits a synthetic lethality between pyrvinium and the Anaphase Promoting

Complex/Cyclosome subunit apc-1. This screen is designed to isolate

suppressor mutations that target the binding cite of pyrvinium on CKIα or genes

that regulate CKIa's activity. This work has the potential to uncover new

information about the regulation of CKIα, as well as early embryonic

development and the role of the APC/Cyclosome.

Future directions – Chapter 2. Wnt signaling.

We have proposed a model whereby UNC-4 negatively regulates the

expression of frizzled receptors MOM-5 and MIG-1 to prevent VA motor neurons

from responding to a posterior EGL-20/Wnt signal. Our work suggests that UNC-4 dependant modulation of this response accounts for the mechanism whereby that UNC-4 controls synaptic choice in posterior subset of VA motor neurons. This model proposes several questions that remain to be answered. Cell-specific microarray experiments found that both *mom-5* and *mig-1* transcripts are elevated in VA motor neurons in *unc-37* mutants but experiments with promotor::GFP fusions have not confirmed that *unc-4* negatively regulates these targets. As an alternative strategy to answer this question, we are collaborating with Rik Korswagen to use a new method of Fluorescent In Situ Hybridization (FISH) that can detect specific transcripts at single cell resolution (Raj et al. 2008). Previous efforts in *C. elegans* to utilize *in situ* hybridization relied on a single RNA probe. Unfortunately, the old methodologies were unable to resolve expression at the single cell level and yielded highly ambiguous data. This new methodology overcomes several technological limitations by using multiple, short, non-overlaping probes designed to complement a single mRNA transcript. Experiments in the Korswagen lab show that this protocol produces a clear punctate signal, which can be used to determine relative expression levels between cells. This methodology, combined with a volumetric scan of the imaged tissue by confocal microscopy, may have the sensitivity required to validate our microarray results. We have initiated a collaboration with Rik Korswagen in order to test the hypothesis that mutations in *unc-4* cause an upregulation in *mom-5* and *mig-1* mRNA in VA motor neurons.

Results reported in Chapter 2 are consistent with a model in which the *lin-17/lin-44* pathway functions in parallel to *unc-4* to antagonize AVB inputs to VA motor neurons. This model predicts that overexpression of the LIN-17/Frizzled protein in VA motor neurons could prevent inappropriate inpust from AVB and therefore restore backward locomotion to an *unc-4* mutant. We can test this model by directly assessing ectopic wiring in an *unc-4; punc-4::LIN-17* animal using our AVB gap junction marker. A different way to test this model would be to overexpress the Wnt ligand LIN-44 globally in an *unc-4* mutant. LIN-44 is normally expressed in the posterior of the animal and potentially in the anchor cell in the midbody region. This restricted pattern of LIN-44 expression may limit its antagonizing effects on *ceh-12* expression in distal VA motor neurons. However, if global overexpression of LIN-44 can rescue the Unc-4 defect, then these results would suggest that the EGL-20 pathway is antagonized by increased LIN-44/LIN-17 pathway activation.

We have proposed that *lin-17* opposes *ceh-12* expression and that this accounts for the observations that (1) *ceh-12::GFP* is ectopically expressed in VA motor neurons in a *lin-17* mutant and (2) *lin-17* mutants enhance the Unc-4 miswiring defect. This model can now be tested by a simple genetic epistasis experiment. If *ceh-12* is required for the *lin-17* miswiring defect, then the *ceh-12* mutant should restore backward locomotion to a *lin-17; unc-4(ts)* double mutant as well as suppress the appearance of ectopic AVB inputs to VAs.

Because our results did not detect a role for canonical signal components in the *lin-17* pathway, it is possible that *lin-17* may antagonize VB inputs by a

non-canonical Wnt signaling pathway. This model can be tested using genetic mutations in established non-canonical pathway genes. For example, if the non-canonical asymmetry pathway functions downstream of *lin-17*, then mutations in the non-canonical asymmetry pathway, such as *lit-1* or *mom-4* should phenocopy mutations in *lin-17* and enhance the Unc-4 defect.

Future directions – Chapter 3. Genetic Screen.

The "stuck" genetic screen for Unc-4 suppressors, or *blr* mutants, isolated over 50 individual mutant lines which suppress the Unc-4 defect. This success, however, came with the realization that I would not be able to fully characterize these alleles within my time in David's lab. My eventual goal for this project was to characterize these mutations at a basic level, such that future graduate students could pick one or two interesting mutants as a PhD project.

During the past 4 years, we have only been able to extensively characterize 6 alleles isolated in this screen, and have found a total of 3 *blr* alleles that function in parallel to *ceh-12*. Due to this trend we can assume that additional loci that function in parallel pathways downstream of UNC-4 will be uncovered. The characterization of these mutations would proceed at a much faster rate due to the tools and techniques we have developed. The first step is to outcross the *blr* mutations, map them to the genome, and perform complementation tests with known *blr* alleles. Second, mutations would need to be subjected to a battery of genetic tests to determine if they function in parallel to *ceh-12* or in the *ceh-12* pathway (Chapter 3). Third, an examination of the

effect that these mutations have on ectopic AVB to VA gap junctions should yield insight as to where these *blr* pathways function.

One potential method of characterizing these mutations that was only partially explored in my studies was the use of GRASP (split-GFP) to characterize the AVA to VA synapses. With this assay it should be possible to determine if *blr* mutants restore normal VA inputs. This outcome seems highly likely given the restoration of backward locomotion in *blr*; *unc-4* doubles but it is important to provide direct confirmation to substantiate this assumption. The GRASP technique has been difficult to utilize, however, due to a weak signal and mosaic expression. Recently, Rachel Skelton has generated new GRASP transgenic lines that show strong AVA to VA puncta and therefore should be useful for addressing this important question.

The identification of Wnt, a secreted morphogen, as a potential determinant of synaptic choice, suggests the possibility that additional local secreted signals may be interpreted as local synaptogenic signals. As described in chapter I, other non-cell autonomous signals like UNC-6/Netrin can also function to regulate the location of specific synapses in *C. elegans*. Thus, it may prove advantagous to test mutants in other morphogens, such as *lin-3*/EGF, *let-22*/FGF, UNC-6/Netrin, SLT-1/Slit, etc, for defects in VA motor neuron wiring.

It is also possible that a *blr* mutant isolated in our genetic screen, could be in a pathway controlled by the Ig domain containing protein, *rig-3*. A split-GFP experiment I performed in collaboration with Clay Spencer, suggested that *rig-3* mutants have reduced AVA to A-class synapses when compared to wildtype

animals. The only known function of *rig-3* is its role in the maintenance of the VNC fascicle, in combination with other IgCAM proteins (Schwarz et al. 2009). However, experiments Clay has performed suggest that the loss of AVA to VA synapses in *rig-3* mutants is not likely to be due to a defasiculated phenotype because *rig-3* mutants alone do not have a defasiculated VNC. *rig-3* is also the only *rig* mutant, to our knowledge, that is backward Unc. This result, along with the GRASP data suggests that *rig-3* may play a role in AVA to VA synaptogenesis. Clay Spencer is currently testing this possibility for his thesis project.

Ultimately the success of this project depends upon the molecular identification of *blr* mutations that function downstream of UNC-4. One of the new techniques used by the *C. elegans* community to identify these mutations is high-throughput genome sequencing (Sarin et al. 2008). This approach provides a robust, fast, and high throughput methodology for identifying novel genes in the *unc-4* pathway. We are currently implementing this protocol to identify the molecular lesion of selected *blr* loci.

Once the specific molecular lesion and loci are known for each mutation, it will be interesting to examine the expression pattern of these *blr* loci in a wildtype and *unc-4* mutant background to determine if *unc-4* regulates their expression. Also, overexpressing these genes in VA motor neurons should induce an Unc-4 defect, similar to that observed by overexpressing CEH-12 or ΔNT-BAR-1 in VA motor neurons. We may find that some *blr* mutant loci are directly regulated by *unc-4*, potentially in anterior VA motor neurons.

We also admit the possibility that some *blr* mutations may lie in genes that suppress the Unc-4 backward locmotion defect, but are not transcriptionally regulated by *unc-4*. It is possible that these *blr* mutations may affect a component of a signaling pathway or protein complex important for synaptic choice. *unc-4* may, instead, regulate the activity of this pathway by repressing the transcription of a different component, key to the pathway's function. For example, although mutations in *egl-20*/Wnt suppress the backward locomotion defect, it is doubtful that *unc-4* directly regulates EGL-20/Wnt expression. In this case, *unc-4* controls the Wnt signaling pathway by modulating the potency of the EGL-20/Wnt ligand in VA motor neurons, but *unc-4* does not exert its influence this pathway by directly controlling *egl-20* transcription. It is plausible that some of these *blr* mutations may also affect other intracellular signaling pathways in similar ways.

Future Directions – Chapter 4. Pyrvinium.

Due to the fortuitous discovery that pyrvinium induces a synthetic lethality in a *mat-2(ax102)* genetic background, we now have the opportunity to perform a genetic screen to identify genes that functionally interact with *kin-19*/CKIα. However, additional experiments that should be perfomed before the genetic screen to potentially optimize this protocol.

First, we should determine if pyrvinium genetically interacts with other components of the APC/C. Many hypomorphic mutants have been isolated in cyclosome components and would be amenable to testing using the existing

lethality assay described in Chapter 4. This survey may provide a better genetic background for the genetic screen than *mat-2(ax102)* as another allele/gene may have a more penetrant lethality with pyrvinium.

Second, it will be informative to perform experiments that verify the activation of *kin-19*/CKIα by pyrvinium. This can be tested by demonstrating that treatment of a *mat-2* animal with pyrvinium leads to an increase in endoderm at the expense of mesoderm in the early embryo, as has been previously characterized (Peters et al. 1999). This effect would be consistent with our model suggesting that pyrvinium functions through *kin-19*/CKIα to block mesoderm development. Antibodies to perform these experiments (using gut-specific monocolonal antibody ICB4 and pharynx specific antibody 3NB12) exist, and GFP reporters that specifically mark these tissues are also available.

One way to extend this analysis is to perform some basic biochemical experiments using *C. elegans* proteins. One set of experiments involves confirming that the pyrvinium target is *kin-19,* by using a *C. elegans* destruction complex reconstituted *in vitro.* In these experiments, the destruction complex components, *kin-19*/CKIα, *pry-1*/Axin, *apr-1*/APC, and *gsk-3*/GSK-3 can be reconstituted *in vitro* and mixed with *bar-1/*β-catenin. The overall phosphorylation of β-catenin can be measured using incorporation of $[\gamma^{32}P]ATP$ onto *bar-1/*β-catenin and SDS-PAGE/autoradiography. By comparing pyrvinium treated or non-treated samples, we can determine if pyrvinium is able to activate a *C. elegans* destruction complex *in vitro*. Furthermore, by using this *in vitro* method, the functional binding site of pyrvinium on *kin-19* can be determined by

mutating conserved domains. We can also test for conservation of function by adding purified KIN-19 to CKIα-depleted Xenopus egg extracts and determining if the destruction complex is able to function normally.

Another mechanism to validate a physical interaction between *kin-19* and pyrvinium is to repeat a biochemical experiment that Curtis Thorne performed in Ethan Lee's lab. Curtis took purified CKIα and other members of the destruction complex and spot-blotted them onto a nitrocellulose membrane. He then washed the membrane with a medium containing pyrvinium. Pyrvinium is blood-red and fluoresces under green light. After several washes, Curtis imaged the nitrocellulose and found that pyrvinium stuck to the spot containing CKIα, but not to Axin, β-catenin, GSK3, or APC. This finding led him to hypothesize that pyrvinium directly interacts with CKIα. This experiment can be readily performed with *C. elegans* KIN-19 and would help verify that pyrvinium also interacts with KIN-19 (Thorne, et al. submitted).

One experiment we can use to verify that pyrvinium blocks KIN-19 is to determine if *kin-19* overactivation is able to overcome GSK3 inhibition. Treatment of adult *C. elegans* with lithium chloride causes embryonic lethality at 20mM. It may be possible to rescue this lethality with pyrvinium treatment. This outcome is predicted by the antagonistic functions of these two compounds on destruction complex function; lithium chloride inhibits the destruction complex from phosphorylating β-catenin, whereas pyrvinium causes an overactivation of the destruction complex. Thus, it is possible that pyrvinium could suppress this LiCl-induced lethal phenotype.

kin-19 is also highly conserved in *C. elegans* and contains over 40% homology to human CKIα (Korswagen 2002). The only mutants available of *kin-19* (deletions) are lethal in *C. elegans*, and it would be interesting to determine if *Drosophila*, *Xenopus*, or human CKIα can rescue the *kin-19* mutant in *C. elegans*. This would suggest a conservation of function between components of the destruction complex and other species.

Experiments using structural analogs of pyrvinium may also be insightful to understand more about the interaction of this compound in *C. elegans*. First, a more potent inhibitor of *kin-19* than pyrvinium may be identified from treatment of N2 animals with pyrvinium analogs. From these experiments, we may be able to identify a compound that induces lethality at a much lower dose in *mat-2(ax102)* animals, and thus, may provide for a more efficient genetic screen.

Overall relevance of the project.

Ultimately, the goal of the UNC-4 project is to identify the determinants of synaptic choice. The experiments presented in this dissertation add to our understanding of this problem: Local signals are interpreted within the post-synaptic neuron to dictate synaptic choice. Specifically, we have learned that *unc-4* antagonizes an EGL-20/Wnt signal that functions through MIG-1 and MOM-5/Frizzled and a canonical pathway to promote *ceh-12* expression and AVB (forward circuit) inputs. An antagonistic LIN-44/Wnt pathway, functions via LIN-17/Frizzled to antagonize *ceh-12* expression in these motor neurons. We have also learned that multiple pathways function downstream of *unc-4* to

coordinate inputs to VA motor neurons along an anterior-posterior axis. Thus, on the basis of these studies and from other work cited in the introduction, we can conclude that the mechanism of synaptic choice is not limited to signaling between adjacent neurons, but may also be regulated by extrinsic, positional cues derived from non-neuronal cells. In other words, the mere presence of an appropriate target may not be the critical step in coordinating the proper synaptic inputs. The local environment, composed of surrounding cells and morphogen concentrations, acts as a functional partner to specify an individual synaptic connection.

REFERENCES

Ahmad-Annuar, A., Ciani, L., Simeonidis, I., Herreros, J., Fredj, N., Rosso, S., Hall, A., Brickley, S., and Salinas, P. 2006. Signaling across the synapse: a role for Wnt and Dishevelled in presynaptic assembly and neurotransmitter release. *J Cell Biol* **174**(1): 127-139.

Ai, Z., Fischer, A., Spray, D.C., Brown, A.M., and Fishman, G.I. 2000. Wnt-1 regulation of connexin43 in cardiac myocytes. *J Clin Invest* **105**(2): 161-171.

Angers, S. and Moon, R.T. 2009. Proximal events in Wnt signal transduction. *Nat Rev Mol Cell Biol* **10**(7): 468-477.

Arber, S., Han, B., Mendelsohn, M., Smith, M., Jessell, T.M., and Sockanathan, S. 1999. Requirement for the homeobox gene Hb9 in the consolidation of motor neuron identity. *Neuron* **23**(4): 659-674.

Ataman, B., Ashley, J., Gorczyca, D., Gorczyca, M., Mathew, D., Wichmann, C., Sigrist, S.J., and Budnik, V. 2006. Nuclear trafficking of Drosophila Frizzled-2 during synapse development requires the PDZ protein dGRIP. *Proc Natl Acad Sci USA* **103**(20): 7841-7846.

Ataman, B., Ashley, J., Gorczyca, M., Ramachandran, P., Fouquet, W., Sigrist, S.J., and Budnik, V. 2008. Rapid activity-dependent modifications in synaptic structure and function require bidirectional wnt signaling. *Neuron* **57**(5): 705-718.

Barnes, T.M. and Hekimi, S. 1997. The Caenorhabditis elegans avermectin resistance and anesthetic response gene unc-9 encodes a member of a protein family implicated in electrical coupling of excitable cells. *J Neurochem* **69**(6): 2251-2260.

Bauer, R., Lehmann, C., Fuss, B., Eckardt, F., and Hoch, M. 2002. The Drosophila gap junction channel gene innexin 2 controls foregut development in response to Wingless signalling. *J Cell Sci* **115**(Pt 9): 1859-1867.

Bauer, R., Löer, B., Ostrowski, K., Martini, J., Weimbs, A., Lechner, H., and Hoch, M. 2005. Intercellular communication: the Drosophila innexin multiprotein family of gap junction proteins. *Chem Biol* **12**(5): 515-526.

Bertrand, V. and Hobert, O. 2009. Linking asymmetric cell division to the terminal differentiation program of postmitotic neurons in C. elegans. *Dev Cell* **16**(4): 563-575.

Brenner, S. 1974. The genetics of Caenorhabditis elegans. *Genetics* **77**(1): 71-94.

Broihier, H.T. and Skeath, J.B. 2002. Drosophila homeodomain protein dHb9 directs neuronal fate via crossrepressive and cell-nonautonomous mechanisms. *Neuron* **35**(1): 39-50.

Ch'ng, Q., Williams, L., Lie, Y.S., Sym, M., Whangbo, J., and Kenyon, C. 2003. Identification of genes that regulate a left-right asymmetric neuronal migration in Caenorhabditis elegans. **164**(4): 1355-1367.

Chalfie, M., Sulston, J.E., White, J.G., Southgate, E., Thomson, J.N., and Brenner, S. 1985. The neural circuit for touch sensitivity in Caenorhabditis elegans. *J Neurosci* **5**(4): 956-964.

Chao, D.L., Ma, L., and Shen, K. 2009. Transient cell|[ndash]|cell interactions in neural circuit formation. *Nat Rev Neurosci* **10**(4): 262.

Chen, B., Liu, Q., Ge, Q., Xie, J., and Wang, Z.-W. 2007a. UNC-1 regulates gap junctions important to locomotion in C. elegans. *Curr Biol* **17**(15): 1334-1339.

Chen, B., Liu, Q., Ge, Q., Xie, J., and Wang, Z.W. 2007b. UNC-1 regulates gap junctions important to locomotion in C. elegans. *Curr Biol* **17**(15): 1334-1339.

Christie, J.M., Bark, C., Hormuzdi, S.G., Helbig, I., Monyer, H., and Westbrook, G.L. 2005. Connexin36 mediates spike synchrony in olfactory bulb glomeruli. *Neuron* **46**(5): 761-772.

Chuang, C.-F., Vanhoven, M.K., Fetter, R.D., Verselis, V.K., and Bargmann, C.I. 2007. An innexin-dependent cell network establishes left-right neuronal asymmetry in C. elegans. *Cell* **129**(4): 787-799.

Clevers, H. 2006. Wnt/beta-catenin signaling in development and disease. *Cell* **127**(3): 469-480.

Colón-Ramos, D.A., Margeta, M.A., and Shen, K. 2007. Glia promote local synaptogenesis through UNC-6 (netrin) signaling in C. elegans. *Science* **318**(5847): 103-106.

Connors, B.W. and Long, M.A. 2004. Electrical synapses in the mammalian brain. *Annu Rev Neurosci* **27**: 393-418.

Coudreuse, D.Y., Roël, G., Betist, M.C., Destrée, O., and Korswagen, H.C. 2006. Wnt gradient formation requires retromer function in Wnt-producing cells. *Science* **312**(5775): 921-924.

Cselenyi, C.S., Jernigan, K.K., Tahinci, E., Thorne, C.A., Lee, L.A., and Lee, E. 2008. LRP6 transduces a canonical Wnt signal independently of Axin degradation by inhibiting GSK3's phosphorylation of beta-catenin. *Proc Natl Acad Sci USA* **105**(23): 8032-8037.

D'hondt, C., Ponsaerts, R., De Smedt, H., Bultynck, G., and Himpens, B. 2009. Pannexins, distant relatives of the connexin family with specific cellular functions? *Bioessays*.

Davis, M., Hammarlund, M., Harrach, T., Hullett, P., Olsen, S., and Jorgensen, E. 2005. Rapid single nucleotide polymorphism mapping in C. elegans. *BMC Genomics* **6**: 118.

Ding, Chao, Wang, and Shen. 2007. Spatial Regulation of an E3 Ubiquitin Ligase Directs Selective Synapse Elimination. *Science*.

Downey, A.S., Chong, C.R., Graczyk, T.K., and Sullivan, D.J. 2008. Efficacy of pyrvinium pamoate against Cryptosporidium parvum infection in vitro and in a neonatal mouse model. *Antimicrob Agents Chemother* **52**(9): 3106-3112.

Du, W.J., Li, J.K., Wang, Q.Y., Hou, J.B., and Yu, B. 2008. Lithium chloride regulates connexin43 in skeletal myoblasts in vitro: possible involvement in Wnt/beta-catenin signaling. *Cell Commun Adhes* **15**(3): 261-271.

Eisenmann, D.M. and Kim, S.K. 2000. Protruding vulva mutants identify novel loci and Wnt signaling factors that function during Caenorhabditis elegans vulva development. **156**(3): 1097-1116.

Fanto, M. and McNeill, H. 2004. Planar polarity from flies to vertebrates. *J Cell Sci* **117**(Pt 4): 527-533.

Feinberg, E.H., Vanhoven, M.K., Bendesky, A., Wang, G., Fetter, R.D., Shen, K., and Bargmann, C.I. 2008. GFP Reconstitution Across Synaptic Partners (GRASP) Defines Cell Contacts and Synapses in Living Nervous Systems. *Neuron* **57**(3): 353-363.

Feldman M, F.L., Brandt, LJ. 2006. *Gastrointestinal and Liver Disease*. Saunders, Philladelphia, PA.

Fire, A., Albertson, D., Harrison, S.W., and Moerman, D.G. 1991. Production of antisense RNA leads to effective and specific inhibition of gene expression in C. elegans muscle. *Development* **113**(2): 503-514.

Forrester, W.C., Kim, C., and Garriga, G. 2004. The Caenorhabditis elegans Ror RTK CAM-1 inhibits EGL-20/Wnt signaling in cell migration. *Genetics* **168**(4): 1951-1962.

Fox, R., Von Stetina, S., Barlow, S., Shaffer, C., Olszewski, K., Moore, J., Dupuy, D., Vidal, M., and Miller, D. 2005a. A gene expression fingerprint of C. elegans embryonic motor neurons. *BMC Genomics* **6**(1): 42.

Fox, R.M., Von Stetina, S.E., Barlow, S.J., Shaffer, C., Olszewski, K.L., Moore, J.H., Dupuy, D., Vidal, M., and Miller, D.M. 2005b. A gene expression fingerprint of C. elegans embryonic motor neurons. *BMC Genomics* **6**(1): 42.

Fry, G.F. and Moore, J.G. 1969. Enterobius vermicularis: 10,000-year-old human infection. *Science* **166**(913): 1620.

Fukuda, T. 2007. Structural Organization of the Gap Junction Network in the Cerebral Cortex. *The Neuroscientist* **13**(3): 199.

Fukuda, T. and Kosaka, T. 2003. Ultrastructural study of gap junctions between dendrites of parvalbumin-containing GABAergic neurons in various neocortical areas of the adult rat. *Neuroscience* **120**(1): 5-20.

Fukuda, T., Kosaka, T., Singer, W., and Galuske, R.A.W. 2006. Gap junctions among dendrites of cortical GABAergic neurons establish a dense and widespread intercolumnar network. *J Neurosci* **26**(13): 3434-3443.

Gleason, J., Korswagen, H., and Eisenmann, D. 2002a. Activation of Wnt signaling bypasses the requirement for RTK/Ras signaling during C. elegans vulval induction. *Genes and Development* **16**(10): 1281.

Gleason, J.E., Korswagen, H.C., and Eisenmann, D.M. 2002b. Activation of Wnt signaling bypasses the requirement for RTK/Ras signaling during C. elegans vulval induction. *Genes and Development* **16**(10): 1281.

Gleason, J.E., Szyleyko, E.A., and Eisenmann, D.M. 2006. Multiple redundant Wnt signaling components function in two processes during C. elegans vulval development. *Dev Biol* **298**(2): 442-457.

Gögel, S., Wakefield, S., Tear, G., Klämbt, C., and Gordon-Weeks, P.R. 2006. The Drosophila microtubule associated protein Futsch is phosphorylated

by Shaggy/Zeste-white 3 at an homologous GSK3beta phosphorylation site in MAP1B. *Mol Cell Neurosci* **33**(2): 188-199.

Gogolla, N., Galimberti, I., Deguchi, Y., and Caroni, P. 2009. Wnt signaling mediates experience-related regulation of synapse numbers and mossy fiber connectivities in the adult hippocampus. *Neuron* **62**(4): 510-525.

Golden, A., Sadler, P.L., Wallenfang, M.R., Schumacher, J.M., Hamill, D.R., Bates, G., Bowerman, B., Seydoux, G., and Shakes, D.C. 2000. Metaphase to anaphase (mat) transition-defective mutants in Caenorhabditis elegans. *J Cell Biol* **151**(7): 1469-1482.

Green, Inoue, and Sternberg. 2007. The C. elegans ROR receptor tyrosine kinase, CAM-1, non-autonomously inhibits the Wnt pathway. *Development*.

Green, J.L., Inoue, T., and Sternberg, P.W. 2008. Opposing Wnt pathways orient cell polarity during organogenesis. *Cell* **134**(4): 646-656.

Hall, A.C., Lucas, F.R., and Salinas, P.C. 2000. Axonal remodeling and synaptic differentiation in the cerebellum is regulated by WNT-7a signaling. *Cell* **100**(5): 525-535.

Harris, J., Honigberg, L., Robinson, N., and Kenyon, C. 1996. Neuronal cell migration in C. elegans: regulation of Hox gene expression and cell position. *Development* **122**(10): 3117-3131.

Hayashi, Y., Hirotsu, T., Iwata, R., Kage-Nakadai, E., Kunitomo, H., Ishihara, T., Iino, Y., and Kubo, T. 2009. A trophic role for Wnt-Ror kinase signaling during developmental pruning in Caenorhabditis elegans. *Nat Neurosci* **12**(8): 981-987.

Henriquez, J.P., Webb, A., Bence, M., Bildsoe, H., Sahores, M., Hughes, S.M., and Salinas, P.C. 2008. Wnt signaling promotes AChR aggregation at the neuromuscular synapse in collaboration with agrin. *Proc Natl Acad Sci USA* **105**(48): 18812-18817.

Herman, M. 2001. C. elegans POP-1/TCF functions in a canonical Wnt pathway that controls cell migration and in a noncanonical Wnt pathway that controls cell polarity. *Development* **128**(4): 581-590.

Hestrin, S. and Galarreta, M. 2005. Electrical synapses define networks of neocortical GABAergic neurons. *Trends Neurosci* **28**(6): 304-309.

Hilliard, M.A. and Bargmann, C.I. 2006. Wnt signals and frizzled activity orient anterior-posterior axon outgrowth in C. elegans. *Dev Cell* **10**(3): 379-390.

Hingwing, K., Lee, S., Nykilchuk, L., Walston, T., Hardin, J., and Hawkins, N. 2009. CWN-1 functions with DSH-2 to regulate C. elegans asymmetric neuroblast division in a beta-catenin independent Wnt pathway. *Dev Biol* **328**(2): 245-256.

Hobert, O. 2002. PCR fusion-based approach to create reporter gene constructs for expression analysis in transgenic C. elegans. *Biotechniques* **32**(4): 728-730.

Horne, P.D. 2002. First evidence of enterobiasis in ancient Egypt. *J Parasitol* **88**(5): 1019-1021.

Huang, S., Shetty, P., Robertson, S.M., and Lin, R. 2007. Binary cell fate specification during C. elegans embryogenesis driven by reiterated

reciprocal asymmetry of TCF POP-1 and its coactivator beta-catenin SYS-1. *Development* **134**(14): 2685-2695.

Inaki, Yoshikawa, Thomas, Aburatani, and Nose. 2007. Wnt4 Is a Local Repulsive Cue that Determines Synaptic Target Specificity. *Curr Biol*.

Inoue, T., Wang, M., Ririe, T.O., Fernandes, J.S., and Sternberg, P.W. 2005. Transcriptional network underlying Caenorhabditis elegans vulval development. *Proc Natl Acad Sci U S A* **102**(14): 4972-4977.

Jing, L., Lefebvre, J.L., Gordon, L.R., and Granato, M. 2009. Wnt signals organize synaptic prepattern and axon guidance through the zebrafish unplugged/MuSK receptor. *Neuron* **61**(5): 721-733.

Kamath, R.S., Martinez-Campos, M., Zipperlen, P., Fraser, A.G., and Ahringer, J. 2001. Effectiveness of specific RNA-mediated interference through ingested double-stranded RNA in Caenorhabditis elegans. *Genome Biology* **2**(1): RESEARCH0002.

Kim, N., Stiegler, A.L., Cameron, T.O., Hallock, P.T., Gomez, A.M., Huang, J.H., Hubbard, S.R., Dustin, M.L., and Burden, S.J. 2008. Lrp4 is a receptor for Agrin and forms a complex with MuSK. *Cell* **135**(2): 334-342.

King, R.S., Maiden, S.L., Hawkins, N.C., Kidd, A.R., Kimble, J., Hardin, J., and Walston, T.D. 2009. The N- or C-terminal domains of DSH-2 can activate the C. elegans Wnt/beta-catenin asymmetry pathway. *Dev Biol* **328**(2): 234-244.

Klassen, M.P. and Shen, K. 2007. Wnt Signaling Positions Neuromuscular Connectivity by Inhibiting Synapse Formation in C. elegans. *Cell* **130**(4): 704-716.

Kokel, D., Li, Y., Qin, J., and Xue, D. 2006. The nongenotoxic carcinogens naphthalene and para-dichlorobenzene suppress apoptosis in Caenorhabditis elegans. *Nat Chem Biol* **2**(6): 338-345.

Korkut, C., Ataman, B., Ramachandran, P., Ashley, J., Barria, R., Gherbesi, N., and Budnik, V. 2009. Trans-synaptic transmission of vesicular Wnt signals through Evi/Wntless. *Cell* **139**(2): 393-404.

Korkut, C. and Budnik, V. 2009. WNTs tune up the neuromuscular junction. *Nat Rev Neurosci* **10**(9): 627-634.

Korswagen, H.C. 2002. Canonical and non-canonical Wnt signaling pathways in Caenorhabditis elegans: variations on a common signaling theme. *Bioessays* **24**(9): 801-810.

Krylova, O., Herreros, J., Cleverley, K., Ehler, E., Henriquez, J., Hughes, S., and Salinas, P. 2002. WNT-3, expressed by motoneurons, regulates terminal arborization of neurotrophin-3-responsive spinal sensory neurons. *Neuron* **35**(6): 1043-1056.

Kühl, M. 2004. The WNT/calcium pathway: biochemical mediators, tools and future requirements. *Front Biosci* **9**: 967-974.

Kummer, T.T., Misgeld, T., and Sanes, J.R. 2006. Assembly of the postsynaptic membrane at the neuromuscular junction: paradigm lost. *Curr Opin Neurobiol* **16**(1): 74-82.

Lee, J.-Y., Marston, D.J., Walston, T., Hardin, J., Halberstadt, A., and Goldstein, B. 2006. Wnt/Frizzled signaling controls C. elegans gastrulation by activating actomyosin contractility. *Curr Biol* **16**(20): 1986-1997.

Lewis, J.A., Wu, C.H., Berg, H., and Levine, J.H. 1980a. The genetics of levamisole resistance in the nematode Caenorhabditis elegans. *Genetics* **95**(4): 905-928.

Lewis, J.A., Wu, C.H., Levine, J.H., and Berg, H. 1980b. Levamisole-resistant mutants of the nematode Caenorhabditis elegans appear to lack pharmacological acetylcholine receptors. *Neuroscience* **5**(6): 967-989.

Li, S., Dent, J.A., and Roy, R. 2003. Regulation of intermuscular electrical coupling by the Caenorhabditis elegans innexin inx-6. *Mol Biol Cell* **14**(7): 2630-2644.

Lo, M.-C., Gay, F., Odom, R., Shi, Y., and Lin, R. 2004. Phosphorylation by the beta-catenin/MAPK complex promotes 14-3-3-mediated nuclear export of TCF/POP-1 in signal-responsive cells in C. elegans. *Cell* **117**(1): 95-106.

Macdonald, B.T., Tamai, K., and He, X. 2009. Wnt/beta-catenin signaling: components, mechanisms, and diseases. *Developmental Cell* **17**(1): 9-26.

Maloof, J.N., Whangbo, J., Harris, J.M., Jongeward, G.D., and Kenyon, C. 1999. A Wnt signaling pathway controls hox gene expression and neuroblast migration in C. elegans. *Development* **126**(1): 37-49.

Maro, G.S., Klassen, M.P., and Shen, K. 2009. A beta-catenin-dependent Wnt pathway mediates anteroposterior axon guidance in C. elegans motor neurons. *PLoS ONE* **4**(3): e4690.

Mathew, D., Ataman, B., Chen, J., Zhang, Y., Cumberledge, S., and Budnik, V. 2005. Wingless signaling at synapses is through cleavage and nuclear import of receptor DFrizzled2. *Science* **310**(5752): 1344-1347.

McMahon, A.P. and Moon, R.T. 1989a. Ectopic expression of the proto-oncogene int-1 in Xenopus embryos leads to duplication of the embryonic axis. *Cell* **58**(6): 1075-1084.

-. 1989b. int-1--a proto-oncogene involved in cell signalling. *Development* **107 Suppl**: 161-167.

Mello, C.C., Kramer, J.M., Stinchcomb, D., and Ambros, V. 1991. Efficient gene transfer in C.elegans: extrachromosomal maintenance and integration of transforming sequences. *The EMBO Journal* **10**(12): 3959-3970.

Miech, C., Pauer, H.-U., He, X., and Schwarz, T.L. 2008. Presynaptic local signaling by a canonical wingless pathway regulates development of the Drosophila neuromuscular junction. *J Neurosci* **28**(43): 10875-10884.

Miller, D. and Niemeyer, C. 1995. Expression of the unc-4 homeoprotein in Caenorhabditis elegans motor neurons specifies presynaptic input. *Development* **121**(9): 2877-2886.

Miller, D., Niemeyer, C., and Chitkara, P. 1993a. Dominant unc-37 mutations suppress the movement defect of a homeodomain mutation in unc-4, a neural specificity gene in Caenorhabditis elegans. *Genetics* **135**(3): 741-753.

Miller, D.M. 2007. Neuroscience. Synapses here and not everywhere. *Science* **317**(5840): 907-908.

Miller, D.M., Niemeyer, C.J., and Chitkara, P. 1993b. Dominant unc-37 mutations suppress the movement defect of a homeodomain mutation in unc-4, a neural specificity gene in Caenorhabditis elegans. **135**(3): 741-753.

Miller, D.M., Shen, M.M., Shamu, C.E., Burglin, T.R., Ruvkun, G., Dubois, M.L., Ghee, M., and Wilson, L. 1992. C. elegans unc-4 gene encodes a homeodomain protein that determines the pattern of synaptic input to specific motor neurons. *Nature* **355**(6363): 841-845.

Mizumoto, K. and Sawa, H. 2007. Two betas or not two betas: regulation of asymmetric division by beta-catenin. *Trends Cell Biol* **17**(10): 465-473.

Moon, R.T. and Kimelman, D. 1998. From cortical rotation to organizer gene expression: toward a molecular explanation of axis specification in Xenopus. *Bioessays* **20**(7): 536-545.

Motulsky, H. 2010. *Intuitive Biostatistics: A Nonmathematical Guide to Statistical Thinking*. Oxford University Press, New York.

Nakamura, K., Kim, S., Ishidate, T., Bei, Y., Pang, K., Shirayama, M., Trzepacz, C., Brownell, D.R., and Mello, C.C. 2005. Wnt signaling drives WRM-1/beta-catenin asymmetries in early C. elegans embryos. *Genes Dev* **19**(15): 1749-1754.

Nakamura, Y., Nishisho, I., Kinzler, K.W., Vogelstein, B., Miyoshi, Y., Miki, Y., Ando, H., Horii, A., and Nagase, H. 1991. Mutations of the adenomatous polyposis coli gene in familial polyposis coli patients and sporadic colorectal tumors. *Int Symp Princess Takamatsu Cancer Res Fund* **22**: 285-292.

Olson, D.J., Christian, J.L., and Moon, R.T. 1991. Effect of wnt-1 and related proteins on gap junctional communication in Xenopus embryos. *Science* **252**(5010): 1173-1176.

Olson, D.J. and Moon, R.T. 1992. Distinct effects of ectopic expression of Wnt-1, activin B, and bFGF on gap junctional permeability in 32-cell Xenopus embryos. *Dev Biol* **151**(1): 204-212.

Packard, M., Koo, E.S., Gorczyca, M., Sharpe, J., Cumberledge, S., and Budnik, V. 2002. The Drosophila Wnt, wingless, provides an essential signal for pre- and postsynaptic differentiation. *Cell* **111**(3): 319-330.

Pan, C.-L., Howell, J.E., Clark, S.G., Hilliard, M., Cordes, S., Bargmann, C.I., and Garriga, G. 2006. Multiple Wnts and frizzled receptors regulate anteriorly directed cell and growth cone migrations in Caenorhabditis elegans. *Dev Cell* **10**(3): 367-377.

Park, F.D., Tenlen, J.R., and Priess, J.R. 2004. C. elegans MOM-5/frizzled functions in MOM-2/Wnt-independent cell polarity and is localized asymmetrically prior to cell division. *Curr Biol* **14**(24): 2252-2258.

Pecho-Vrieseling, E., Sigrist, M., Yoshida, Y., Jessell, T.M., and Arber, S. 2009. Specificity of sensory-motor connections encoded by Sema3e-Plxnd1 recognition. *Nature* **459**(7248): 842-846.

Peters, J.M., McKay, R.M., McKay, J.P., and Graff, J.M. 1999. Casein kinase I transduces Wnt signals. *Nature* **401**(6751): 345-350.

Peters, M.A., Teramoto, T., White, J.Q., Iwasaki, K., and Jorgensen, E.M. 2007. A Calcium Wave Mediated by Gap Junctions Coordinates a Rhythmic Behavior in C. elegans. *Curr Biol* **17**(18): 1601-1608.

Pflugrad, A., Meir, J., Barnes, T., and Miller, D. 1997a. The Groucho-like transcription factor UNC-37 functions with the neural specificity gene unc-4 to govern motor neuron identity in C. elegans. *Development* **124**(9): 1699-1709.

Pflugrad, A., Meir, J.Y., Barnes, T.M., and Miller, D.M. 1997b. The Groucho-like transcription factor UNC-37 functions with the neural specificity gene unc-4 to govern motor neuron identity in C. elegans. *Development* **124**(9): 1699-1709.

Poon, V.Y., Klassen, M.P., and Shen, K. 2008. UNC-6/netrin and its receptor UNC-5 locally exclude presynaptic components from dendrites. *Nature* **aop**(current).

Raj, A., van den Bogaard, P., Rifkin, S.A., van Oudenaarden, A., and Tyagi, S. 2008. Imaging individual mRNA molecules using multiple singly labeled probes. *Nat Meth* **5**(10): 877-879.

Rappleye, C.A., Tagawa, A., Lyczak, R., Bowerman, B., and Aroian, R.V. 2002. The anaphase-promoting complex and separin are required for embryonic anterior-posterior axis formation. *Dev Cell* **2**(2): 195-206.

Robinson, J.A., Chatterjee-Kishore, M., Yaworsky, P.J., Cullen, D.M., Zhao, W., Li, C., Kharode, Y., Sauter, L., Babij, P., Brown, E.L., Hill, A.A., Akhter, M.P., Johnson, M.L., Recker, R.R., Komm, B.S., and Bex, F.J. 2006. Wnt/beta-catenin signaling is a normal physiological response to mechanical loading in bone. *J Biol Chem* **281**(42): 31720-31728.

Rocheleau, C.E., Downs, W.D., Lin, R., Wittmann, C., Bei, Y., Cha, Y.H., Ali, M., Priess, J.R., and Mello, C.C. 1997. Wnt signaling and an APC-related gene specify endoderm in early C. elegans embryos. *Cell* **90**(4): 707-716.

Rocheleau, C.E., Yasuda, J., Shin, T.H., Lin, R., Sawa, H., Okano, H., Priess, J.R., Davis, R.J., and Mello, C.C. 1999. WRM-1 activates the LIT-1 protein kinase to transduce anterior/posterior polarity signals in C. elegans. *Cell* **97**(6): 717-726.

Roos, J., Hummel, T., Ng, N., Klämbt, C., and Davis, G.W. 2000. Drosophila Futsch regulates synaptic microtubule organization and is necessary for synaptic growth. *Neuron* **26**(2): 371-382.

Rosso, S., Sussman, D., Wynshaw-Boris, A., and Salinas, P. 2005. Wnt signaling through Dishevelled, Rac and JNK regulates dendritic development. *Nat Neurosci* **8**(1): 34-42.

Sarin, S., Prabhu, S., O'meara, M., Pe'er, I., and Hobert, O. 2008. Caenorhabditis elegans mutant allele identification by whole-genome sequencing. *Nat Meth*: 3.

Schlesinger, A., Shelton, C.A., Maloof, J.N., Meneghini, M., and Bowerman, B. 1999. Wnt pathway components orient a mitotic spindle in the early Caenorhabditis elegans embryo without requiring gene transcription in the responding cell. *Genes Dev* **13**(15): 2028-2038.

Schwarz, V., Pan, J., Voltmer-Irsch, S., and Hutter, H. 2009. IgCAMs redundantly control axon navigation in Caenorhabditis elegans. *Neural Development 2009 4:16* **4**: 13.

Shen, K. and Bargmann, C.I. 2003. The immunoglobulin superfamily protein SYG-1 determines the location of specific synapses in C. elegans. *Cell* **112**(5): 619-630.

Shen, K., Fetter, R.D., and Bargmann, C.I. 2004. Synaptic specificity is generated by the synaptic guidepost protein SYG-2 and its receptor, SYG-1. *Cell* **116**(6): 869-881.

Shin, T.H., Yasuda, J., Rocheleau, C.E., Lin, R., Soto, M., Bei, Y., Davis, R.J., and Mello, C.C. 1999. MOM-4, a MAP kinase kinase kinase-related protein, activates WRM-1/LIT-1 kinase to transduce anterior/posterior polarity signals in C. elegans. *Mol Cell* **4**(2): 275-280.

Slusarski, D.C., Yang-Snyder, J., Busa, W.B., and Moon, R.T. 1997. Modulation of embryonic intracellular Ca2+ signaling by Wnt-5A. *Dev Biol* **182**(1): 114-120.

Starich, T., Starich, T., Xu, J., Xu, J., Skerrett, I.M., Skerrett, I.M., Nicholson, B., Nicholson, B., Shaw, J., and Shaw, J. 2009a. Interactions between innexins UNC-7 and UNC-9 mediate electrical synapse specificity in the Caenorhabditis elegans locomotory nervous system. *Neural Development 2009 4:16* **4**(1): 16.

Starich, T.A., Herman, R.K., and Shaw, J.E. 1993. Molecular and genetic analysis of unc-7, a Caenorhabditis elegans gene required for coordinated locomotion. *Genetics* **133**(3): 527-541.

Starich, T.A., Lee, R.Y., Panzarella, C., Avery, L., and Shaw, J.E. 1996. eat-5 and unc-7 represent a multigene family in Caenorhabditis elegans involved in cell-cell coupling. *J Cell Biol* **134**(2): 537-548.

Starich, T.A., Xu, J., Skerrett, I.M., Nicholson, B.J., and Shaw, J.E. 2009b. Interactions between innexins UNC-7 and UNC-9 mediate electrical synapse specificity in the Caenorhabditis elegans locomotory nervous system. *Neural Development 2009 4:16* **4**: 16.

Sternberg, P.W. 2005. Vulval development. *WormBook : the online review of C elegans biology*: 1-28.

Sulston, J. 1976. Post-embryonic development in the ventral cord of Caenorhabditis elegans. *Philos Trans R Soc Lond B Biol Sci* **275**(938): 287-297.

Sulston, J.E. and Horvitz, H.R. 1977. Post-embryonic cell lineages of the nematode, Caenorhabditis elegans. *Dev Biol* **56**(1): 110-156.

Sulston, J.E., Schierenberg, E., White, J.G., and Thomson, J.N. 1983. The embryonic cell lineage of the nematode Caenorhabditis elegans. *Dev Biol* **100**(1): 64-119.

Tahinci, E., Thorne, C.A., Franklin, J.L., Salic, A., Christian, K.M., Lee, L.A., Coffey, R.J., and Lee, E. 2007. Lrp6 is required for convergent extension during Xenopus gastrulation. *Development* **134**(22): 4095-4106.

Thompson, R.J., Zhou, N., and MacVicar, B.A. 2006. Ischemia opens neuronal gap junction hemichannels. *Science* **312**(5775): 924-927.

Torres, M.A., Yang-Snyder, J.A., Purcell, S.M., DeMarais, A.A., McGrew, L.L., and Moon, R.T. 1996. Activities of the Wnt-1 class of secreted signaling factors are antagonized by the Wnt-5A class and by a dominant negative cadherin in early Xenopus development. *J Cell Biol* **133**(5): 1123-1137.

Van Der Giessen, R.S., Koekkoek, S.K., van Dorp, S., De Gruijl, J.R., Cupido, A., Khosrovani, S., Dortland, B., Wellershaus, K., Degen, J., Deuchars, J., Fuchs, E.C., Monyer, H., Willecke, K., De Jeu, M.T.G., and De Zeeuw, C.I. 2008. Role of olivary electrical coupling in cerebellar motor learning. *Neuron* **58**(4): 599-612.

van der Heyden, M.A., Rook, M.B., Hermans, M.M., Rijksen, G., Boonstra, J., Defize, L.H., and Destrée, O.H. 1998. Identification of connexin43 as a functional target for Wnt signalling. *J Cell Sci* **111 (Pt 12)**: 1741-1749.

Vashlishan, A.B., Madison, J.M., Dybbs, M., Bai, J., Sieburth, D., Ch'ng, Q., Tavazoie, M., and Kaplan, J.M. 2008. An RNAi screen identifies genes that regulate GABA synapses. *Neuron* **58**(3): 346-361.

Von Stetina, S., Fox, R., Watkins, K., Starich, T., Shaw, J., and Miller, D. 2007a. UNC-4 represses CEH-12/HB9 to specify synaptic inputs to VA motor neurons in C. elegans. *Genes Dev* **21**(3): 332-346.

Von Stetina, S.E., Fox, R.M., Watkins, K.L., Starich, T.A., Shaw, J.E., and Miller, D.M. 2007b. UNC-4 represses CEH-12/HB9 to specify synaptic inputs to VA motor neurons in C. elegans. *Genes Dev* **21**(3): 332-346.

Walston, T., Tuskey, C., Edgar, L., Hawkins, N., Ellis, G., Bowerman, B., Wood, W., and Hardin, J. 2004. Multiple Wnt Signaling Pathways Converge to Orient the Mitotic Spindle in Early C. elegans Embryos. *Dev Cell* **7**(6): 831-841.

Wang, J., Jing, Z., Zhang, L., Zhou, G., Braun, J., Yao, Y., and Wang, Z.-Z. 2003. Regulation of acetylcholine receptor clustering by the tumor suppressor APC. *Nat Neurosci* **6**(10): 1017-1018.

Wang, J., Ruan, N.-J., Qian, L., Lei, W.-l., Chen, F., and Luo, Z.-G. 2008. Wnt/beta-catenin signaling suppresses Rapsyn expression and inhibits acetylcholine receptor clustering at the neuromuscular junction. *J Biol Chem* **283**(31): 21668-21675.

Weatherbee, S.D., Anderson, K.V., and Niswander, L.A. 2006. LDL-receptor-related protein 4 is crucial for formation of the neuromuscular junction. *Development* **133**(24): 4993-5000.

Westfall, T.A., Brimeyer, R., Twedt, J., Gladon, J., Olberding, A., Furutani-Seiki, M., and Slusarski, D.C. 2003. Wnt-5/pipetail functions in vertebrate axis formation as a negative regulator of Wnt/beta-catenin activity. *J Cell Biol* **162**(5): 889-898.

Whangbo, J. and Kenyon, C. 1999. A Wnt signaling system that specifies two patterns of cell migration in C. elegans. *Mol Cell* **4**(5): 851-858.

White, J., Southgate, E., and Thomson, J. 1992a. Mutations in the Caenorhabditis elegans unc-4 gene alter the synaptic input to ventral cord motor neurons. *Nature* **355**(6363): 838-841.

White, J., Southgate, E., Thomson, J., and Brenner, S. 1976a. The structure of the ventral nerve cord of Caenorhabditis elegans. *Philos Trans R Soc Lond B Biol Sci* **275**(938): 327-348.

White, J.G., Southgate, E., and Thomson, J.N. 1992b. Mutations in the Caenorhabditis elegans unc-4 gene alter the synaptic input to ventral cord motor neurons. *Nature* **355**(6363): 838-841.

White, J.G., Southgate, E., Thomson, J.N., and Brenner, S. 1976b. The structure of the ventral nerve cord of Caenorhabditis elegans. *Philos Trans R Soc Lond B Biol Sci* **275**(938): 327-348.

Winnier, A.R., Meir, J.Y., Ross, J.M., Tavernarakis, N., Driscoll, M., Ishihara, T., Katsura, I., and Miller, D.M. 1999. UNC-4/UNC-37-dependent repression of motor neuron-specific genes controls synaptic choice in Caenorhabditis elegans. *Genes Dev* **13**(21): 2774-2786.

Wu, M. and Herman, M.A. 2007. Asymmetric localizations of LIN-17/Fz and MIG-5/Dsh are involved in the asymmetric B cell division in C. elegans. *Dev Biol* **303**(2): 650-662.

Yeh, E., Kawano, T., Ng, S., Fetter, R., Hung, W., Wang, Y., and Zhen, M. 2009. Caenorhabditis elegans innexins regulate active zone differentiation. *J Neurosci* **29**(16): 5207-5217.

Yu, D.-H., Macdonald, J., Liu, G., Lee, A.S., Ly, M., Davis, T., Ke, N., Zhou, D., Wong-Staal, F., and Li, Q.-X. 2008. Pyrvinium targets the unfolded protein response to hypoglycemia and its anti-tumor activity is enhanced by combination therapy. *PLoS ONE* **3**(12): e3951.

Zhang, B., Luo, S., Dong, X.-P., Zhang, X., Liu, C., Luo, Z., Xiong, W.-C., and Mei, L. 2007. Beta-catenin regulates acetylcholine receptor clustering in muscle cells through interaction with rapsyn. *J Neurosci* **27**(15): 3968-3973.

Zufall, F. 2005. Connexins and olfactory synchronicity: toward the olfactory code. *Neuron* **46**(5): 693-694.